THE UNIVERSITY OF CALGARY

Effect of Network Self Interference on the Performance of a Slow Frequency Hopped Spread Spectrum Network

by

Kevin Dale Altman

A THESIS

SUBMITTED TO THE FACULTY OF GRADUATE STUDIES

IN PARTIAL FUFILLMENT OF THE REQUIREMENTS FOR THE

DEGREE OF MASTER OF SCIENCE

DEPARTMENT OF ELECTRICAL AND COMPUTER ENGINEERING

CALGARY, ALBERTA

NOVEMBER, 1998

ABSTRACT

Capacity of CDMA (code division multiple access) networks is known to be interference limited, as such the reduction of interference is an important design criteria in optimizing network performance. Self-interference is one of the largest sources of interference in a CDMA network and possibly the only source of interference over which the system designer has direct control. This thesis is a study of a wireless indoor slow frequency hopped CDMA Ad Hoc network and how it performs as a function of parameters which have a direct effect on self-interference.

Self-interference is due to the sources of interference occurring through the physical layer such as transmitter parameters, hop code characteristics and the immunity of the system through receiver rejection. Transmitter characteristics analyzed to reduce self-interference are fast and slow power control. Frequency hopped code characteristics analyzed are uniform distribution codes, orthogonal uniform distribution codes and orthogonal uniform distribution codes without adjacent channel interference. Non-ideal transceiver characteristics included the transmitter modulation bandwidth, receiver selectivity and receiver linearity.

ACKNOWLEDGEMENTS

I would like to thank Dr. Abu Sesay for his support, guidance and helpful comments during the course of my masters. I would also like to thank Jason Sokolosky for his help and comments.

Finally I would like to thank my wife, Janet, for her patience, understanding and sacrifice throughout this long endeavor.

TABLE OF CONTENTS

LIST OF TABLES

LIST OF FIGURES

LIST OF ABBREVIATIONS AND ACRONYMS

ACI	adjacent channel interference
AWGN	additive white gaussian noise
BER	bit error rate
CDMA	code division multiple access
CIR	carrier to interference ratio
CMTP	continuous maximum transmit power
CPFSK	continuous phase frequency shift keying
FCC	federal communications commission
FH-CDMA	frequency hopping code division multiple access
FHSS	frequency hopped spread spectrum
FM	frequency modulation
FPC	fast power control
GMSK	gaussian minimum shift keying
IF	intermediate frequency
IMPL	interference mean path loss
ISI	intersymbol interference
ISM	industrial, scientific and medical

MSK	minimum shift keying
O-UMC	orthogonal uniformly distributed memoryless frequency hopping codes
O-UMC without ACI	orthogonal uniformly distributed memoryless frequency hopping codes without adjacent channel interference
PBX	private branch exchange
PN	pseudo-random
Rx	receiver
SFH-CDMA	slow frequency hopping code division multiple access
SMPL	signal mean path loss
SPC	slow power control
TDD	time division duplex
Tx	transmitter
UMC	uniformly distributed memoryless frequency hopping codes

Chapter 1

INTRODUCTION

1.1 MOTIVATION

The growth of wireless applications in the Industrial, Scientific and Medical (ISM) bands has been enormous since the adoption of spread spectrum certification in the FCC Part 15 licensing requirements and the increasing availability of wireless components. Market studies predict the digital cordless telephone market to reach 25.5 billion dollars worldwide by 2000 from 319 million dollars in 1995 [Weber95]. Wireless LAN's are also predicted to reach 1 billion dollars by 2000 in the U.S. from less than 200 million dollars in 1996 [Molta96]. Such systems are and will typically be designed in the ISM bands in North America and similar bands worldwide. As such, the use and density of the ISM bands will continue to increase over the coming years.

With growth in any wireless service, capacity becomes an important factor in the continued success of products and services. In the case of the ISM bands, two main issues can be seen driving the need for increased capacity. Firstly, the growth of general uses and applications requiring mobility has increased both the variety of products and the numbers of a particular product utilizing these bands. Secondly, the growing trend of communication networking between various devices in both the home and business environments. Such forces driving the market are now requiring improved performance levels and interoperability while increasing the densities of the traffic within a particular band and location.

This thesis studies capacity/performance metrics of a slow frequency hopped code division multiple access (SFH-CDMA) network as a function of physical layer parameters. Since FH-CDMA is an interference limited system [Wang95], the focus of this thesis is to investigate methods of reducing self-interference in the network. Self-interference is generally the key source of interference in a SFH-CDMA network and the only one that can be controlled by the system designer. Areas that have an effect on self-interference are receiver performance levels (selectivity and linearity), modulation bandwidth, transmitter power control and finally hop code characteristics.

1.2 RELATED RESEARCH

Published research on frequency hopping spread spectrum systems can be separated into two broad categories: fast frequency hopping and slow frequency hopping. If the hop rate equals or exceeds the symbol rate than the system is termed fast frequency hopping. Most published research deals with fast frequency hopping most likely because of the early interest in fast frequency hopping for military applications. The following paragraph contains a listing of some of the work that has been published on slow frequency hopping but is not meant to be exhaustive.

E. A. Geraniotis et al. [Geraniotis82] developed bounds and approximations for the average probability of error for an asynchronous multiple access communication system over fading channels. W. E. Stark [Stark85_1, Stark85_2] evaluates the performance of coding on a slow frequency hopping communication link. T. Ishifuji et al. [Ishifuji94] analyzes the retransmission probability and throughput characteristics for an indoor communication system operating at 2.4 GHz. A. M. C. Correia et al. [Correia94] analyzed the

average probability of error for an asynchronous multiple access system operating in cellular channels. T. Matsumoto et al. [Matsumoto92] derives the performance of Reed-Solomon coded M-ary FSK over the mobile radio propagation channel. M. V. Hegde et al. [Hegde90] analyzes the capacity of a multiple access communication system for both asynchronous and synchronous hopping cases.

1.3 GENERAL NETWORK DESCRIPTION

The network studied consists of 11 ($K = 11$) paired units operating in an indoor environment, the 900 MHz Industrial Scientific & Medical (ISM) band and compliant with FCC Part 15 regulations regarding frequency hopped spread spectrum systems. The regulations require the specifications listed in Table 1.1 to be followed for a frequency hopped spread spectrum system operating in the 902 - 928 MHz ISM band.

SPECIFICATION	REQUIREMENT
Hopping Channels	> 50
Bandwidth per Channel	< 500 kHz (20 dB)
Hop Dwell Period	< 0.4 sec in 20 sec period
Transmit Power	< 1 Watt

Table 1.1 FCC Part 15 Section 247 Regulations

The Multiple Access technique is frequency hopped code division multiple access (FH-CDMA). Full duplex operation is achieved between the forward and reverse link using Time Division Duplex (TDD). The network is based on a paired peer-to-peer structure with communication occurring exclusively between each pair while in the presence of

other communicating pairs [Woerner94]. Such a network is representative of certain wireless modem networks, wireless PBX networks or a transient connection in a true peer-to-peer network allowing multiple simultaneous communication links.

The protocol for this network consists of hopping to a specific channel, transmitting/receiving a forward link packet then transmitting/receiving a reverse link packet and then hopping to the next channel specified by the hopping pattern. The network is a fully symmetric peer-to-peer network implying that the forward and reverse link packet structure and hardware are identical. As a base condition for this network, the frequency hops of all units in the network are synchronous in comparison to the asynchronous hopping case. This condition reduces probability of a collision or hit between operating units by ½ for large q (channels) [Kim94] which improves capacity. As well. the occurrence of a hit amongst users affects the full packet versus a random fraction of the packet simplifying the simulation.

Figure 1.1 shows an example of the random nature of the type of network analyzed in this thesis. Such networks are referred to as Ad Hoc networks to denote the variability in the relation of units to each other. Units denoted by **F** transmit during the forward link time slot while units denoted by **R** receive during the forward link time slot. Subscripts refer to the communicating pair that consists of a single **F** and **R**.

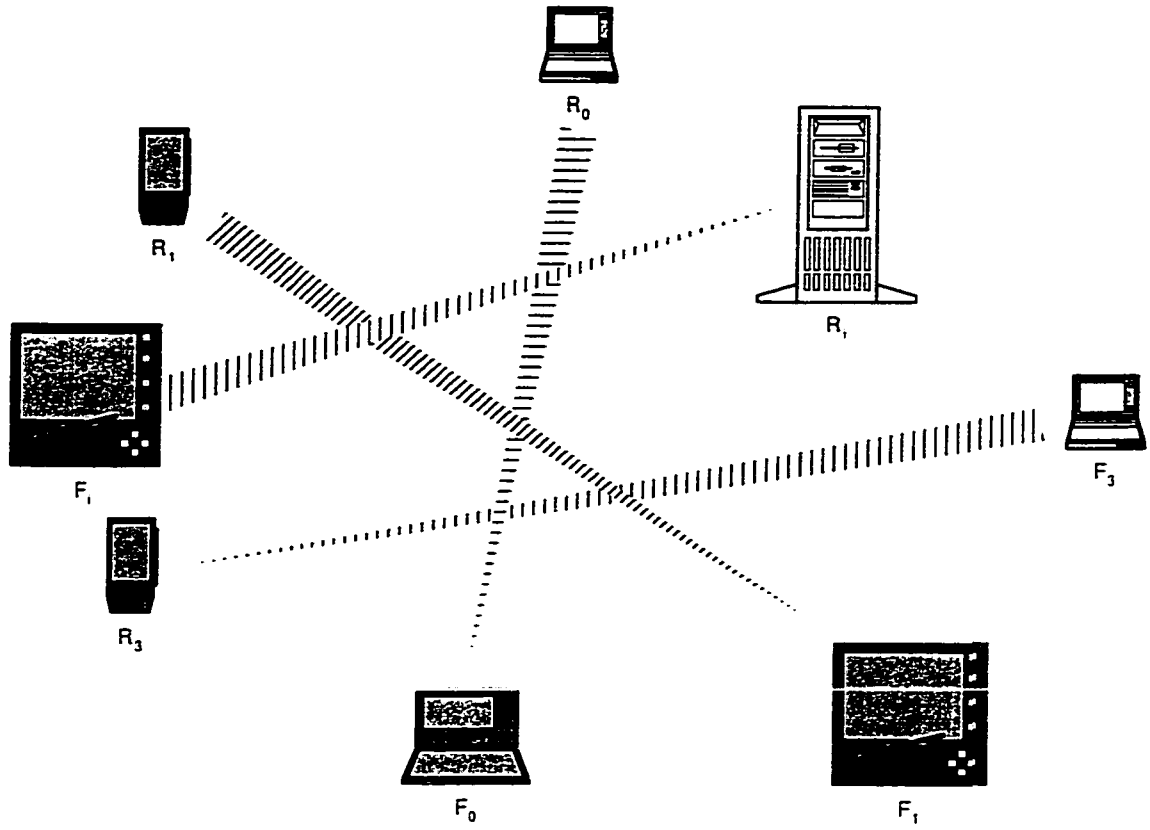

Figure 1.1 Ad Hoc Network Diagram

The objective of this analysis is to maximize the network spatial density (and hence effective capacity) for a fixed number of units while meeting the required performance criteria for all units in the network under varying physical layer characteristics.

The fixed physical layer characteristics of the network are GMSK modulation, a raw data rate of 128 kilobits/second, 128 channels and 200 kHz separation between channels while fitting within the constraints of the 900 MHz ISM band. GMSK modulation was chosen because it provides several useful benefits. Firstly, the ability to restrict the transmit occupied bandwidth over that of MSK. Secondly, GMSK (and MSK) is a continuous envelope modulation allowing for transmit power amplifiers with high efficiency. Finally,

GMSK can be detected with a limiter discriminator which is cost effective and widely available in integrated circuit form. The data rate of 128 kbits/second is chosen to support full duplex high quality voice and/or medium rate data communications.

In CDMA multi-access, the code characteristics have a large effect on the self-interference of the network. Hence the code characteristics are varied to determine the effects on network performance. For this study, uniformly distributed memoryless codes, orthogonal uniformly distributed memoryless codes and orthogonal uniformly distributed memoryless codes without adjacent channel interference (ACI) are analyzed.

The transmit power level also has a significant effect on the self interference of a SFH-CDMA network. Three power control strategies are analyzed in this thesis: continuous maximum transmit power, fast power control based on the channel loss of each hop and slow power control based on the mean channel loss. The transmit power is constrained to be within a maximum level of 10 mWatts and a minimum level of 0.01 mWatt. To study the effects of power control on networks of differing operational characteristics, several spatial distribution models based on differing probability density functions for the separation between linked pairs are investigated.

The hop dwell time is constrained to be less than the 100 mSec coherence time of the 900 MHz indoor channel. This ensures that the channel can be modeled as stationary for the duration of each hop. This restriction translates to a maximum limit on the packet size of 6400 bits for both the forward and reverse link. The 6400 bits would also include the overhead associated with a TDD based system which would reduce the actual data rate to below that of the raw data rate of 128 kbits/second.

The receiver model contains four elements of which only one was variable: noise figure, 3rd order input intercept point (IIP_3), IF filter selectivity and the demodulator. The

noise figure was fixed at 5 dB for this thesis. This was determined based on practical experience of what could be readily achieved with current technology in the 900 MHz ISM band. The 3rd order input intercept point had two values that were simulated -5 dBm, 5 dBm. The linear dynamic range of the receiver is dependent on IIP_3 which in turn affects the isolation of the desired signal from undesired signals in the band. These values are analyzed in order of achievability in a low cost, mobile radio product. -5 dBm is readily achievable and 5 dBm can be achieved at a higher cost. The demodulator chosen is the limiter-discriminator which has been analyzed extensively and available in integrated circuit form.

1.4 PERFORMANCE CRITERIA

The network performance is evaluated on the basis of the minimum required spatial separation between a receiving unit and any interfering transmitters while achieving a BER of 10^{-3}. When viewed in spatial density terms, this criteria maximizes the number of simultaneous links that can be established in a given coverage area and hence directly corresponds to increasing capacity. This approach differs from other capacity analysis in that most evaluate capacity based on average user densities and statistical models for determining which units are part of an active link. This would provide average density estimates for the network performance. In this case, a desire to support a fixed number of units in the absolute minimum coverage area under differing environmental conditions led to these analysis objectives. Often this approach may be desirable as the environment into which the system is being deployed is unknown with the installation being performed by

laymen, however, a minimum guaranteed number of users is often required before installing the network.

Chapter 2

NETWORK MODELS AND SIMULATION DESCRIPTION

2.1 INTRODUCTION

This chapter describes in detail the overall structure of the network simulated and the background theory. Specifically, topics covered include the network system description, simplifications used to reduce simulation complexity and run time and finally the basic models of each of the blocks that where used in representing the network, transceivers and indoor channel.

2.2 NETWORK SYSTEM DESCRIPTION

The network system under analysis is composed of a simple air interface and physical layer. Each are described in detail under the headings of network protocol and system link structure respectively.

2.2.1 NETWORK PROTOCOL

The protocol is illustrated by Figure 2.1. A paired unit selects one of the 128 channels (or slots q) based on CDMA code characteristics. Then, a forward packet is transmitted by the forward unit and received by the reverse unit. This is then followed by a reverse packet transmitted by the reverse unit and received by the forward unit. At this point a new channel (slot) is selected and the units repeat the forward/reverse packet transmission.

The frame period, which is the transmission of a forward and reverse packet, is limited to less than 100 msec. This is to insure that the channel can be modeled as stationary for the duration of the frame and is explained in more detail in the section on the channel model.

The illustration in Figure 2.1 only shows the $(\mathbf{F_0}, \mathbf{R_0})$ pair, however, the illustration is applicable to any operational pair in the network. As $(\mathbf{F_0}, \mathbf{R_0})$ is hopping through the available channels so are the other operational pairs. Note that the overall network is constrained by the current characteristics of the FHSS CDMA code being analyzed. Thus depending on the code attributes, each pair may require knowledge of what frequencies / hopping patterns are currently being used by other units in the network.

Several means of achieving this knowledge are possible depending on the structure of the overall system that the wireless network is part of but the means by which this may be

accomplished is not within the scope of this thesis. For the purpose of this thesis this knowledge is assumed to be readily available.

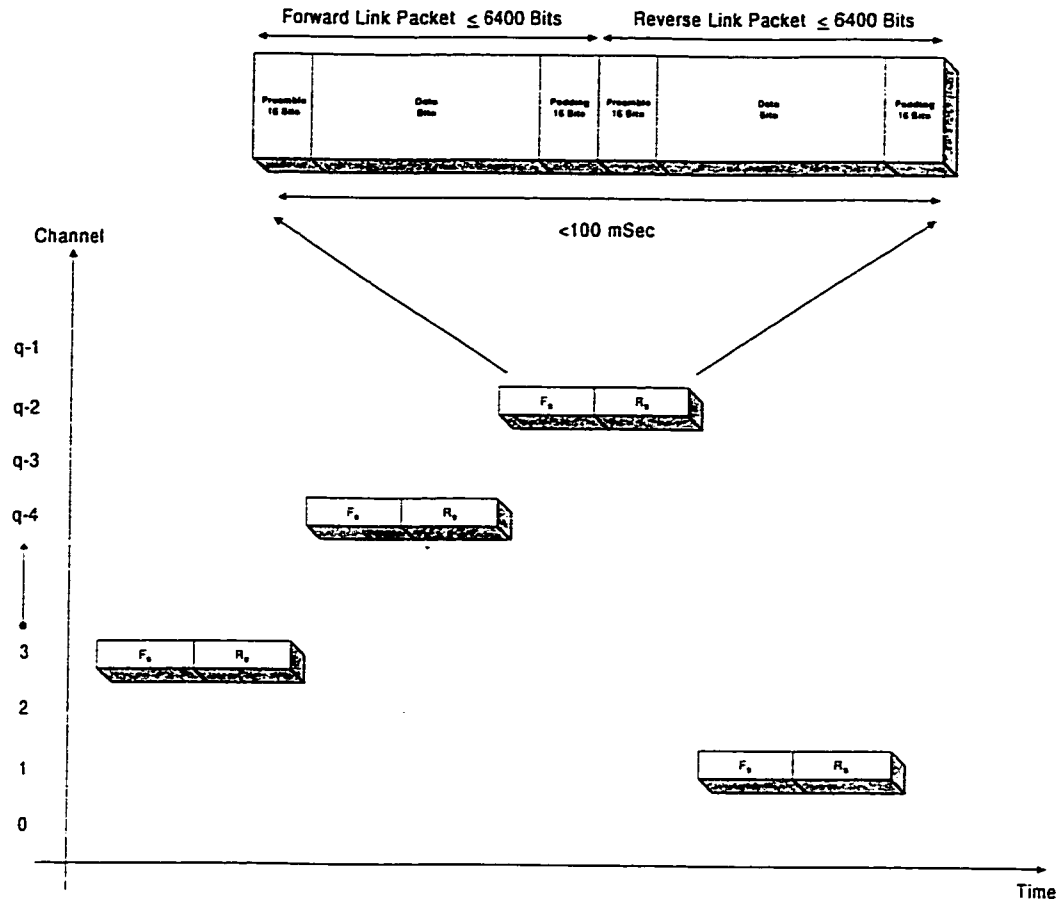

Figure 2.1 Protocol Structure for ($\mathbf{F_0}$, $\mathbf{R_0}$) Pair

The packet simulated consists of preamble bits, data bits and padding bits. The determination of the effective bit error rate is based only on the data bits. Perfect bit synchronization is used to demodulate the bits at the receiver.

Perfect packet transmission synchronization between all the operational pairs insures that the network is synchronous and collisions (hits) occurs over the full packet length.

2.2.2 SYSTEM LINK STRUCTURE

The forward and reverse link hardware structure are identical in design. This is consistent with the nature of low cost TDD systems in which the object is to maximize the amount of design re-use and minimize design time.

The system link elements, representing the wireless physical layer, are contained in three main simulation modules: a generic transmitter, a complex channel and a generic receiver. This allows the generic transmitter/receiver modules to contain the elements that are present in all configurations. The complex channel contains elements that change in complexity or are dependent on the channel and/or other elements such as channel loss, power control and CDMA characteristics.

Figure 2.2 illustrates the blocks used in simulating the network as referenced to the ($\mathbf{F_0}$, $\mathbf{R_0}$) pair. Other $\mathbf{F_i}$ units transmit packets that are added to that of $\mathbf{F_0}$ to represent the interference of the other units on the reception of the $\mathbf{R_0}$ unit.

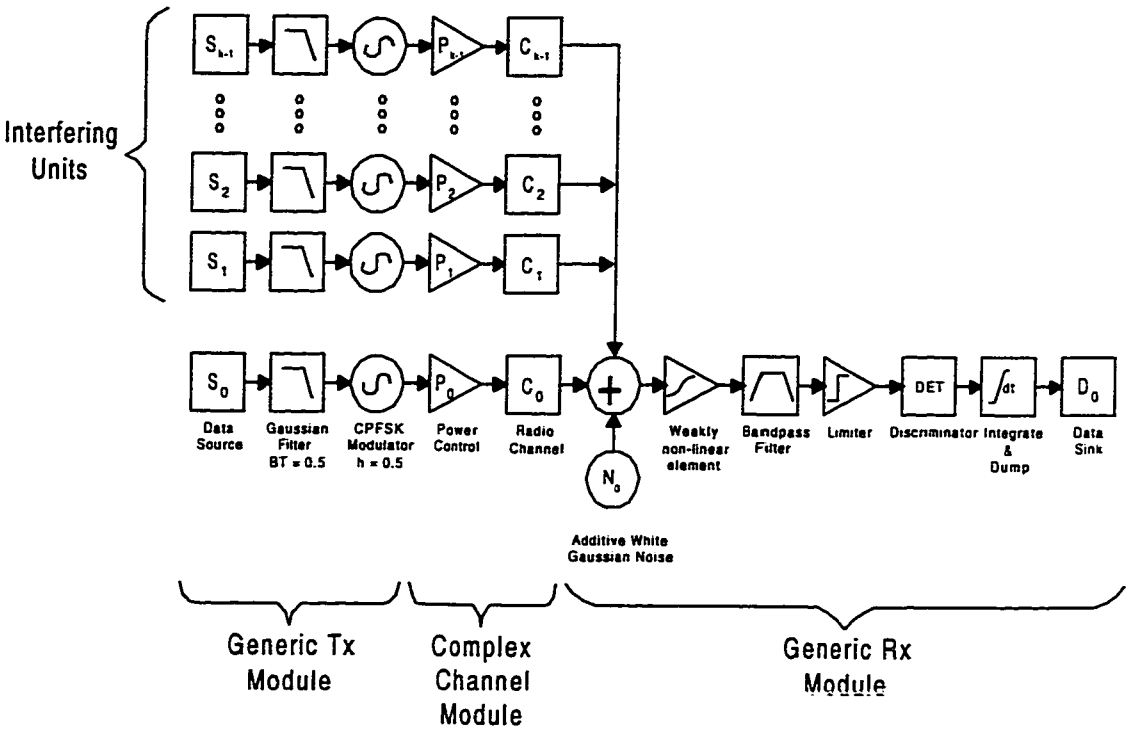

Figure 2.2 Forward/Reverse Link Simulation Block Diagram

Generic Transmitter Module

The generic transmitter model represents the basic aspects of the transmitter and consists of a data source, pulse shaping filter and frequency shift keying modulator. The data source is modeled by a maximal length PN code appended by a zero bit to create the data body of the packet. The data is prefixed by a 1010101010101010 preamble sequence and suffixed by 0000000000000000 padding sequence to insure the transmitter and receiver filter models are at steady state for the data body of the packet. The Tx filter is a Gaussian filter with a cutoff frequency of $0.5/T$ where T is the bit period. This creates the desired time-bandwidth product (BT) of 0.5. Since the impulse response of a Gaussian filter is

infinite, a truncated version was required for simulation purposes. A truncated impulse response of $\pm T$ duration was used in the simulation. The modulator then generates a continuous phase frequency shift keying (CPFSK) waveform [Proakis] from the Gaussian filtered data. This creates the desired GMSK signal with a $BT = 0.5$ and whose magnitude spectrum is illustrated in Figure 2.3.

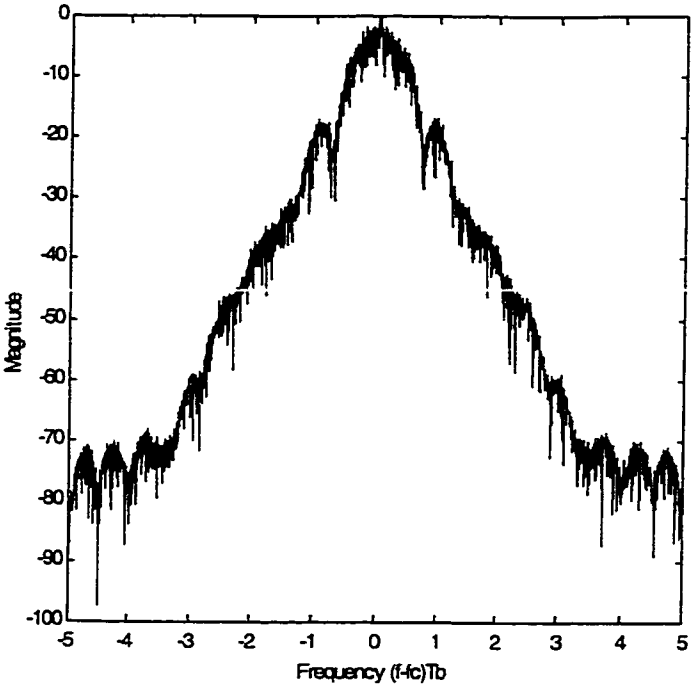

Figure 2.3 GMSK Modulation Spectrum $BT = 0.5$

Complex Channel Module

The complex channel contains models of power control, radio channel, interference tracking, hop code characteristics, and spatial distributions. These items are inter-related

yielding characteristics that are highly dependent, requiring them to be analyzed in concert within a single module.

The power control model functions by using a specified algorithm to compensate for macro path loss and fading but constrains the transmit power to be within a maximum and minimum output.

The radio channel model sums the macro and micro path loss to determine the overall loss for the current channel. The macro path loss is a function of the separation between the transmit and receive units. The micro path loss is a random variable based on the fading model. For this thesis, a Rayleigh random variable is used to represent the indoor channel fading model.

The interference model calculates the interference based on the occupied slots due to other users. Interference due to direct, adjacent channel, alternate channel and second alternate channel hits as well as intermodulation product hits are tracked to generate the proper interference for each hop.

The hop code characteristic models are probability-based and generate the occupied slots due to each operational pair which are then used by the interference model. This model controls which slots can be occupied by each transceiver in the network under the current code characteristics.

The spatial distribution model contains the locations of all $\mathbf{F_i}$, where $\mathbf{F_i}$ $\{ i \neq 0 \}$ are all equidistant from $\mathbf{R_0}$. As well, the probability based separation between ($\mathbf{F_i}$, $\mathbf{R_i}$) pairs $\{ i \neq 0 \}$ are calculated in this section from hop to hop.

Generic Receiver Module

The generic receiver contains the elements of the receiver that are basic to all network configurations. These elements include the additive white Gaussian noise (AWGN) source, weakly non-linear element, Rx IF filter, FM detector and data sink.

The AWGN source adds noise to the front end of the receiver creating the lower limit for sensitivity. The amount of noise added is determined from the noise figure of the receiver.

The weakly non-linear element represents the deviation from linear amplification and ideal mixing which occur in all receivers. The degree of non-linearity is determined by the third order input intercept point.

The receiver IF filter provides the model of the overall receiver selectivity, which in an actual receiver is due to several stages of filtering. The various filter rejection levels for signals on different channel offset allows for accurate modeling of the non-infinite selectivity of the receiver and the effects of CDMA code characteristics and power control.

The FM demodulator is made of three elements, the limiter, quadrature discriminator and matched filter. This block is standard in many FM systems studied in the literature and the performance has been analyzed extensively.

2.3 NETWORK SIMULATION SIMPLIFICATION

Several conditions are met with the network structure that allow the utilization of a major simulation simplification whereby the analysis of the forward link of a single transceiver pair will provide performance/coverage results for the full network.

The first condition is synchronous hopping which yields synchronous transmission, as all forward link units transmit simultaneously and all reverse link units transmit simultaneously. The second condition is the identical packet structure, protocol and hardware between the forward and reverse links. The third condition is hop periods are less than the coherence time of the radio channel, therefore the channel is considered static for each hop period. The fourth condition is the reciprocity principle where the channel characteristics, excluding interference and noise, are symmetrical for observation periods less than the coherence time. Therefor due to reciprocity, the forward and reverse link radio channels are considered identical for the duration of a hop. The fifth condition is omni-directional antennae on both **F** and **R** units.

The third, fourth and fifth conditions result in a simplified path loss model which is only a function of unit separation. Under the stated conditions and a simplified path loss model, there is no difference between the forward and reverse link as they relate to the channel. This allows the analysis of the forward link of the $(\mathbf{F_0}, \mathbf{R_0})$ pair to represent the performance of either the forward or reverse link with no loss of accuracy.

As mentioned earlier, this simplification holds only for the performance of the analyzed pair as it relates to the channel parameters. The performance of the pair in relationship to the interference of other pairs does not allow this simplification unless another condition is met. The requirement is that the minimum separation I_{min} that must be main-

tained between the receiving reverse link unit $\mathbf{R_0}$ and all $\mathbf{F_i}$ $\{ i \neq 0 \}$ must also simultaneously apply when reverse and forward link unit are exchanged. Explicitly, all $\mathbf{R_i}$ $\{ i \neq 0 \}$ must be separated from $\mathbf{F_0}$ by at least I_{min} at the same time all $\mathbf{F_i}$ $\{ i \neq 0 \}$ are separated from $\mathbf{R_0}$ by at least I_{min}. As well the zeroth pair ($\mathbf{F_0}$, $\mathbf{R_0}$) are not extraordinary in these requirements since the minimum interferer separation I_{min} also applies in regards to every transceiver pair ($\mathbf{F_i}$, $\mathbf{R_i}$) $\{ i \in 0, \ldots, K-1 \}$ thus any pair could be the reference pair under analysis.

To determine I_{min}, an interference analysis for fixed K units must be simulated over all applicable ranges of separation between interfering units $\mathbf{F_i}$ $\{ i \neq 0 \}$ from $\mathbf{R_0}$ and all applicable ranges separation of the forward and reverse link pair ($\mathbf{F_0}$, $\mathbf{R_0}$). This will provide two inter-related regions of operation denoted **U** and **I** referenced to $\mathbf{R_0}$. **U** and **I** are physical three dimensional regions, which are potentially overlapping, defined fully in spherical co-ordinate representation. However, due to the conditions of analysis and the simplified path loss model, the angular components have no bearing on the simulation. Hence, **U** and **I** are bounded and defined fully for the purpose of this thesis by a magnitude range consisting of a minimum and maximum value $\mathbf{U} = (r_{min} , r_{max})$ and $\mathbf{I} = (I_{min} , \infty)$. **U** is a region over which the performance of the forward link of ($\mathbf{F_0}$, $\mathbf{R_0}$) meets the minimum BER objective if all interfering units are operating within the second region **I**. The regions are illustrated in two dimensions for simplicity by Figure 2.4.

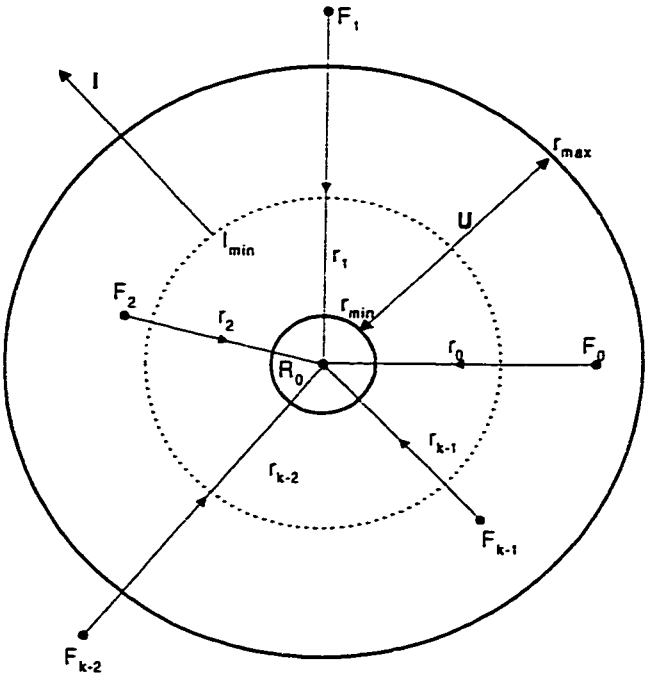

Figure 2.4 Regions **U** and **I** relative to $\mathbf{R_0}$

The performance results derived represent the performance of an Ad Hoc network when all pairs in the network meet the limits of each region, **U** and **I**, for both the forward and reverse link units as illustrated in Figure 2.5. All units are enclosed in a **U** and **I** region but for clarity only half the regions are shown.

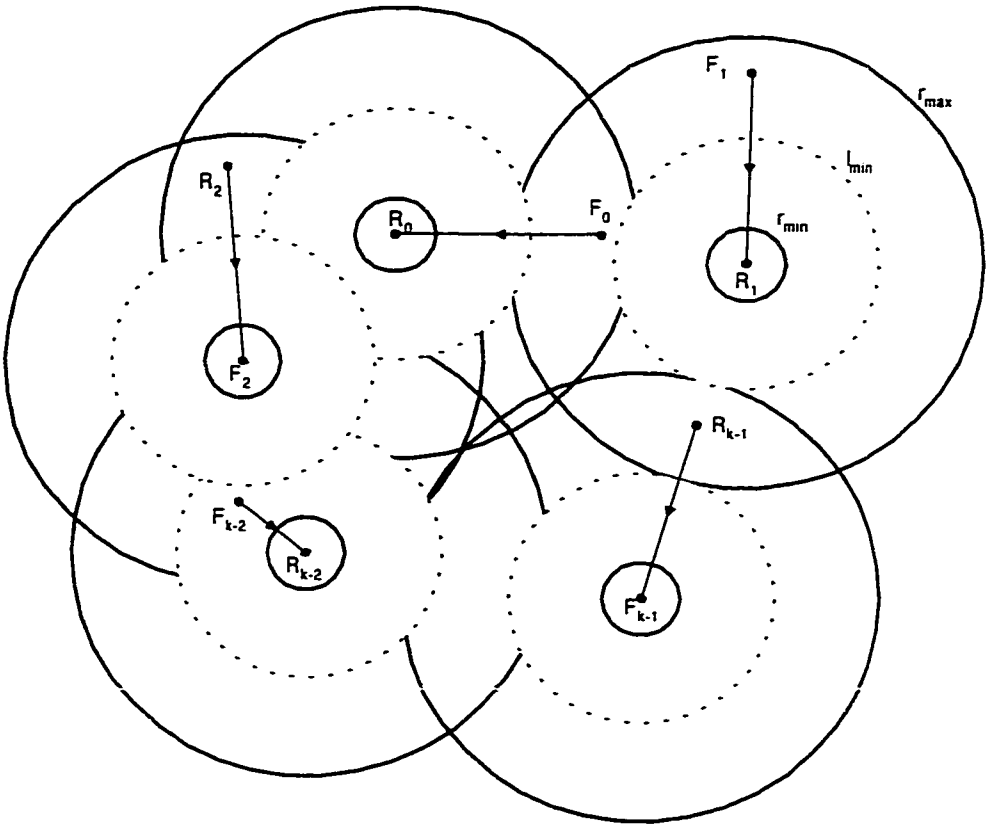

Figure 2.5 Region of Operation for Each Pair in an Ad Hoc Network

If these restrictions are met, then the results derived for the pair ($\mathbf{F_0}$, $\mathbf{R_0}$) can be used to represent the performance of any pair in the network. The optimal design objective for the network, or a single pair, is to attempt to maximize the two regions until **U** is the same as that of a network that consists of a single pair while $\mathbf{I} = (r_{min} , \infty)$.

To simplify the analysis further, the interfering units $\mathbf{F_i}$ $\{ i \neq 0 \}$ are analyzed at the same fixed distance r_i away from the receiving unit $\mathbf{R_0}$. This generates a worst case lower bound condition for I_{min}. However as improvements in the network reduce I_{min} the realism of the worst case simplification is lessoned. This is because as I_{min} is reduced (say below 2 m), it becomes physically unlikely to have 10 forward link units in such close

proximity to one reverse link unit as well as to each other. The results are still useful for small I_{min} but would tend to err on the pessimistic side for most applications.

2.4 SYSTEM MODELS

This sections details the basic models used to represent the physical network. Topics covered are the indoor channel model, spatial models representing the unit range distribution, models representing the radio transmitter, models representing the radio receiver and finally the probability models used to represent the different FHSS CDMA code options.

2.4.1 INDOOR CHANNEL MODEL

The indoor channel model is derived from well known prior work on the subject. The indoor channel is slowly varying with a Doppler rate of $2 \leq f_d \leq 10$ Hz [Pahlavan] and therefore a coherence time which is ≥ 100 mSec. The indoor channel's impulse response has also been measured in many environments [Pahlavan,Devasirvatham87] with a maximum rms delay spread generally less than 500 ns indoors which determines a coherence bandwidth of 2.0 MHz or greater. The 902 - 928 MHz ISM band, which is 26 MHz and obviously greater than the 2 MHz coherence bandwidth, is therefore considered frequency selective. This implies that a wideband channel model is required to properly describe the 902 - 928 MHz frequency band. The implementation of a wideband channel model increases the complexity of the simulation so an effort to simplify the characteristics of the ISM band channel with respect to the SFH-CDMA network under analysis was undertaken. To do this, two areas were exploited to provide simplification. The ongoing work to achieve hop codes to reduce the effects of frequency selective environments [Maric95] and the full band of operation being much greater than the 2.0 MHz coherence bandwidth. Therefore, sequential channels in the hop pattern are assumed to be far enough

apart in frequency such that they can be considered uncorrelated. As well, channels which are separated in frequency by less than the coherence bandwidth will have a minimum of the coherence time between the occurrence of the channels in the hop pattern. Based on these restrictions, the wideband channel model is simplified sufficiently so that each hop is considered to be independently faded from the previous hop.

Because the modulation bandwidth, approximately ~128 kHz, is much less than the coherence bandwidth and the hop dwell period is constrained to be less than the coherence time, the indoor channel is considered to be slowly varying flat fading [Proakis] with respect to a single channel and static for the duration of a hop period. Fading in the indoor channel can exhibit Rician or Rayleigh distributions depending on the environment. However, the Rayleigh fading model is used over the full range of operation because it allows for deeper fades and hence more detrimental fades than Rician fading and has been found to represent fading in cluttered office environments [Devasirvatham87].

Therefore the channel model is simplified significantly by allowing the channel characteristics on each hop to be independent of the previous hop and a static, fixed for the hop duration, Rayleigh distributed random variable for the envelope.

The macro path loss model is based on models proposed and used elsewhere [Parsons, Kasahara96,Devasirvatham87]. The model given by equation (2.1) is a modified form of the Friis Transmission equation [Balanis]. Instead of the standard $1/r^2$ relationship used in the free space propagation model, the exponent has been experimentally found to vary between 2 and 6 depending on the structure of the local measurement site.

This model was chosen to allow wide variability in propagation conditions that can occur in an indoor environment to be accounted for by changing the exponent of the range and repeating the simulation run. This process will achieve results that can be studied

under various propagation exponents for both the analyzed pair and the interfering pairs. The result of simulating the system in this manner will provide an upper and lower performance bound that can be used to estimate the best and worst case performance of a S-FHSS network.

$$ChannelLoss_i = \left(\frac{\lambda}{4 \cdot \pi}\right)^2 \cdot \frac{\Re^2}{r_i^{n_i}} \tag{2.1}$$

$$p_{\Re}(y) = \frac{1}{\sigma^2} \cdot e^{-y^2/(2\sigma^2)} \tag{2.2}$$

$$E[\Re] = \sqrt{\frac{\pi}{2}} \cdot \sigma \tag{2.3}$$

$$E[\Re^2] = \left(2 - \frac{\pi}{2}\right) \cdot \sigma^2 \tag{2.4}$$

$$i \in \{0, 1, \ldots, (K-2), (K-1)\} \tag{2.5}$$

$$n_i \in \{2, 3, 4, 5, 6\} \tag{2.6}$$

Where $\Re$ is a Rayleigh distributed random variable; λ is the wavelength at 915 MHz in free space; r_i is the separation of $\mathbf{R_i}$ and $\mathbf{F_i}$ units.

2.4.2 SPATIAL MODELS

There are two spatial models used in this thesis. The first model is for the separation of all forward link units from the zeroth reverse link unit. The second model describes the

separation of the forward and reverse link units of the interfering pairs for use by the power control algorithm.

Spatial Model for Separation of F_i and R_0

The spatial model shown in Figure 2.6 is a simplified pictorial representation of a three dimensional region showing the separation of (F_i , R_0). This is a simple three dimensional extension of Kocaturk's two dimensional model [Kocaturk94]. Because the system is based on an omni-directional radiation and reception of signals and a generic path loss model that is only dependent on distance, the angle aspects of the spherical coordinate system can be ignored as only the absolute separation of the units is required.

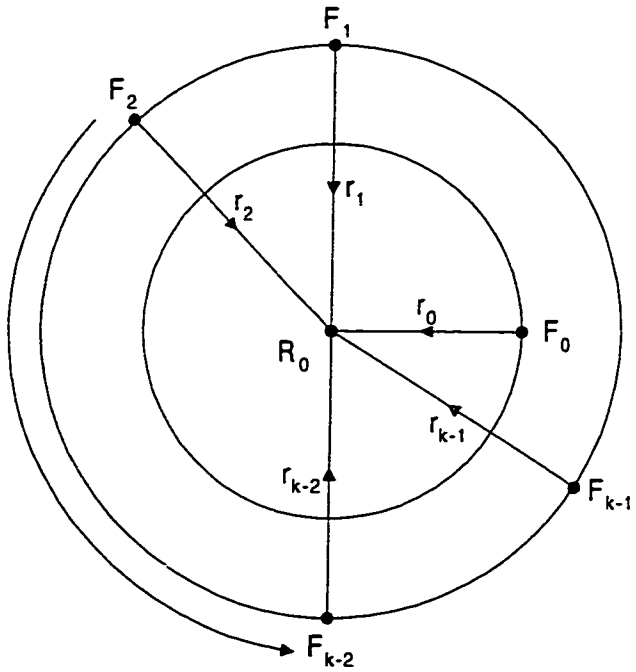

Figure 2.6 Spatial Model of the Forward Link For (F_0 , R_0) With Interfering Units F_i

Where r_0 is the distance between zeroth pair ($\mathbf{F_0}$, $\mathbf{R_0}$), r_i is the distance between $\mathbf{F_i}$ and $\mathbf{R_0}$. The minimum separation between a **F** and **R** pair is r_{min} and is approximately 1 m. The 1 m limit is chosen to represent what is felt to be a realistic worst case separation while not saturating the receiver front end under the specified transmit power and invalidating the weakly non-linear model used in the receiver. The maximum separation r_{max} between a **F** and **R** pair which allows a minimum BER of 10^{-3} in a Rayleigh fading channel with no interference. *K* is the number of operational pairs in the network.

This model allows $\mathbf{F_0}$ to be located anywhere on a circle of radius r_0 with $\mathbf{R_0}$ at the centre. The interfering $\mathbf{F_i}$ are located on another circle of radius r_i with $\mathbf{R_0}$ at the centre where $r_i = r_j \{i,j \neq 0\}$. This creates a spatial model that minimizes the number of combinations while insuring that the performance limiting conditions exist to determine an accurate estimate of the operational range of the network.

Probability Based Spatial Model for Separation of ($\mathbf{F_i}$, $\mathbf{R_i}$) Units

A probability based spatial model is required for the separation of ($\mathbf{F_i}$, $\mathbf{R_i}$) pairs to evaluate the effects of power control on the capacity of the network. To understand how the network will perform under differing topologies, three separate probability models are investigated. It is noted that there exists an infinite number of potential models, however, due to a lack of published studies on the distribution of wireless modems, LANS or cordless telephones in the indoor environment, 3 generic cases representing 3 intuitive conditions were created and studied.

The first spatial interference model is based on a uniform probability of separation between r_{min} and r_{max} , the probability density function (pdf) is shown in Figure 2.7.

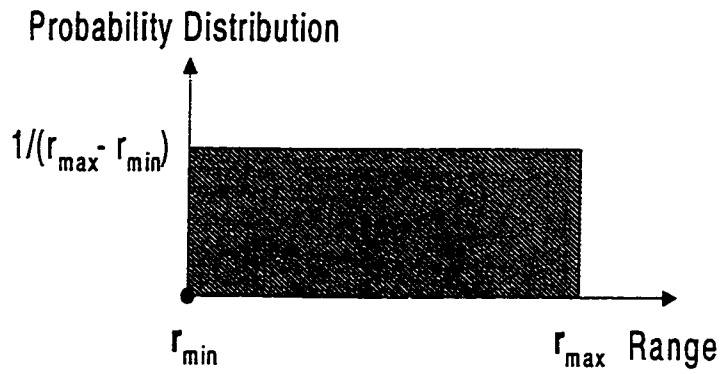

Figure 2.7 Uniform Spatial Distribution

The second spatial distribution, shown by Figure 2.8, is based on a triangular probability function where the highest probability occurs at r_{min} and the lowest probability is at r_{max} . This distribution would represent the case when the separation between units is typically small. Such a spatial distribution might occur in networks where the transceivers are cost effective and mobility an asset but not required.

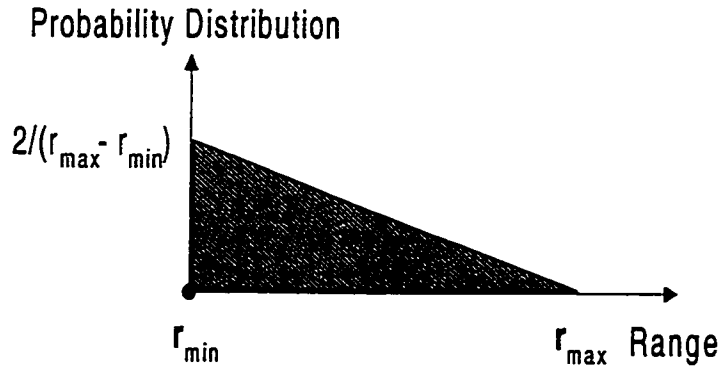

Figure 2.8 Short Range Spatial Distribution

The final spatial distribution, shown in Figure 2.9, is based on a triangular probability function where the lowest probability occurs at r_{min} and the highest probability is at r_{max}. This distribution would represent the case when the separation between units is typically large. Such a distribution might occur where the cost of the transceivers are high and therefore used in 'must' wireless links which might tend to be longer.

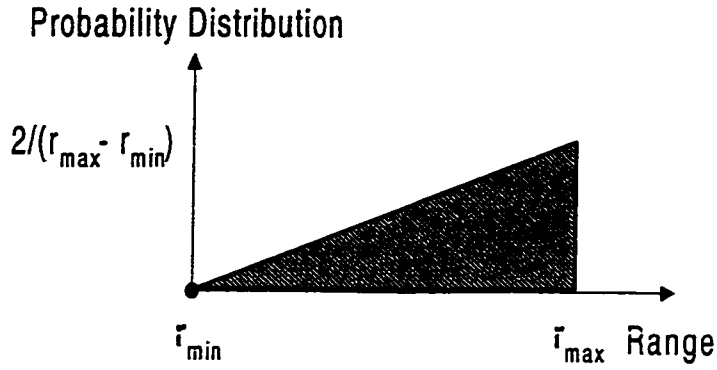

Figure 2.9 Long Range Spatial Distribution

2.4.3 TRANSMITTER MODELS

The transmitter contains two parameters which are deemed to have a significant effect on performance of the network. These are power control and modulation bandwidth.

Power Control Strategies

Three power control strategies have been analyzed to determine the effects on capacity. Continuous maximum transmit power (CMTP), fast power control (FPC) based on path loss of each hop and slow power control (SPC) based on the mean path loss.

Continuous maximum transmit power is the simplest power control strategy to implement and model. For this case the transmitters of all units are set to the maximum level of 10 mW independent of the signal power received. Obviously, this will maximize the amount of network self-interference.

Fast power control calculates the path loss between ($\mathbf{F_i}$, $\mathbf{R_i}$) for each hop and transmits at a level that is 3 dB higher than that required to achieve a BER of 10^{-3}, which is at an E_b/N_o=16.0 dB. The transmit power is constrained to be in the region 0.01 mW $\leq TxP_i \leq$ 10 mW at all times. TxP_i represents the transmit power level of the i^{th} forward link transceiver $\mathbf{F_i}$.

Slow power control effectively keeps the transmit power level at 3 dB above the average level required to achieve a BER of 10^{-3} in a Rayleigh fading environment. which is at E_b/N_o=33 dB. The transmit power is also constrained to be in the region 0.01 mW $\leq TxP_i$ $\leq$ 10 mW at all times.

The choice of TxP_i being constrained below 10 mW was based on the practical knowledge of the region of operation for the weakly non-linear model. A constraint on the received signal power to be below -20 dBm at the receiver input is due to the breakdown of the Input Intercept Model for the weakly non-linear component of the receiver model. The model is only accurate for input power levels that are less than IIP_3 by about 15 dB from practical experience. So, with the minimum IIP_3 of -5 dBm being analyzed and a lower bound on r_{min} and I_{min} of approximately 1 m, a maximum value of TxP_i = 10 mW is determined to ensure that the weakly non-linear model is accurate.

Modulation Bandwidth

A modulation time-bandwidth of $BT = 0.5$ is simulated to represent pulse shaping which would reduce the modulation sidebands while introducing a tolerable amount of intersymbol interference such that equalization would not be required. The transmit filter used is a FIR filter with an impulse response corresponding to a truncated Gaussian filter impulse response of ± 1 bit period shown in Figure 2.10 and frequency response shown in Figure 2.11.

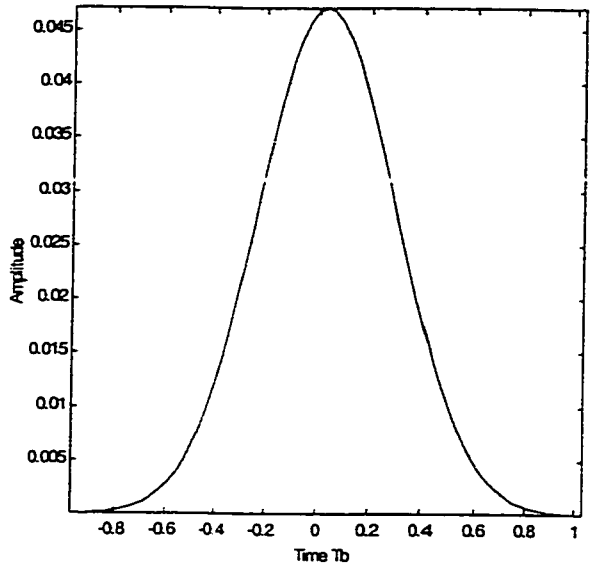

Figure 2.10 Truncated Gaussian Filter Impulse Response

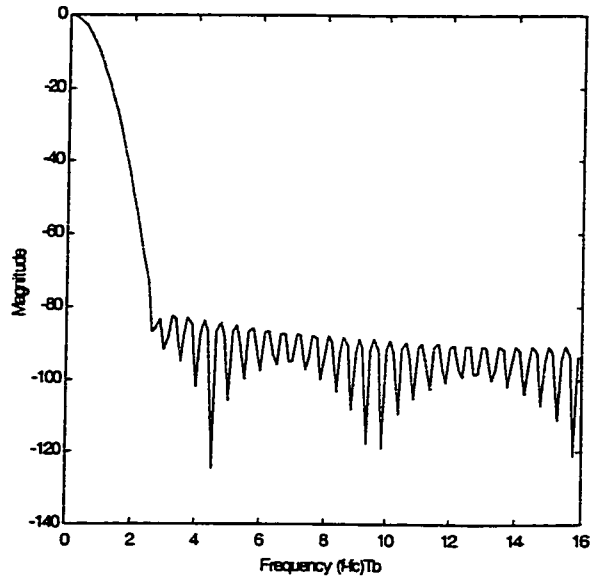

Figure 2.11 Truncated Gaussian Filter Response

2.4.4 RECEIVER MODEL

Four separate elements are incorporated in the receiver model to represent the parameters that have the greatest effect on receiver performance. Thermal noise, non-linear element, selectivity and detector are arguably the most important aspects to a receiver. Each is heavily dependent on the receiver architecture and the quality of the components. As such it is important to understand how each component affects the network performance to minimize cost and complexity.

Thermal Noise

Thermal noise has been analyzed extensively and the results are well known, hence only a summary is included with the addition of a correction factor needed for the receiver noise figure. The power of the thermal noise is given by equation (2.7).

$$N_I = Vn^2 = 4kT_kBR \tag{2.7}$$

Where $k = 1.38\ 10^{-23}$ Joules per Kelvin; R is the resistance in ohms; B is the bandwidth in Hz; T_k is the temperature in degrees Kelvin.

Using the Friis formula given by equation (2.8), the receiver noise can be reduced to the noise model represented in Figure 2.12. This allows the addition of N_{SYS} to represent the additional noise added by the receiver such that the blocks following the summation can be considered noiseless without any loss of accuracy.

$$Fsys = F_1 + \frac{F_2 - 1}{G_1} + \frac{F_3 - 1}{G_1 \cdot G_2} + \frac{F_4 - 1}{G_1 \cdot G_2 \cdot G_3} + \ldots \tag{2.8}$$

$$NF = 10 \cdot \log(Fsys) \tag{2.9}$$

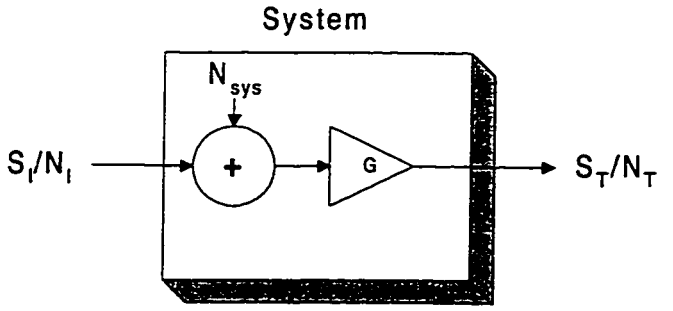

Figure 2.12 Thermal Noise/Noise Figure Block Diagram

$$S_T = G \cdot S_I \tag{2.10}$$

$$N_T = G \cdot [N_I + N_{SYS}] \tag{2.11}$$

$$NF \equiv 10 \cdot \log\left[\frac{SNR_T}{SNR_I}\right] = 10 \cdot \log\left[\frac{S_I/N_I}{S_T/N_T}\right] \tag{2.12}$$

Substituting (2.10) and (2.11) into (2.12) gives

$$NF = 10 \cdot \log\left[\frac{N_{SYS}}{N_I} + 1\right] \tag{2.13}$$

obviously,

$$N_{SYS} = N_I \cdot (10^{NF/10} - 1) \tag{2.14}$$

and hence,

$$N_T = G \cdot \overline{N_I} \tag{2.15}$$

$$\overline{N_I} = N_I \cdot 10^{NF/10} \tag{2.16}$$

Equation (2.16) allows the simplification shown in Figure 2.13 to be made to the system to account for the receiver noise figure independent of the receiver gain.

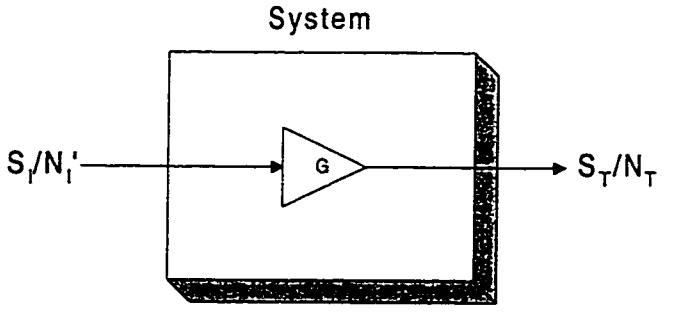

Figure 2.13 Simplified Receiver Thermal Noise / Noise Figure Model

This is a simple method for achieving the correct noise levels for simulation purposes such that any subsequent signal processing blocks can be considered noiseless.

Weakly Non-Linear Model

When two or more signals are passed through a non-linear device, the non-linearities generate new frequency components not present in the input signal which give rise to distortion of the original signal. The resulting products are called intermodulation products and the process is referred to as intermodulation and are graphically shown in Figure 2.14.

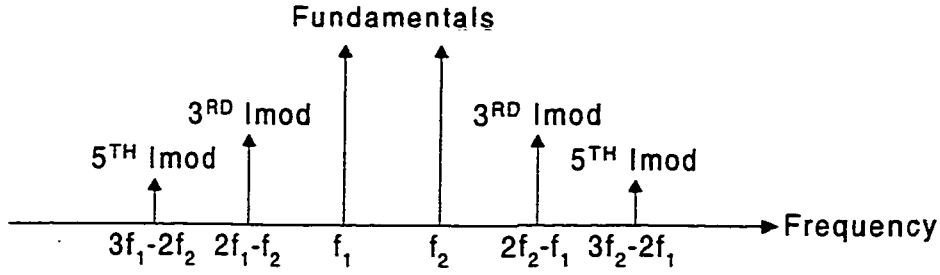

Figure 2.14 Intermodulation Products

In the case of narrowband wireless receivers, it is the odd exponent non-linearities which generally cause interference [Maxemchuk77]. As well, the 3rd order intermodulation products are typically stronger than the 5th which are in turn stronger than the 7th and so on. Only the 3rd order products are considered in the analysis of intermodulation interference as these products tend to dominate for the majority of a receiver's dynamic range.

A standard measure of the linearity of a device is the input (or output) 3rd order intercept point [Sagers82]. This is a theoretical input (or output) power at which the power in

one of two distinct input frequencies equals the power of one of the two intermodulation products created by the 3rd order non-linearity and shown graphically in Figure 2.15. This figure of merit can be specified for individual blocks or cascaded to achieve an equivalent system result in much the same way as noise figure using equation (2.17).

$$IIP_{3SYS} = \left\{ \frac{1}{IIP_{3_1}} + \frac{G_1}{IIP_{3_2}} + \frac{G_1 G_2}{IIP_{3_3}} + \frac{G_1 G_2 G_3}{IIP_{3_4}} + \ldots \right\}^{-1} \tag{2.17}$$

Where IIP_{3SYS} is the equivalent linear system input intercept point; IIP_{3i} is the linear block input intercept point and G_i is the linear block gain.

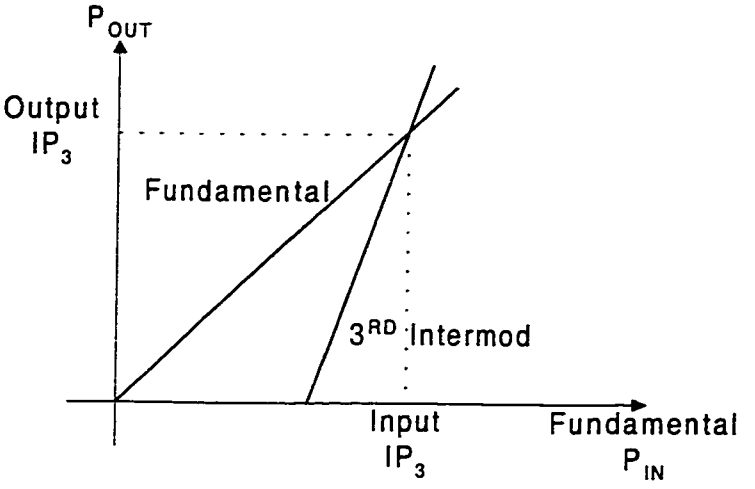

Figure 2.15 3rd Order Intercept Point

As the intercept point is a standard measure of receiver non-linearity it is important to relate this measure to the power series representation of a non-linear gain stage in equation (2.18).

$$V_{OUT}(t) = \sum_{i=1}^{\infty} a_i \cdot V_{IN}^{i}(t) \tag{2.18}$$

As mentioned previously, only the odd intermodulation products are of concern in narrowband receivers and of these the 3RD order non-linearities dominate for the operational range of concern. The odd order intermods are generated from the odd order exponents so the following simplification can be made to the power series representation of the non-linear component yielding equation (2.19).

$$V_{OUT}(t) \cong a_1 \cdot V_{IN}(t) + a_3 \cdot (V_{IN}(t))^3 \tag{2.19}$$

Where $V_{OUT}(t)$ is the output signal voltage; $V_{IN}(t)$ is the input signal voltage; a_1 is the linear gain term and a_3 is the non-linear gain term.

Analyzing the case when the input signal, equation (2.20), is composed of two sinusoids of frequencies f_1 and f_2, amplitude terms A_1 and A_2, phase change $\theta_1(t)$ and $\theta_2(t)$ due to CPFSK modulation, and finally initial random phase offset ϕ_1 and ϕ_2. We can then derive a relationship between the 3RD Order Intercept Point and the coefficients of the power series expansion. This relationship will allow a simple method of modeling the non-linearity of a receiver.

$$V_{IN}(t) = A_1 \cdot \cos(2\pi f_1 t + \theta_1(t) + \phi_1) + A_2 \cdot \cos(2\pi f_2 t + \theta_2(t) + \phi_2) \tag{2.20}$$

$$\theta_1(t) = 2\pi \cdot \frac{h}{2T} \int_{-\infty}^{t} s_1(t)dt \tag{2.21}$$

$$\theta_2(t) = 2\pi \cdot \frac{h}{2T} \int_{-\infty}^{t} s_2(t)dt \tag{2.22}$$

For equations (2.21) and (2.22), T is the bit period in seconds, h is the modulation index and $s_1(t), s_2(t)$ are the binary ± 1 data streams.

Substituting equation (2.20) into (2.19) gives (2.23) which can be expanded into (2.24).

$$\therefore V_{OUT}(t) \equiv a_1 \langle A_1 \cdot \cos(2\pi f_1 t + \theta_1(t) + \phi_1) + A_2 \cdot \cos(2\pi f_2 t + \theta_2(t) + \phi_2) \rangle + a_3 \langle A_1 \cdot \cos(2\pi f_1 t + \theta_1(t) + \phi_1) + A_2 \cdot \cos(2\pi f_2 t + \theta_2(t) + \phi_2) \rangle^3 \quad (2.23)$$

$$\begin{aligned}
\therefore V_{OUT}(t) \equiv\ & a_1 A_1 \cdot \cos(2\pi f_1 t + \theta_1(t) + \phi_1) + a_1 A_2 \cdot \cos(2\pi f_2 t + \theta_2(t) + \phi_2) \\
& + \frac{3a_3 A_1^3}{4} \cdot \cos(2\pi f_1 t + \theta_1(t) + \phi_1) + \frac{3a_3 A_2^3}{4} \cdot \cos(2\pi f_2 t + \theta_2(t) + \phi_2) \\
& + \frac{3a_3 A_1^2 A_2}{2} \cdot \cos(2\pi f_1 t + \theta_1(t) + \phi_1) + \frac{3a_3 A_1 A_2^2}{2} \cdot \cos(2\pi f_2 t + \theta_2(t) + \phi_2) \\
& + \frac{3a_3 A_1^2 A_2}{4} \cdot \cos\{2(2\pi f_1 t + \theta_1(t) + \phi_1) - (2\pi f_2 t + \theta_2(t) + \phi_2)\} \\
& + \frac{3a_3 A_1 A_2^2}{4} \cdot \cos\{2(2\pi f_2 t + \theta_2(t) + \phi_2) - (2\pi f_1 t + \theta_1(t) + \phi_1)\} \\
& + \frac{3a_3 A_1^2 A_2}{4} \cdot \cos\{2(2\pi f_1 t + \theta_1(t) + \phi_1) + (2\pi f_2 t + \theta_2(t) + \phi_2)\} \\
& + \frac{3a_3 A_1 A_2^2}{4} \cdot \cos\{2(2\pi f_2 t + \theta_2(t) + \phi_2) + (2\pi f_1 t + \theta_1(t) + \phi_1)\} \\
& + \frac{a_3 A_1^3}{4} \cdot \cos\{3(2\pi f_1 t + \theta_1(t) + \phi_1)\} + \frac{a_3 A_2^3}{4} \cdot \cos\{3(2\pi f_2 t + \theta_2(t) + \phi_2)\}
\end{aligned} \quad (2.24)$$

Because the receiver in this system is narrowband, only the signals at f_1 , f_2 , $2f_2$-f_1 and $2f_1$-f_2 frequencies are important so equation (2.24) can be reduced to (2.25).

$$V_{OUT}(t) \equiv a_1 A_1 \cdot \cos(2\pi f_1 t + \theta_1(t) + \phi_1) + a_1 A_2 \cdot \cos(2\pi f_2 t + \theta_2(t) + \phi_2) \quad (2.25)$$
$$+ \frac{3a_3 A_1^3}{4} \cdot \cos(2\pi f_1 t + \theta_1(t) + \phi_1) + \frac{3a_3 A_2^3}{4} \cdot \cos(2\pi f_2 t + \theta_2(t) + \phi_2)$$
$$+ \frac{3a_3 A_1^2 A_2}{2} \cdot \cos(2\pi f_1 t + \theta_1(t) + \phi_1) + \frac{3a_3 A_1 A_2^2}{2} \cdot \cos(2\pi f_2 t + \theta_2(t) + \phi_2)$$
$$+ \frac{3a_3 A_1^2 A_2}{4} \cdot \cos\{2(2\pi f_1 t + \theta_1(t) + \phi_1) - (2\pi f_2 t + \theta_2(t) + \phi_2)\}$$
$$+ \frac{3a_3 A_1 A_2^2}{4} \cdot \cos\{2(2\pi f_2 t + \theta_2(t) + \phi_2) - (2\pi f_1 t + \theta_1(t) + \phi_1)\}$$

Now equation (2.25) needs to be related to the 3RD order input intercept point in equation (2.26).

$$IIP_3 \equiv P_{IN} + \frac{\Delta IM_3}{2} \quad (2.26)$$

In equation (2.26), IIP_3 is the 3RD Order Input Intercept Point in dBm which is defined as a theoretical point where the input signals to a device would create intermodulation products of the same power as one of the input signals. ΔIM_3 is the difference in dB between the fundamental power level and the power level of the 3RD intermodulation products. IIP_3 is independent of the gain of the device or system which allows direct comparisons of different devices. Note that by definition A_1=A_2 in determining IIP_3 or OIP_3.

$$OIP_3 = IIP_3 + G \quad (2.27)$$

$$OIP_3 \equiv P_{OUT} + \frac{\Delta IM_3}{2} \tag{2.28}$$

OIP_3 is the 3RD Order Output Intercept Point is defined as the output power where the fundamental signal(s) power equals the 3RD order intermodulation product(s) power. G is the linear gain of the device or system.

The power of one of the 3RD order intermodulation products is obtained by taking the expectation shown in equation (2.29). The result is given in linear scale by equation (2.30) and dB scale by equation (2.31).

$$P_{IMOD_3}\Big|_{LIN} = E\left[\frac{3a_3A_1^2A_2}{4} \cdot \cos\{2(2\pi f_1 t + \theta_1(t) + \phi_1) - (2\pi f_2 t + \theta_2(t) + \phi_2)\}\right]^2 \tag{2.29}$$

$$P_{IMOD_3}\Big|_{LINEAR} = \left(\frac{3a_3A_1^2A_2}{4}\right)^2 \cdot \frac{1}{2} \tag{2.30}$$

$$P_{IMOD_3} = 10 \cdot \log\left[\left(\frac{3a_3A_1^2A_2}{4}\right)^2 \cdot \frac{1}{2}\right] \tag{2.31}$$

The power of the input signal is given by equation (2.32) in dB, and the gain of the system or device is given in (2.33) in dB.

$$P_{IN} = 10 \cdot \log\left[\frac{A_1^2}{2}\right] \tag{2.32}$$

$$G = 10 \cdot \log[a_1] \tag{2.33}$$

Equation (2.34) is derived from equations (2.31) , (2.32) and from the previous condition that A_1=A_2 in defining IIP_3 or OIP_3.

$$\Delta IM_3 = P_{IN} - P_{IMOD_3} = 10 \cdot \log\left(\frac{4}{3a_3 A_1^2}\right)^2 \tag{2.34}$$

Substituting (2.32) , (2.33) , (2.34) into (2.28) yields equation (2.35) which can be simplified into (2.36).

$$OIP_3 = P_{IN} + G + \frac{\Delta IM_3}{2} = 10 \cdot \log\left[\frac{A_1^2}{2}\right] + 10 \cdot \log[a_1] + \frac{10}{2} \cdot \log\left(\frac{4}{3a_3 A_1^2}\right)^2 \tag{2.35}$$

$$OIP_3 = 10 \cdot \log\left[\left|\frac{2a_1}{3a_3}\right|\right] \tag{2.36}$$

Using the relationships in equations (2.27), (2.33) and (2.36), equation (2.37) can be derived. Thus, we have derived the mathematical relationship between the common receiver figure of merit IIP_3 and the coefficients of the power series expansion for a nonlinear element.

$$IIP_3 = 10 \cdot \log\left[\left|\frac{2}{3a_3}\right|\right] \tag{2.37}$$

By rearranging equation (2.37) we can easily determine the proper a_3 coefficient value for a given IIP_3.

$$a_3 = -\frac{2}{3} \cdot 10^{-IIP_3/10} \tag{2.38}$$

Using this result the interference for double beat intermodulation products can be derived and the result is expressed in equation (2.39) .

$$V_{IMOD_2}(t) = -\frac{2}{3} \cdot 10^{-IIP_3/10} \cdot \frac{3A_1^2 A_2}{4} \cdot \cos(2\pi f_c t + \vartheta_2(t) + \varphi_2) \tag{2.39}$$

$$\vartheta_2(t) = 2\pi \cdot \frac{h}{2T} \int_{-\infty}^{t} (2s_1(t) - s_2(t))dt \tag{2.40}$$

$$\varphi_2 = 2\phi_1 - \phi_2 \tag{2.41}$$

Where A_1 is the amplitude of the carrier that is closest to the desired channel and A_2 is the amplitude of the carrier that is farthest from the desired channel. f_c is the desired channel, $\vartheta_2(t)$ is the double beat modulation phase, h is the modulation index, T is the bit period, ϕ_1 , ϕ_2 are the initial random phases of the two signals, and $s_1(t)$, $s_2(t)$ are the binary data streams for the two original signals.

Note that this result applies to a double beat intermodulation product which is created from two carriers. There are also triple beat intermodulation products which are the result of three carriers. The resulting interference for triple beat intermodulation can be derived similarly, the end result of the derivation is equation (2.42).

$$V_{IMOD_3}(t) = -\frac{2}{3} \cdot 10^{-IIP_3/10} \cdot \frac{6A_1 A_2 A_3}{4} \cdot \cos(2\pi f_c t + \vartheta_3(t) + \varphi_3) \tag{2.42}$$

$$\vartheta_3(t) = 2\pi \cdot \frac{h}{2T} \int_{-\infty}^{t} (s_1(t) + s_2(t) + s_3(t))dt \tag{2.43}$$

$$\varphi_3 = \phi_1 + \phi_2 + \phi_3 \tag{2.44}$$

Where A_1 , A_2 , A_3 are the amplitudes of the original signals, f_c is the desired channel, $\vartheta_3(t)$ is the triple beat intermodulation phase, h is the modulation index, T is the bit

period, ϕ_1 , ϕ_2 , ϕ_3 are the initial random phases of the input signals, and $s_1(t)$, $s_2(t)$, $s_3(t)$ are the binary data streams for the three original signals.

The significance of these results is the capability of analytically determining what the proper intermodulation products level should be based on the power of the originating signals, and then creating the product directly. The other option would be to simulate all 128 channels simultaneously with the required oversampling and then pass the resulting signals through a non-linear stage in the simulator. This approach would have a significant impact on simulation time and hence is undesirable.

By using the relation derived between the input intercept point and a_3, the resulting interference can be added to the desired signal as it enters the receiver independent of the subsequent stages which can be considered completely linear. This is due to the similar nature of this parameter to that of the system noise figure in that these parameters are derived for the full system but referenced to the input. Thus, when a double or triple beat intermodulation product occupies the desired channel, the product amplitude is calculated based on the amplitude of the creating components and the input intercept point and summed directly with the desired signal. This process obviously simplifies the simulation as the sample rate is reduced substantially by not having to simulate the original carriers and there is no effect on accuracy.

Selectivity

Selectivity of a receiver is based on the filtering that occurs in the system prior to the detection process. The filtering that typically occurs in stages at differing frequencies has been combined into a single filter, the IF filter. This can be accomplished without loss of

accuracy since equivalent system noise and linearity models have been derived. Figure 2.16 plots the magnitude response of the IF filter used in the simulation.

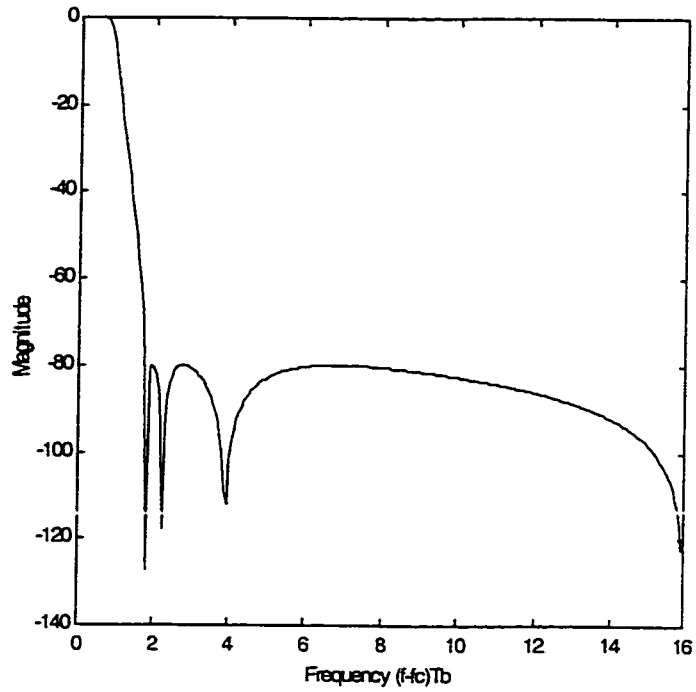

Figure 2.16 IF Filter Response

The selectivity template for the IF filter has been derived to represent the overall filtering result that can be readily achieved with current technology.

FM Detector

The FM detector is the bandpass limiter discriminator with integrate and dump filtering. It has been analyzed extensively in regards to performance in AWGN [Pawula81,Tjhung70]. The method outlined here is based on the work of Pawula for both

the AWGN and Rayleigh fading cases. Pawula's work is a simplified method for analyzing the performance of a limiter discriminator with various IF filter types but contains restrictions in the modulation index ($h < 1.5$) and the IF filter ($1< BT <3$). These restrictions are not violated in this analysis so this method is ideal because, to the knowledge of the author, the IF filter simulated in this thesis has not been analyzed in literature. For Rayleigh fading, Pawula's results were used with the addition of a slow fading Rayleigh environment.

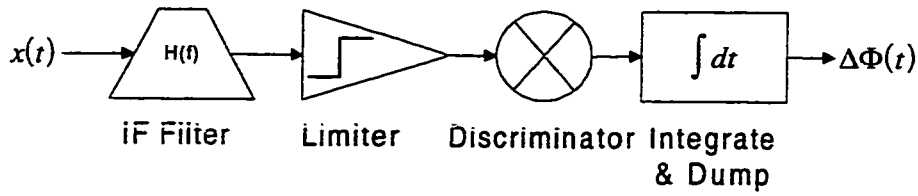

Figure 2.17 Bandpass Limiter Discriminator Model

The input signal is represented in equation (2.45).

$$x(t) = \sqrt{2S} \cdot \cos(\omega_o t + \theta(t)) + w(t) \tag{2.45}$$

$$\theta(t) = 2\pi \cdot f_d \int_{-\infty}^{t} s_1(t)dt \tag{2.46}$$

Equation (2.47) represents the binary data modulation.

$$s_1(t) = \pm 1 \tag{2.47}$$

$$\omega_o = 2\pi fo \tag{2.48}$$

$$h = 2Tf_d \tag{2.49}$$

S is the signal power; $w(t)$ is the white gaussian noise term with single-sided spectral density N_0 ; f_d is the modulation deviation and h is the modulation index.

The bandpass limiter output is represented by $Z(t)$.

$$Z(t) = \frac{\sqrt{2S}\cdot\cos(\omega_o t+\theta(t))+w(t)}{\left|\sqrt{2S}\cdot\cos(\omega_o t+\theta(t))+w(t)\right|} = I(t)+jQ(t) \tag{2.50}$$

And the output of the discriminator is represented by $\Psi(t)$.

$$\Psi(t) = \frac{I(t)Q'(t)-I'(t)Q(t)}{I^2(t)+Q^2(t)} \tag{2.51}$$

Based on (2.50) and (2.51) Pawula derives the probability of bit error for binary CPFSK using a limiter discriminator demodulator with integrate and dump post detection filtering [Pawula81]. The equations (2.52) to (2.72) briefly outline Pawula's derivation.

The total probability of error is the summation, equation (2.52), of a continuous component $P_{continous}$, equation (2.60), and an FM click component P_{click}, equation (2.53).

$$P_e = P_{click}+P_{continous} \tag{2.52}$$

$$P_{click} = \frac{h}{4}\cdot e^{-R_d} + \int_0^{\pi}\left(\frac{d}{dx}\left\{\operatorname{atan}\left(\frac{-m\cdot\cos(x)}{1-n\cdot\cos(2x+\delta)}\right)\right\}\right. \tag{2.53}$$
$$\left.\cdot\exp\left(-R_a\frac{[1-n\cdot\cos(2x+\delta)]^2+m^2\cdot[\cos(x)]^2}{[1-n\cdot\cos\delta]^2+m^2}\right)\right)\frac{dx}{4\pi}$$

Parameter δ, given in equation (2.54), represents the effects of non-linear phase of the IF filter $H(f)$ and with T in (2.55) being the bit period.

$$\delta = \angle H(2f_1) - 2\angle H(f_1) \tag{2.54}$$

$$f_1 = \frac{1}{2T} \tag{2.55}$$

The parameters m and n defined in equations (2.56) and (2.57) respectively, relate the effects of the modulation index h and filter characteristic for both the continuous and click error.

$$m = \frac{2h^2 \cdot |H(f_1)|}{1-h^2} \cdot \cos\left(\frac{\pi \cdot h}{2}\right) \tag{2.56}$$

$$n = \frac{2h^2 \cdot |H(f_1)|}{4-h^2} \tag{2.57}$$

Parameters R_a and R_d defined by equations (2.58) and (2.59) respectively, also relate the effects of the modulation index and filter characteristic but include the ratio of bit energy to noise spectral density.

$$R_a = \frac{E_b}{N_o}\left\{\frac{\sin(\pi h/2)}{\pi h/2}\right\}^2 \cdot \frac{(1-n\cos\delta)^2 + m^2}{T\int |H(f)|^2 df} \tag{2.58}$$

$$R_d = \frac{E_b}{N_o} \cdot \frac{|H(f_d)|^2}{T\int |H(f)|^2 df} \tag{2.59}$$

The $P_{continous}$ error component is derived by the average error rate for three representative bit patterns 111, 010 and 011 and is given in equation (2.60).

$$P_{continous} = \frac{1}{4}[P\{\psi > \Delta\phi | 111\} + P\{\psi > \Delta\phi | 010\} + 2P\{\psi > \Delta\phi | 011\}] \tag{2.60}$$

The continuous probability of error for each of the three bit patterns by the selection of $\Delta\phi$, U and V are given in equations (2.61) and (2.62).

$$P\{\psi > \psi_o\} = \int_{\psi_o}^{\pi} p(\psi) d\psi \tag{2.61}$$

$$p(\psi) = \frac{e^{-U}}{4\pi}\int_0^{\pi} \{\sin\alpha \cdot [1 + U + V \cdot \cos\alpha + W \cdot \sin\alpha \cdot \cos\psi] \cdot \exp[V \cdot \cos\alpha + W \cdot \sin\alpha \cdot \cos\psi]\} \cdot d\alpha \tag{2.62}$$

$$W^2 = U^2 + V^2 \tag{2.63}$$

The parameters for the bit pattern 111 are specified in equations (2.64), (2.65) and (2.66).

$$\Delta\phi|111 = \pi h \tag{2.64}$$

$$U|111 = R_d \tag{2.65}$$

$$V|111 = 0 \tag{2.66}$$

The parameters for the bit pattern 010 are specified in equations (2.67), (2.68) and (2.69).

$$\Delta\phi|010 = 2\,\text{atan}\frac{m}{1 - n \cdot \cos\delta} \tag{2.67}$$

$$U|010 = R_a \tag{2.68}$$

$$V|010 = 0 \tag{2.69}$$

The parameters for the bit pattern 011 are specified in equations (2.70), (2.71) and (2.72).

$$\Delta\phi|011 = \frac{\pi h}{2} + \text{atan}\frac{m}{1 - n \cdot \cos\delta} \tag{2.70}$$

$$U|011 = \frac{R_a + R_d}{2} \tag{2.71}$$

$$V|011 = \frac{R_a - R_d}{2} \tag{2.72}$$

Figure 2.18 graphs the performance of the bandpass limiter discriminator detector with the simulation IF filter in AWGN for both theory and the simulation. A small (< 0.5 dB) discrepancy can be noted between theory and the simulation results. This can be attributed to the ISI due to the IF filter model. Pawula's results are derived under the assumption that ISI only occurs due to adjacent bits. The filter used in the simulation, while having a BT within Pawula's limits, has an extremely steep roll-off which causes non-negligible amounts of ISI due to bits more than 1 bit period away.

Figure 2.19 graphs the performance of the bandpass limiter discriminator for both MSK and GMSK $BT = 0.5$ in AWGN. It can be noted that using GMSK over MSK causes a 2 dB degradation in required signal levels at 0.001 BER with the limiter discriminator detector.

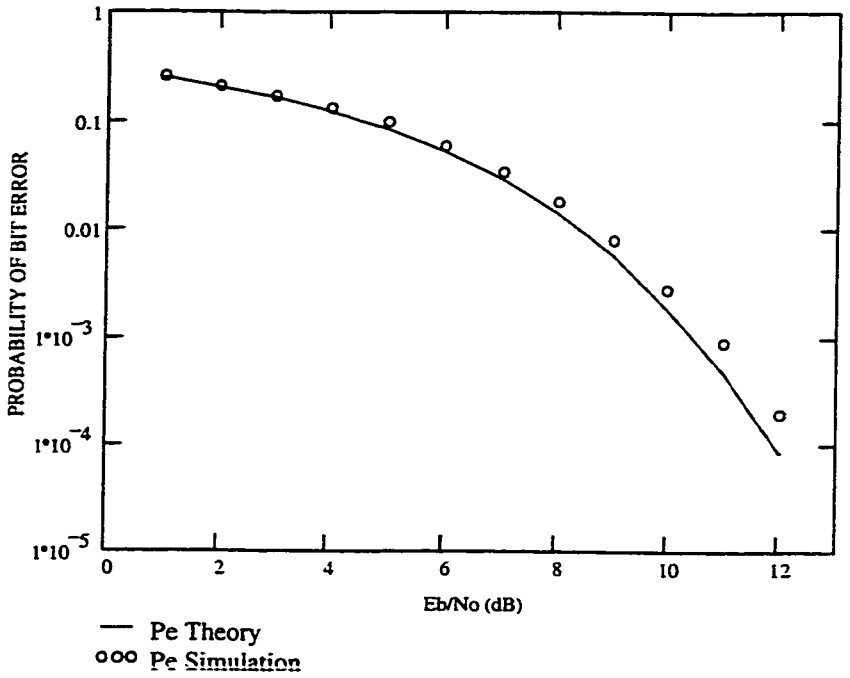

Figure 2.18 Performance of MSK with Limiter Discriminator Detection in AWGN

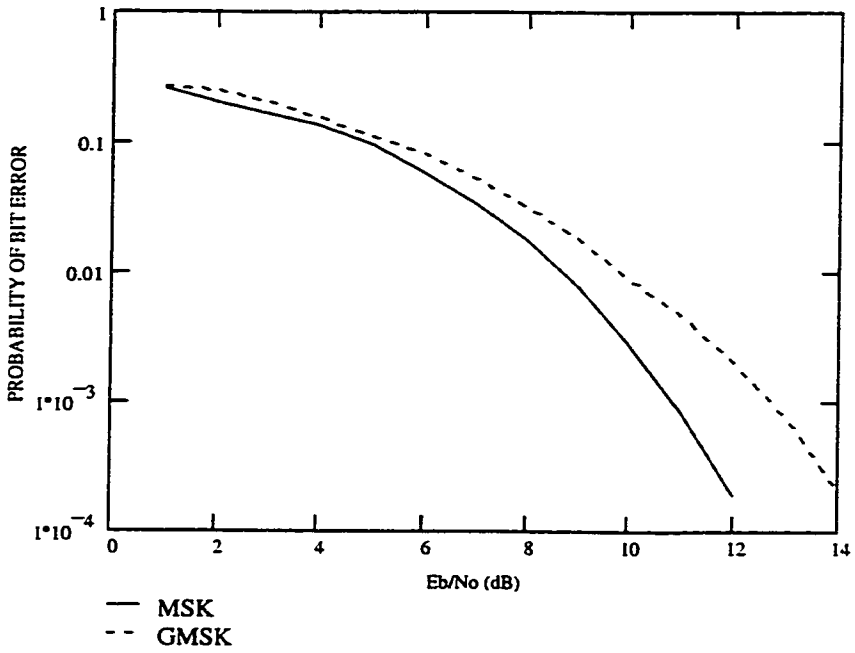

Figure 2.19 Simulation of BER for MSK and GMSK $BT = 0.5$ with Limiter Discriminator Detection in AWGN

The performance of the bandpass limiter discriminator with GMSK modulation $BT = 0.5$ in AWGN is shown in the following figures for various types of interference. This is an illustration of the rejection capability of the receiver to the different types of interference that are used in the simulation. Figure 2.20 shows the probability of bit error with co-channel interference. Figure 2.21 shows the probability of bit error with adjacent channel interference. Figure 2.22 and Figure 2.23 show the probability of bit error with alternate and 2nd alternate channel interference respectively.

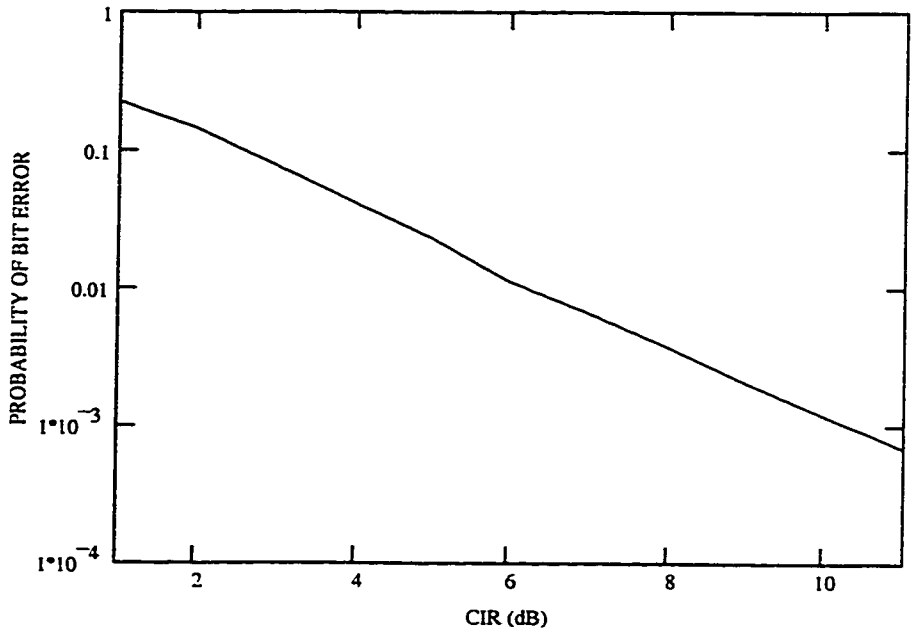

Figure 2.20 Simulation of BER for GMSK $BT = 0.5$ with Limiter Discriminator Detection and Co-channel Interference $\frac{Eb}{No}$ = 16 dB

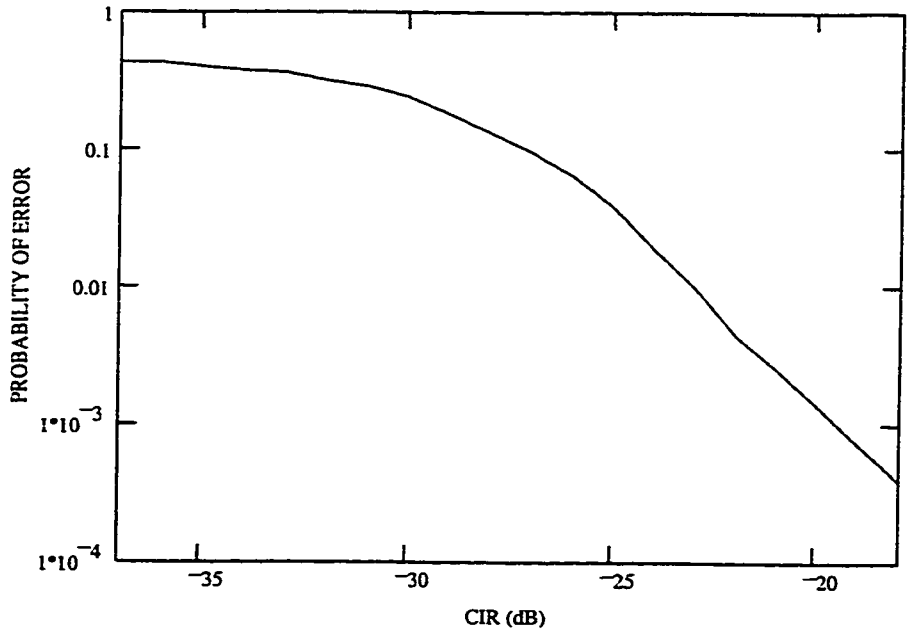

Figure 2.21 Simulation of BER for GMSK $BT = 0.5$ with Limiter Discriminator Detection and Adjacent Channel Interference $\frac{Eb}{No}$ = 16 dB

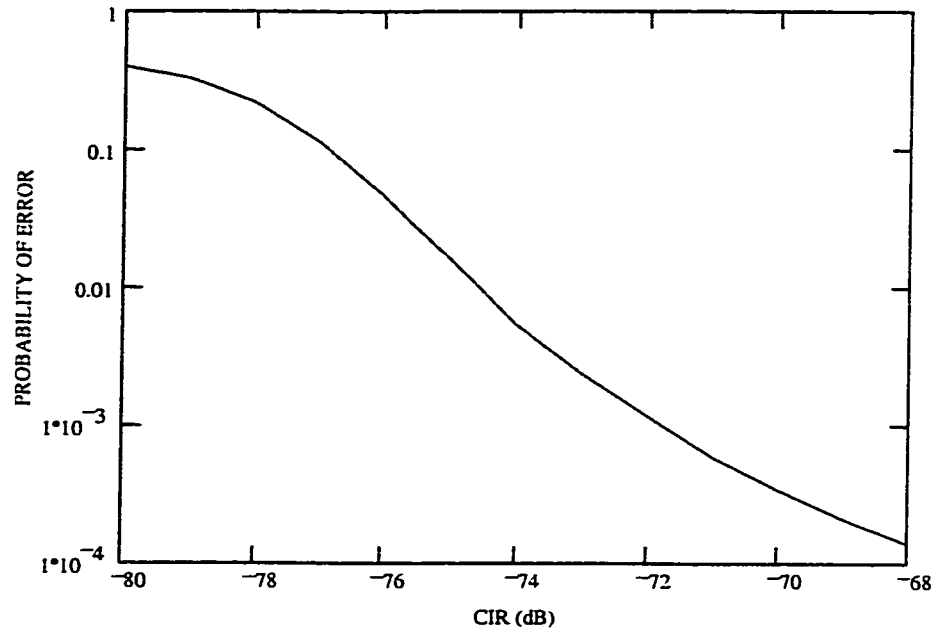

Figure 2.22 Simulation of BER for GMSK $BT = 0.5$ with Limiter Discriminator Detection and Alternate Channel Interference $\frac{Eb}{No}$ = 16 dB

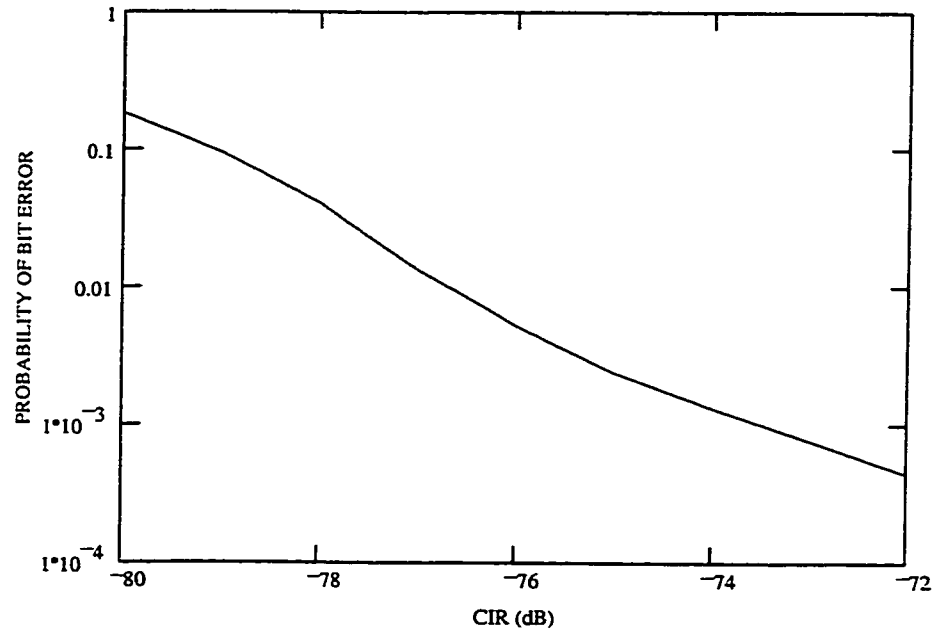

Figure 2.23 Simulation of BER for GMSK $BT = 0.5$ with Limiter Discriminator Detection and 2nd Alternate Channel Interference $\frac{Eb}{No}$ = 16 dB

To derive the theoretical performance of the bandpass limiter discriminator in Rayleigh fading, equations (2.73) and (2.74) are combined with Pawula's work. The result is not included here since it is a minor modification to the mathematical software used to calculate the bit error rate curve.

$$P_{eRayleigh} = \int_0^\infty P\left(\frac{E_b}{N_o}\right) \cdot p\left(\frac{E_b}{N_o}\right) d\frac{E_b}{N_o} \tag{2.73}$$

$$p\left(\frac{E_b}{N_o}\right) = \frac{1}{\overline{\frac{E_b}{N_o}}} \cdot \exp\left(\frac{E_b}{N_o} \Big/ \overline{\frac{E_b}{N_o}}\right) \tag{2.74}$$

with P_e being equation (2.52)

$$P\left(\frac{E_b}{N_o}\right) = P_e \tag{2.75}$$

Figure 2.24 graphs the performance of the bandpass limiter discriminator theory versus simulation in a Rayleigh fading channel. Figure 2.25 compares the limiter discriminator detection of MSK and GMSK $BT = 0.5$ in Rayleigh fading. Figure 2.26 shows the performance of the limiter discriminator with GMSK $BT = 0.5$ in the presence of co-channel interference and Rayleigh fading.

Figure 2.24 illustrates the relatively close correspondence between theory and the simulation results.

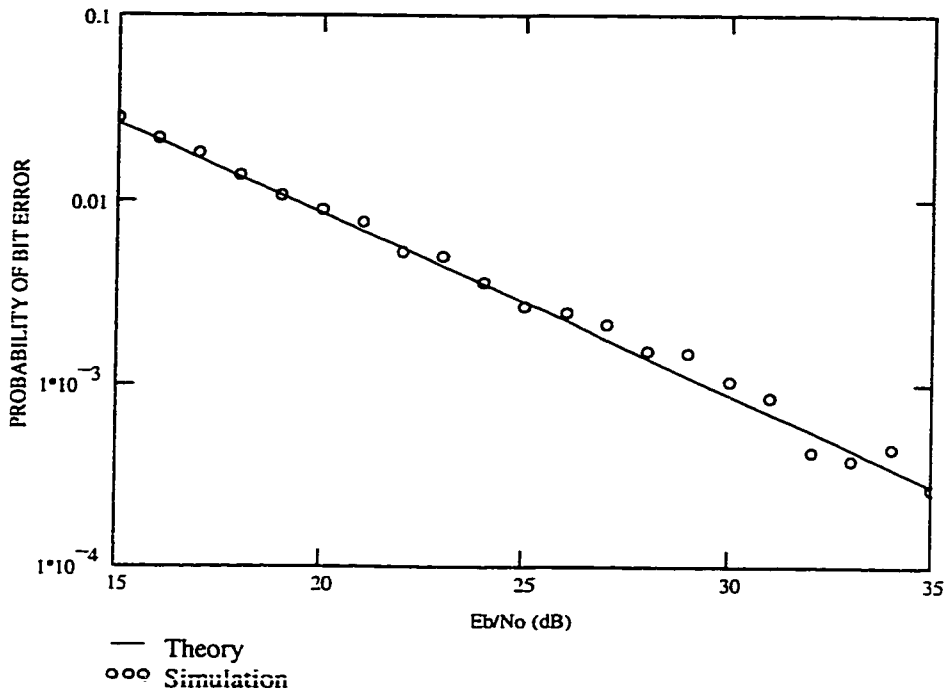

Figure 2.24 Performance of MSK with Limiter Discriminator Detection in Rayleigh Fading

From Figure 2.25 the difference between MSK and GMSK $BT = 0.5$ in Rayleigh fading is less than 1dB. This is a small reduction from the 2 dB difference in a non-fading AWGN channel. For GMSK $BT = 0.5$ the required $\frac{Eb}{No}$ to achieve a BER of 10^{-3} is approximately 30 dB.

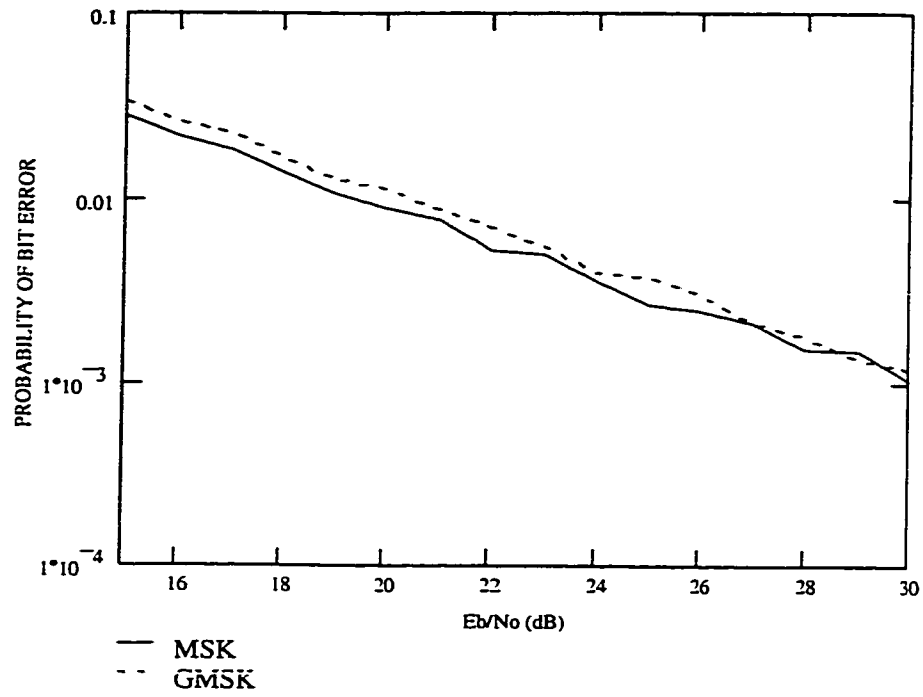

Figure 2.25 Simulation Comparison of MSK and GMSK $BT = 0.5$ with Limiter Discriminator Detection in Rayleigh Fading

From Figure 2.26 the required carrier to interference ratio (CIR) to achieve a BER of 10^{-3} in Rayleigh fading is approximately 30 dB.

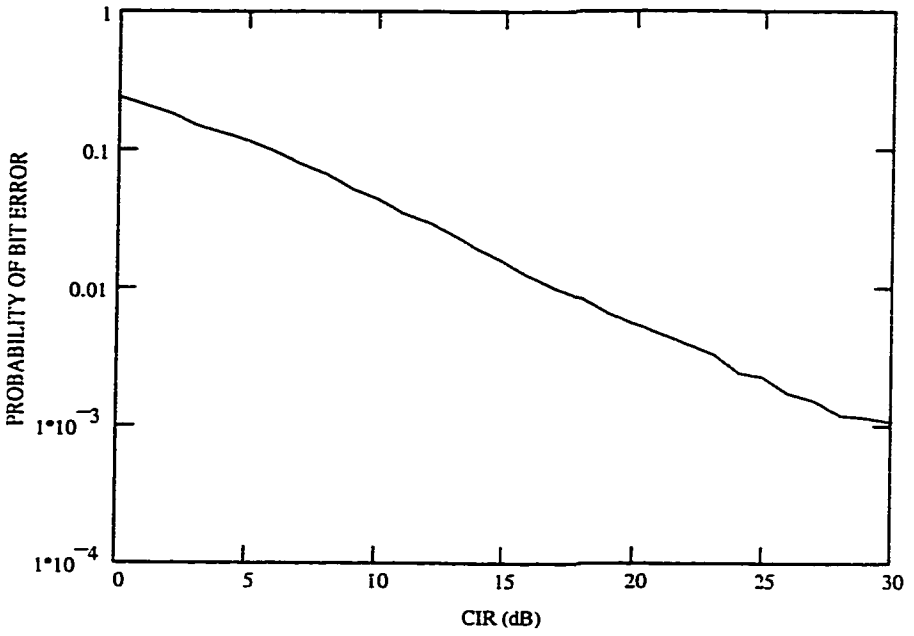

Figure 2.26 Performance of GMSK $BT = 0.5$ with Limiter Discriminator Detection in Rayleigh Fading with Co-channel Interference $\frac{Eb}{No}$ = 33 dB

2.4.5 FH-CDMA INTERFERENCE MODELS

Three types of hopping patterns are investigated to determine the effects of specific characteristics of code division multiple access codes on the performance of the network. The characteristics of the codes were uniformly distributed memoryless hopping (UMC), orthogonal uniformly distributed memoryless hopping (O-UMC) and orthogonal uniformly distributed memoryless hopping without adjacent channel interference (O-UMC without ACI). These specific attributes decrease the amount of network self interference but increase the complexity of designing the codes.

Five main interference types exist that are related to the characteristics of the hopping patterns. The types are listed in decreasing order of effect on the performance of the net-

work. The first type and the most damaging is the case of a direct hit or also termed co-channel interference. This occurs when 2 or more pairs occupy the same channel at the same time. Obviously, the interference is at the highest possible level while the receiver's interference immunity is at the lowest. The second type is termed adjacent channel interference. This type of interference occurs when one or more pairs occupy the channel directly above or below the current channel of the pair being analyzed. The adjacent channel rejection of the receiver is greater than that of co-channel rejection, however, it is usually far below the rejection of signals that are 2 or more channels away.

The third and fourth types of interference are due to the non-linear nature of the receiver. As discussed in Section "Weakly Non-Linear Model" on page 34, the reception of 2 or more separate frequency components into a receiver give rise to intermodulation components that are not present in the original signal. Obviously, these components may or may not exist on a particular channel that will cause degradation in network performance. As such a probability model or occupied channel tracking is required to determine if an intermodulation product occupies the desired channel. The third type is based on the triple beat products and the fourth type is based on the double beat.

The fifth type is due to the rejection of the receiver to signals that are 2 or more channels away from the desired channel. There exist several other interference cases, however after careful study it is obvious these particular cases dominate the BER performance of the network.

Uniformly Distributed Memoryless Hopping Codes

Identical, independent uniformly distributed (i.i.d.) memoryless hopping codes (UMC) are used extensively as models for actual hopping patterns in the analysis of FH-CDMA [Kim94_2]. Each pair uses a frequency hopping pattern that randomly hops among q frequency slots with probability 1/q of occupying a given slot independent of previous hop frequencies.

The probability of a direct hit is listed in (2.76) taken from reference [Kim94_2].

$$P_{DIRECT} = \sum_{m=1}^{K-1} \binom{K-1}{m} P_h^{\,m} \cdot (1-P_h)^{K-1-m} \tag{2.76}$$

Where the probability of a pair occupying any particular channel is given by equation (2.77).

$$P_h = \frac{1}{q} \tag{2.77}$$

Where q is the number of channels; $\binom{K-1}{m}$ is the Binomial coefficient; K is the number of operational pairs.

Figure 2.27 shows the probability of a direct hit for various numbers of operational pairs, both theory and simulation are shown. Once the sampling error is averaged out of the simulation results the correspondence to theory is exact.

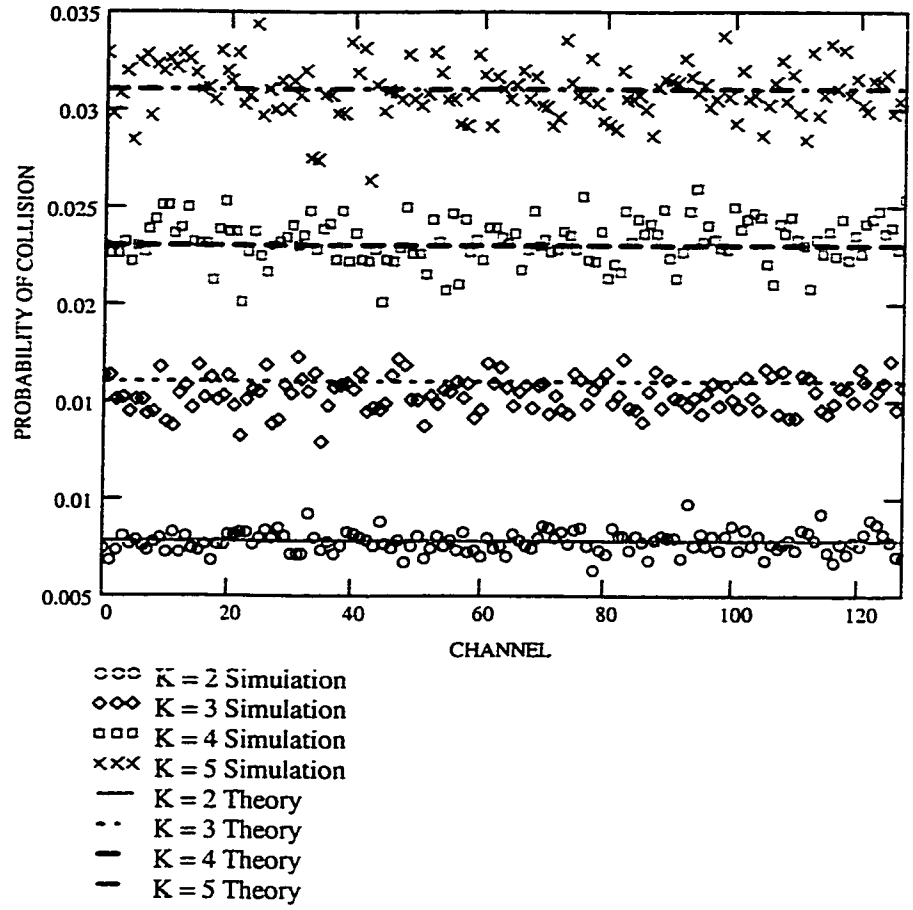

Figure 2.27 Probability of a Direct Hit $K = 2,3,4,5$ q=128

The probability of an adjacent hit in equation (2.78) can be easily derived by extending equation (2.76).

$$P_{ADJACENT} = \sum_{m=1}^{K-1} \binom{K-1}{m} P_{ADJ}^{\ m} \cdot (1 - P_{ADJ})^{K-1-m} \tag{2.78}$$

Where the probability of another pair occupying either adjacent channels in the interior channels being listed in (2.79).

$$P_{ADJ}(Q \neq 0, q-1) = \frac{2}{q} \tag{2.79}$$

The probability of another pair occupying the adjacent channel for the end channels being (2.80), Q is the current channel ($0 \leq Q \leq q$-1).

$$P_{ADJ}(Q = 0, q-1) = \frac{1}{q} \tag{2.80}$$

Figure 2.28 illustrates the probability of an adjacent channel hit for various number of users for both theory and simulation. Again, once the sampling error is averaged out for the simulation results the correspondence with theory is exact.

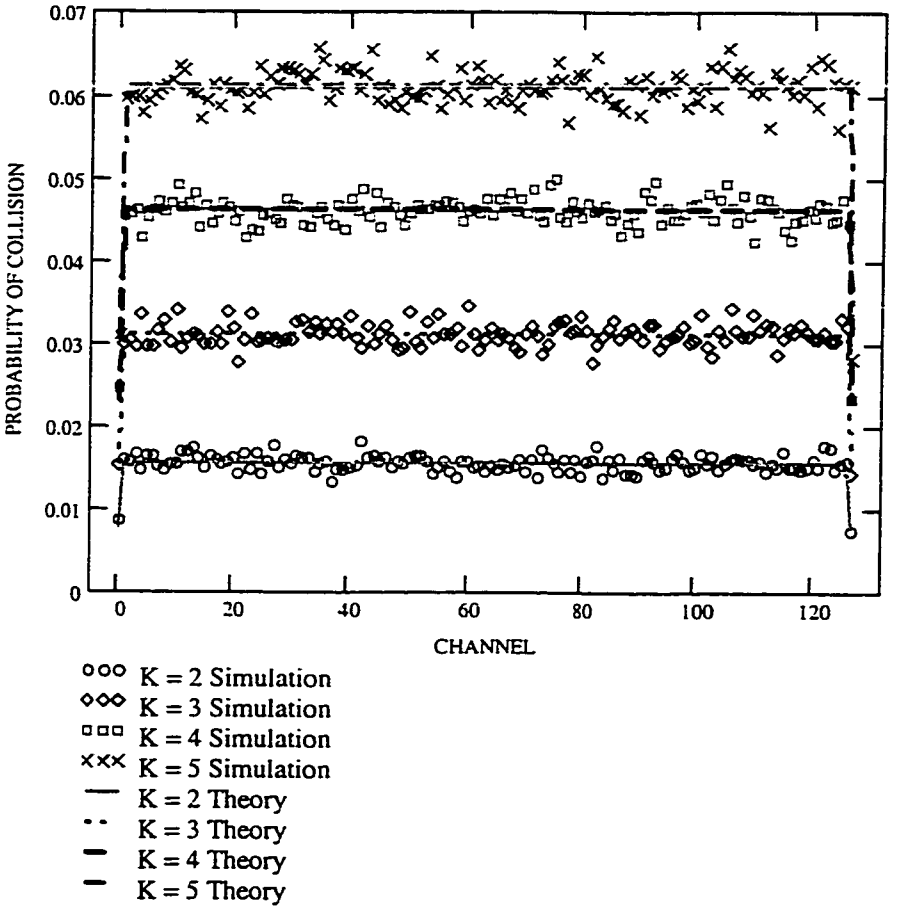

Figure 2.28 Probability of an Adjacent Hit K = 2,3,4,5 q=128

The double beat intermodulation probability of a hit on the desired channel has been derived and is listed in equation (2.81) for the case of an even number of channels and K=3.

$$P_{IMOD_D}(K=3) = \frac{2}{q^2} \cdot \left\{ \frac{q}{2} - 1 \right\} \tag{2.81}$$

This result has been derived to be independent of the occupied channel, note that this can only be done for the cases where there are an even number of channels. This is because a relationship independent of the occupied channel can not be found for the odd number of channels case as the number of potential slot combinations creating a product on the occupied channel varies with the channel under consideration.

Unfortunately, a convenient expression for the exact probability of a double beat intermodulation hit for $K > 3$ is not easily found for either the odd or even number of channels cases. This is due to the probabilities of 2 or more simultaneous intermodulation hits being a function of two conditions. Firstly, for 2 or more hits, each hit is no longer independent of the other hits, i.e., each pair of channels that create an intermodulation hit at the current channel have varying probabilities that one of the members of the pair can create another double beat intermodulation product also at the current channel with another carrier. Secondly, the probability of 2 or more double beat intermodulation hits becomes a function of the current channel.

Figure 2.29 shows the probability of a double beat intermodulation hit for various numbers of users.

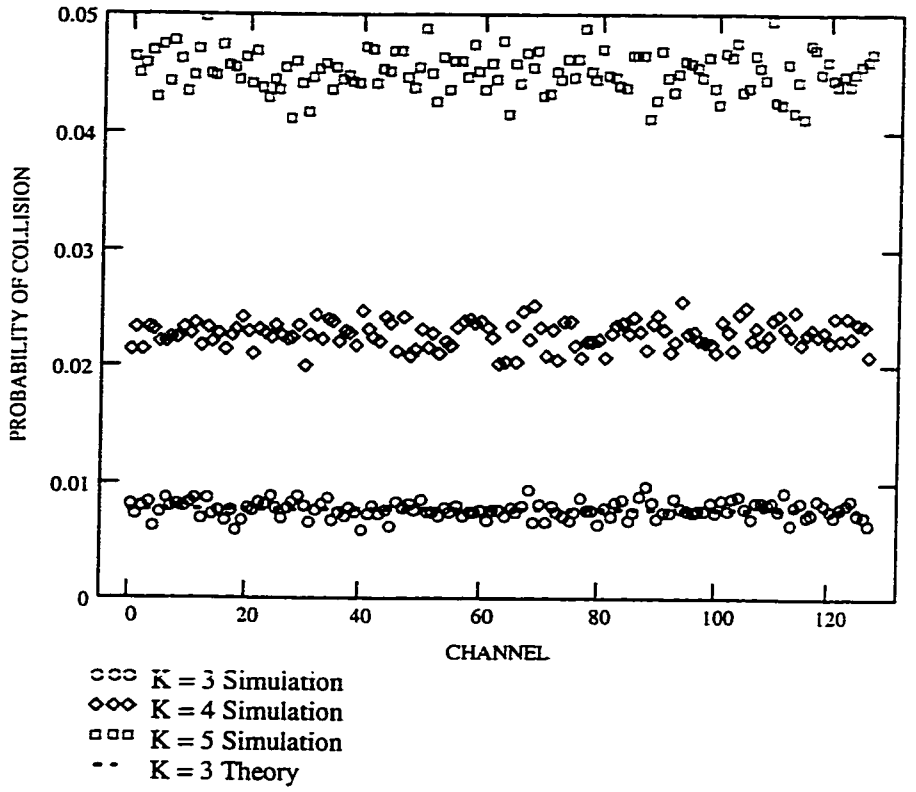

Figure 2.29 Probability of Double Beat Intermodulation Product Hits $K = 3,4,5$ q=128

The triple beat intermodulation product hit probability cannot be summarized into a convenient closed form for variable numbers of channels q, independent of which channel is being considered even for $K = 4$. This is due to the number of channel combinations which create a triple beat intermodulation product at a given channel also being a function of the channel under consideration.

The variation of possible hit combinations as a function of the current channel is shown in Figure 2.30 for $q = 128$. Of interest is parabolic shape to the number of combinations and that the number of possible triple beat intermodulation products is approximately 50% higher at the centre channel ($Q = 64$) than the two outer channels.

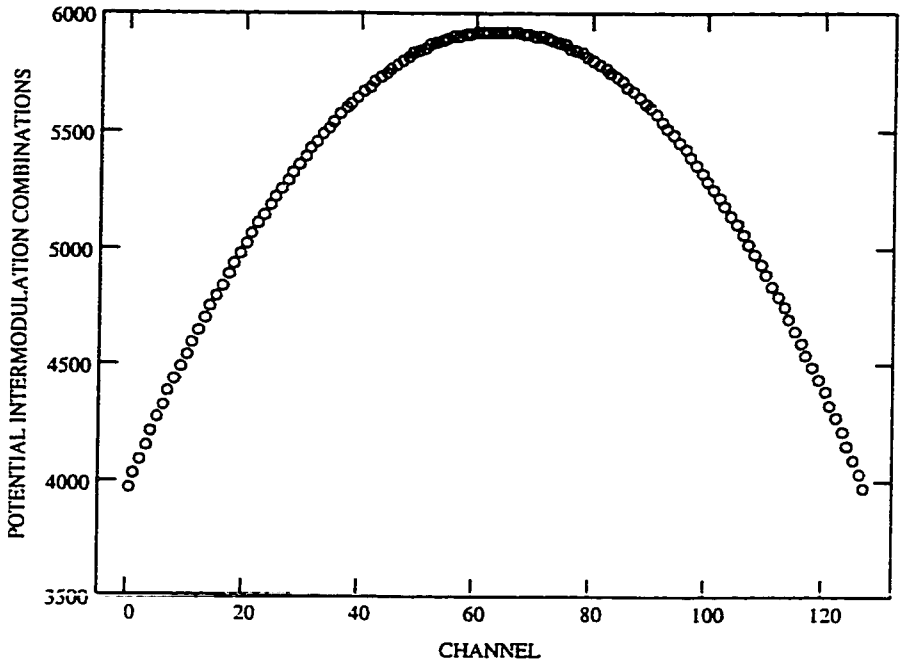

Figure 2.30 Number of Channel Combinations that can Create Triple Beat Intermodulation Products at a Given Channel

Figure 2.31 plots the probabilities of a triple beat intermodulation product hit for various numbers of users.

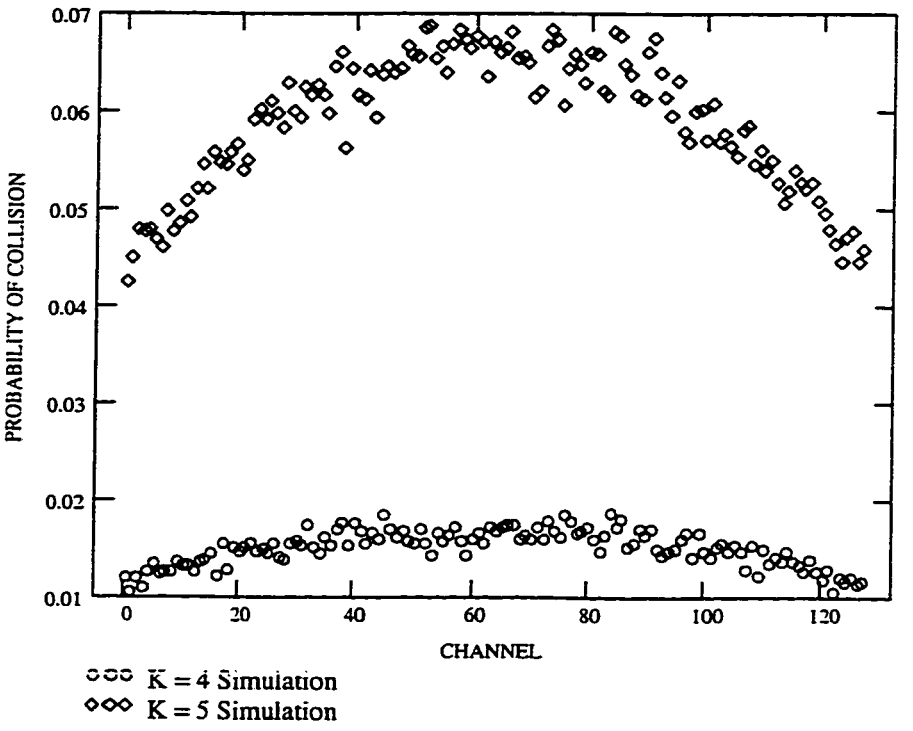

Figure 2.31 Probability of Triple Beat Intermodulation Product Hits $K = 4,5$ q=128

Orthogonal Uniformly Distributed Memoryless Hopping Codes

The prime characteristic of orthogonal uniformly distributed memoryless hopping codes (O-UMC) is the criteria that any two users cannot occupy the same slot at the same time. This removes what is termed a direct hit from being a possible source of error, consequently P_{DIRECT} is identically zero for all operational pairs.

$$P_{DIRECT} = 0 \tag{2.82}$$

Equation (2.83) is the probability of an adjacent channel hit for the interior channels. Equation (2.84) is the probability of an adjacent channel hit for the two outside channels, channels $Q = 0$ or $Q = 127$ when $q = 128$.

$$P_{ADJACENT}(Q \neq 0, q-1) = 2P_{SINGLE} + P_{DOUBLE} \tag{2.83}$$

$$P_{ADJACENT}(Q = 0, q-1) = P_{SINGLE} \tag{2.84}$$

P_{SINGLE} and P_{DOUBLE} are defined in equations (2.85) and (2.86) respectively. P_{SINGLE} is the probability of only one of the two adjacent channels being occupied by another operational pair. P_{DOUBLE} is the probability of both adjacent channels being occupied.

$$P_{SINGLE} = \sum_{m=1}^{K-1} \left[\frac{1}{q-m} \cdot \frac{\prod_{n=1}^{K-1} \left[\left(1-\frac{2}{q-n}\right) \cdot \left(1-\frac{1}{q-n}\right) \right]}{\left\{ \prod_{p=m}^{K-1} \left(1-\frac{2}{q-p}\right) \right\} \cdot \left\{ \prod_{r=1}^{m} \left(1-\frac{1}{q-r}\right) \right\}} \right] \tag{2.85}$$

$$P_{DOUBLE} = \sum_{m=1}^{K-2} \left[\frac{2}{q-m} \cdot \frac{\prod_{n=1}^{K-2} \left(1-\frac{2}{q-n}\right)}{\prod_{p=m}^{K-2} \left(1-\frac{2}{q-p}\right)} \cdot \sum_{r=m+1}^{K-1} \left\{ \frac{1}{q-r} \cdot \frac{\prod_{s=m+1}^{K-1} \left(1-\frac{1}{q-s}\right)}{\prod_{t=r}^{K-1} \left(1-\frac{1}{q-t}\right)} \right\} \right] \tag{2.86}$$

Figure 2.32 illustrates the probability of an adjacent channel hit for various numbers of users. In comparing Figure 2.28 and Figure 2.32, the probability of an adjacent channel hit is slightly greater for Orthogonal UMC than for UMC. This is due to the reduction in the possible channel options for each operating pair since only a single pair can occupy any

one channel. The difference in probability between the two code types increases with increasing K.

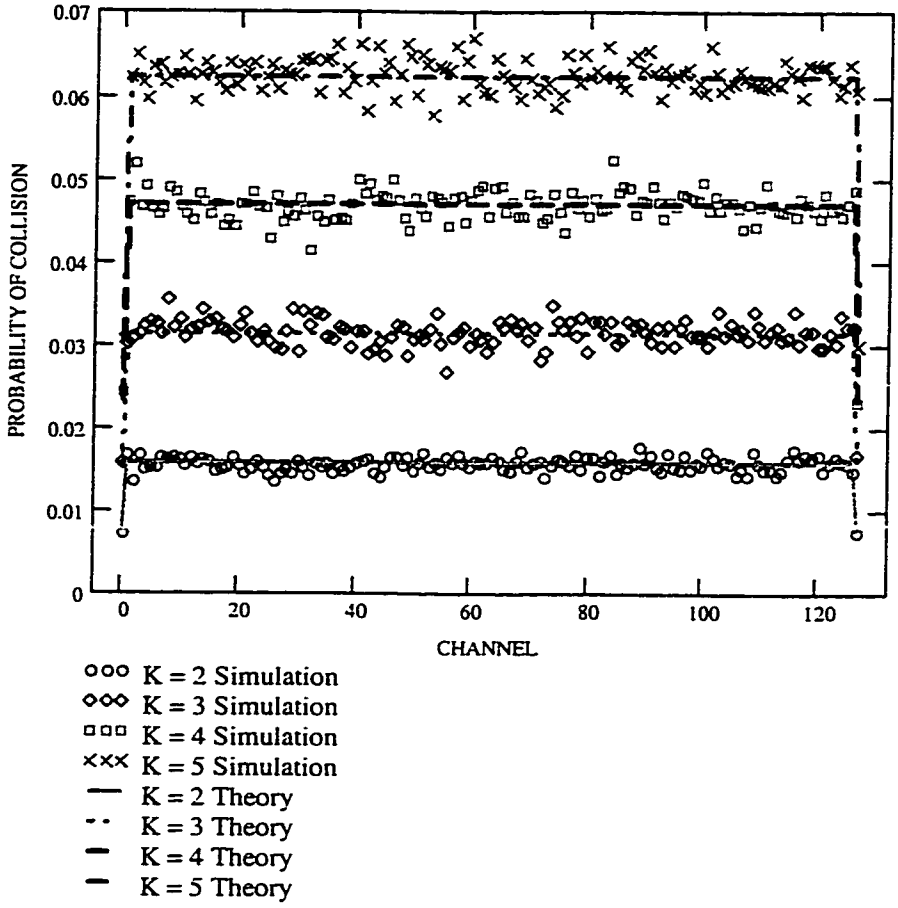

Figure 2.32 Probability of Adjacent Channel Hits $K = 2,3,4,5$ q=128 $P_{DIRECT} = 0$

Figure 2.33 illustrates the simulation results for the probability of a double beat intermodulation hit for various numbers of users. A closed form expression is not readily found for the probability of a double beat intermodulation hit. It can be noted that the probability of a double beat intermodulation hit for Orthogonal UMC is more likely than for UMC. For small K the difference is not large which can be seen by comparing Figure 2.29 and

Figure 2.33. However, the difference in probability between the two codes increases with increasing K.

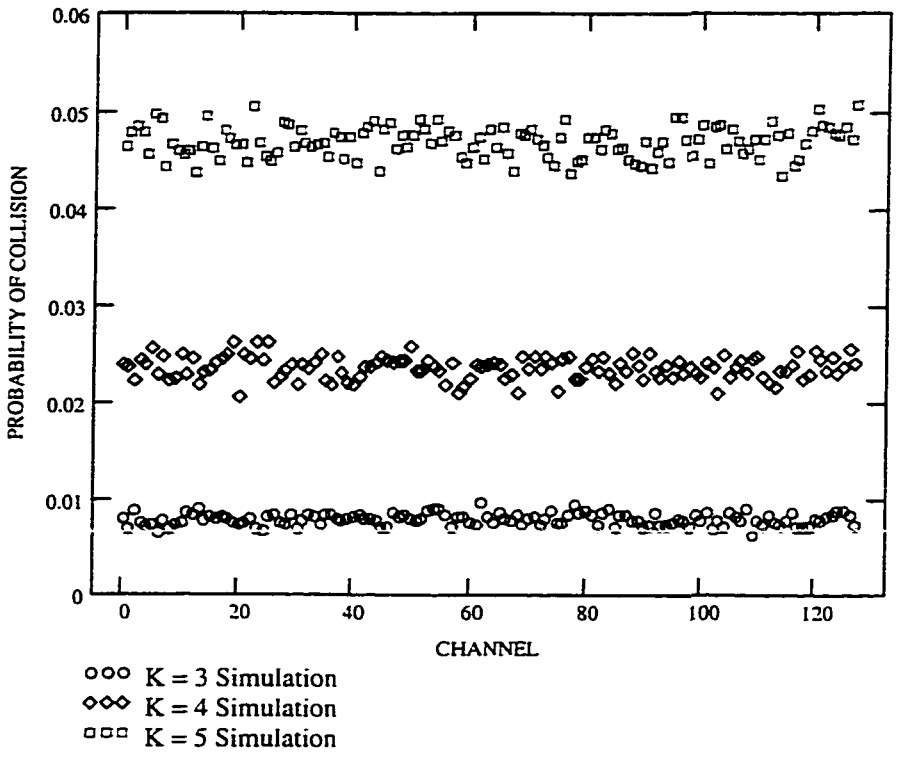

Figure 2.33 Probability of Double Beat Intermodulation Product Hits $K = 3,4,5$ $q=128$ $P_{DIRECT} = 0$

Figure 2.34 illustrates the simulation results for the probability of triple beat intermodulation hits. As in the case of the double beat intermodulation products, a closed form expression is not readily found for the probability of an intermodulation hit. As well, hits for Orthogonal UMC are more probable than for UMC and the difference increases with increasing K.

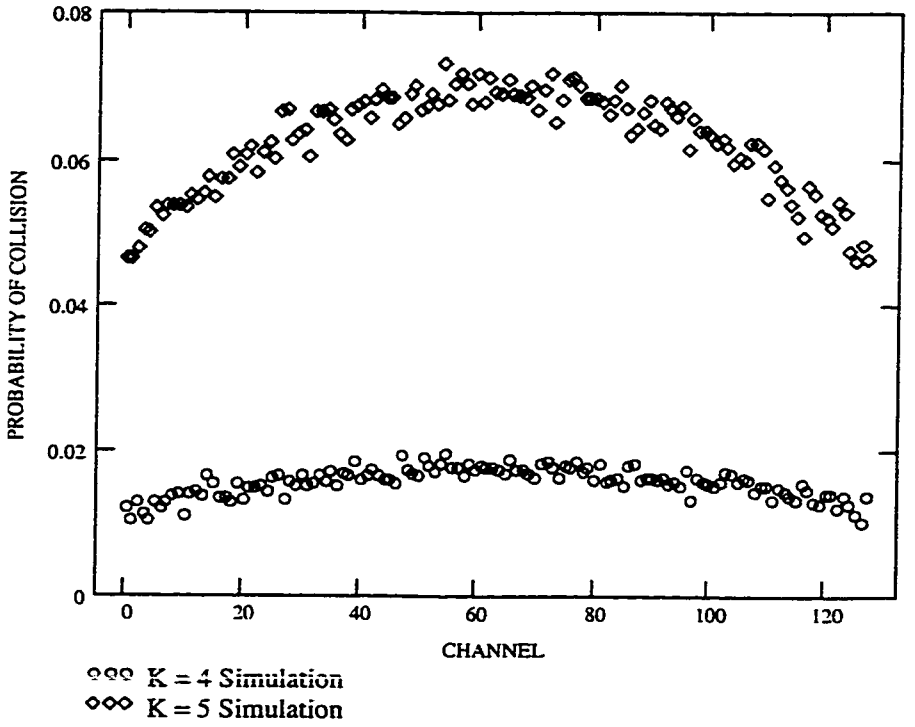

Figure 2.34 Probability of Triple Beat Intermodulation Product Hits $K = 4, 5$ $q = 128$ $P_{DIRECT} = 0$

Orthogonal Uniformly Distributed Memoryless Hopping Codes Without Adjacent Channel Interference

Orthogonal Uniformly Distributed Memoryless Hopping Codes Without Adjacent Channel Interference (O-UMC without ACI) removes the first and second strongest sources of network self interference, a direct hit and adjacent channel hit respectively. Therefore P_{DIRECT} and $P_{ADJACENT}$ are identically zero for each operational pair.

$$P_{DIRECT} = 0 \tag{2.87}$$

$$P_{ADJACENT} = 0 \tag{2.88}$$

With these codes, an operational pair effectively occupies 2 or 3 channels per hop which are then un-available for use by other communicating pairs in the network. The probabilities of double and triple intermodulation product hits do not have an intuitive closed form expression so the probabilities from simulation for various conditions are shown in Figure 2.35 and Figure 2.36.

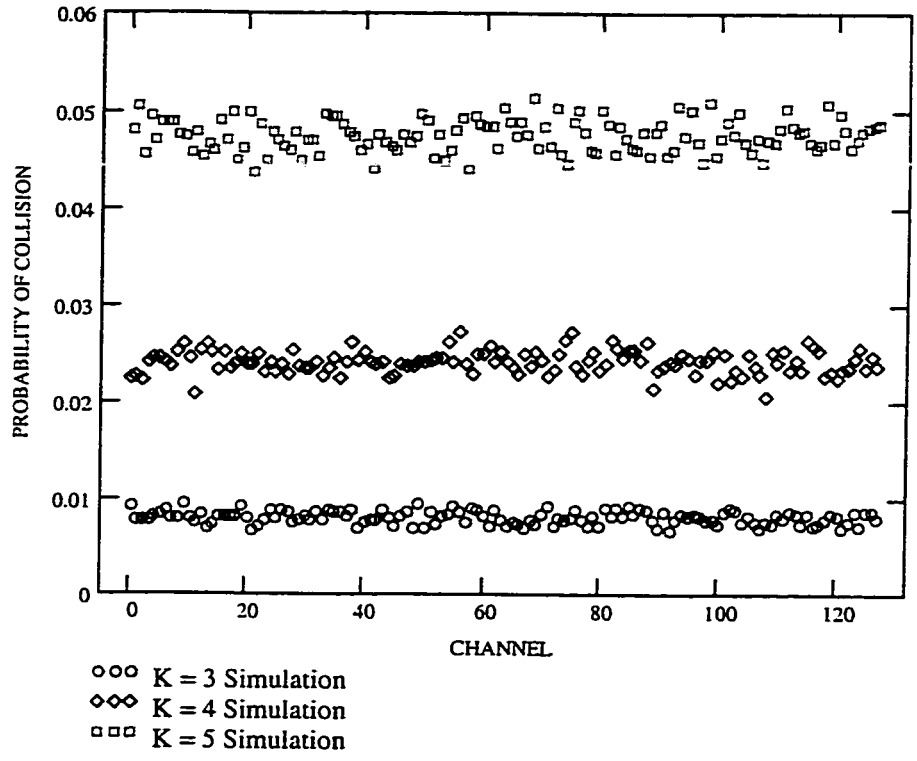

Figure 2.35 Probability of Double Beat Intermodulation Product Hits $K = 3,4,5$ q=128 $P_{DIRECT} = 0$, $P_{ADJACENT} = 0$

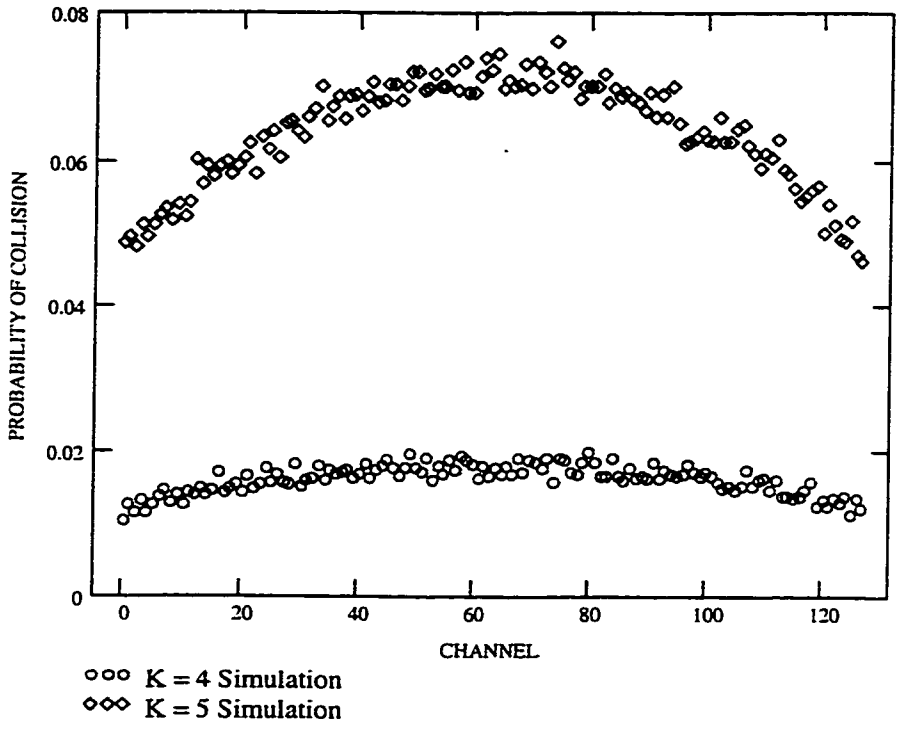

Figure 2.36 Probability of Triple Beat Intermodulation Product Hits $K = 4, 5$ $q = 128$ $P_{DIRECT} = 0$, $P_{ADJACENT} = 0$

It can be noted that the probabilities of double and triple beat intermodulation product hits for Orthogonal UMC without ACI are slightly higher than Orthogonal UMC or UMC. This would be due to the more uniform distribution of occupied channels with increasing code complexity. In the case of UMC, the occupied channels can be bunched together which does not create as large a number of diverse intermodulation products. As the code complexity increases removing co-channel and then adjacent channel interference, the occupied channels are forced to become more uniformly spread across all channels. Therefore, at any one time, the occupied channels can no longer group together to the same level as before. A uniform distribution leads to more unique intermodulation prod-

ucts being created and hence a larger probability that any one channel would have a product occupy it.

Chapter 3

SIMULATION RESULTS

3.1 INTRODUCTION

In the analysis results that follow, each of the code types are evaluated using three power control strategies, various spatial models and input intercept points. The desired performance goal is to exceed a 10^{-3} BER over the same operational range as a single pair operating in an environment where the performance is unimpaired by any possible interference (effectively an interference free environment relative to the pair being analyzed). Graphically, this is illustrated in Figure 3.1 as the optimal performance objective to evaluate the subsequent results against.

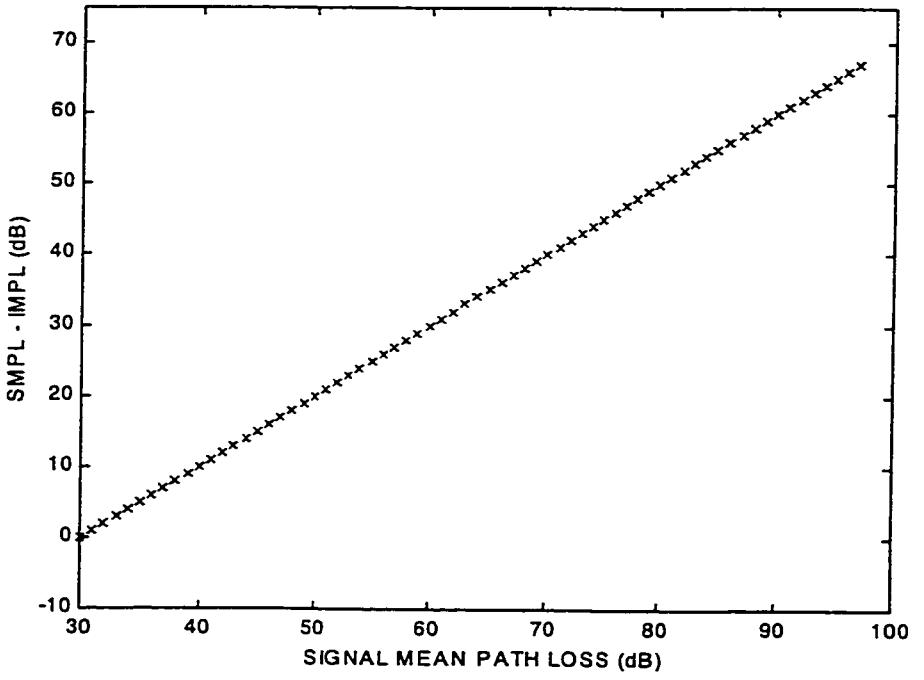

Figure 3.1 Optimal Performance Plot

In Figure 3.1, and the subsequent plots, the x axis is the signal mean path loss (SMPL) which is the path loss between the ($\mathbf{F_0}$, $\mathbf{R_0}$) pair. SMPL is analyzed from 30 dB to 97 dB, which brackets the separation between a ($\mathbf{F_0}$, $\mathbf{R_0}$) pair from approximately 1 m to the maximum path loss that achieves a 10^{-3} BER in a Rayleigh fading environment.

The y axis is the difference between SMPL and IMPL (interference mean path loss) in dB. Therefore in the optimal performing network, shown in Figure 3.1, as SMPL increases so does SMPL minus IMPL. This can be physically explained as the interfering units $\mathbf{F_i}$ are fixed at the minimum separation r_{min} (30 dB IMPL) from $\mathbf{R_0}$ while $\mathbf{F_0}$ can be at any distance between r_{min} (30 dB SMPL) and r_{max} (97 dB SMPL). When the interfering units $\mathbf{F_i}$ and the desired transmitter $\mathbf{F_0}$ are at the minimum separation distance of r_{min} from the receiver $\mathbf{R_0}$ then the optimum SMPL minus IMPL value is 0 dB. When the interfering units are at r_{min} and desired transmitter is at r_{max} then SMPL minus IMPL is 67 dB.

SMPL and SMPL minus IMPL were chosen instead distance for the axes because of path loss model independence. A desire for this thesis was to achieve results that were effectively insensitive to the path loss model. This would provide generic results that could be easily applied to a wide variety of applications utilizing specific path loss models for the local environment. Unfortunately, as will be seen in the following results, there is a small but significant divergence in the results between the 2 and 6 path loss exponents with the SPC and FPC power control algorithms. Depending on the application, the differences may be ignored and an approximation using one of the two results provided can be used with the desired path loss model. However the results are not as generic and versatile as initially hoped and the application of these results to other path loss models should be done with care.

SMPL minus IMPL was chosen instead of IMPL as the y axis for visual clarity in determining which option performed better than another. Using SMPL minus IMPL ensures that a result with a larger y axis value outperforms a result with a lower y axis value.

For the analysis results that follow, a network consisting of 11 user pairs (10 interfering pairs for each operational pair) was simulated. The choice of 11 pairs was made to simulate a statistically significant number of units while ensuring that the simulation time did not become excessive. For completeness the main simulation parameters from chapter 2 are summarized in Table 3.1 .

SPECIFICATION	SETTING
Users	11
Data Rate	128 kbit/s
Hopping Channels	128
Channel Spacing	200 kHz
Hop Dwell Period	< 100 msec
Maximum Transmit Power	10 mWatt
Minimum Transmit Power	.01 mWatt
GMSK Modulation BT	0.5
Noise Figure	5 dB
Sensitivity (Eb/No)	13 dB
Co-channel Rejection (CIR)	10 dB
Adjacent Channel Rejection (CIR)	-20 dB
Alternate Channel Rejection (CIR)	-72 dB
2^{ND} Alternate Channel Rejection (CIR)	-74 dB

Table 3.1 Listing of Main Simulation Parameters

3.2 NETWORK PERFORMANCE WITH UNIFORMLY DISTRIBUTED MEMORYLESS FREQUENCY HOPPING CDMA CODES

This section contains the simulation results for Uniformly Distributed Memoryless Frequency Hopping Codes (UMC). Section 3.2.1 contains the results for the continuous maximum transmit power strategy, section 3.2.2 contains the results for the slow power control strategy and finally section 3.2.3 contains the results for the fast power control strategy.

UMC was evaluated with only the uniform spatial model and IIP_3 = -5 dBm for SPC and FPC. Since the UMC performance was significantly below the desired performance level for the simulations completed, the other cases were not undertaken due to the significant computing time required and the minimal importance of the results.

3.2.1 CONTINOUS MAXIMUM TRANSMIT POWER

Figure 3.2 contains the simulation results for IIP_3 = -5 dBm and IIP_3 = +5 dBm. As can be seen from the plot there is no significant difference in performance between the two IIP_3 values. Performance for UMC is dominated by direct hits hence the linearity of the receiver has no effect on increasing performance levels. For UMC with a continuous maximum transmit power (CMTP), the path loss exponent has no effect on the performance result thus making the CMTP results independent of the path loss model.

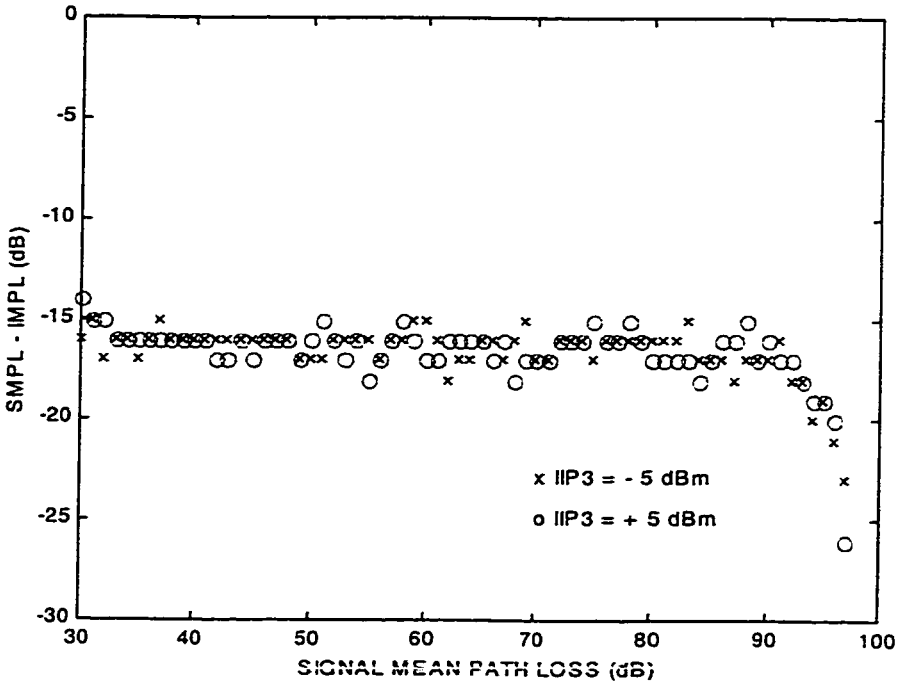

Figure 3.2 UMC with CMTP, IIP_3 = -5 and +5 dBm

3.2.2 SLOW POWER CONTROL

Figure 3.3 contains the results for the slow power control strategy (SPC). As can be seen from the results, the slow power control strategy performs significantly worse than the continuous maximum transmit power strategy for the full SMPL range. This is attributed to the simplicity of the power control algorithm implemented in that interference levels or BER performance is not evaluated. The algorithm only uses the mean path loss between the transmitter and receiver to determine the transmit power level. For SMPL greater than 64 dB, slow power control does begin to improve in performance. As SMPL increases the transmit power increases to compensate which suppresses interference.

Changing the path loss exponent effects the performance with n = 6 outperforming n = 2 slightly.

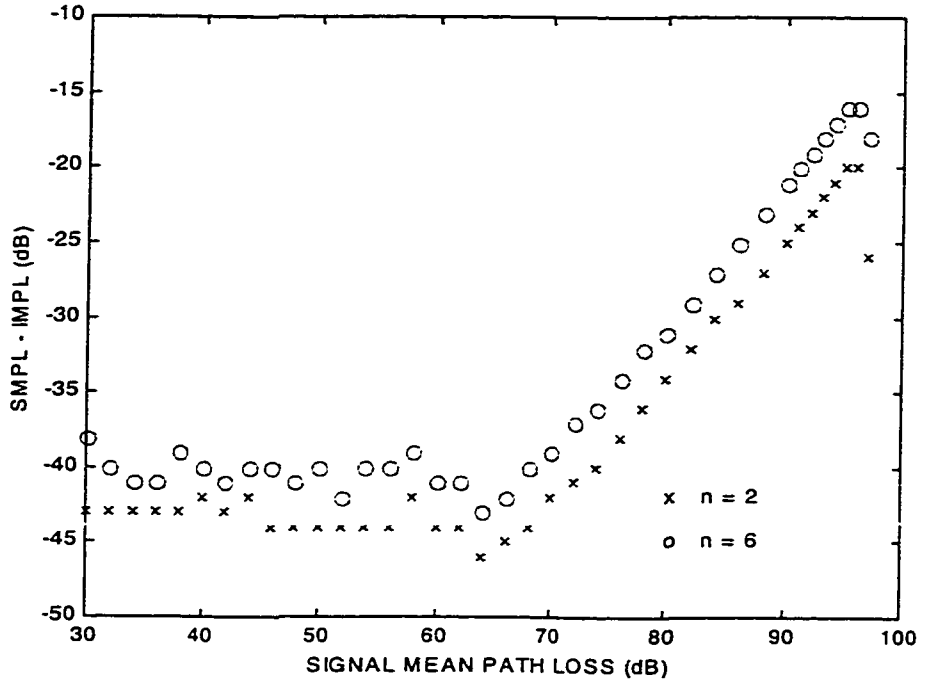

Figure 3.3 UMC with SPC, Uniform Spatial Distribution, IIP_3 = -5 dBm, Path Loss Exponents 2 and 6

3.2.3 FAST POWER CONTROL

Figure 3.4 contains the results for the fast power control strategy (FPC). Fast power control strategy performs significantly worse than the continuous maximum transmit power (CMTP) strategy but does outperform the slow power control strategy. The poor performance for SMPL less than 94 dB is attributed to the lack of interference estimation or BER performance evaluation in the power control algorithm. For SMPL greater than 94 dB, FPC does outperform CMTP for n = 6 and is approximately equivalent for n = 2. As

with SPC, FPC performance begins to increase at about 64 dB as the power control algorithm begins to compensate for increasing SMPL.

Changing the path loss exponent also effects the performance with n = 6 outperforming n = 2 over the full SMPL range of 30 to 97 dB.

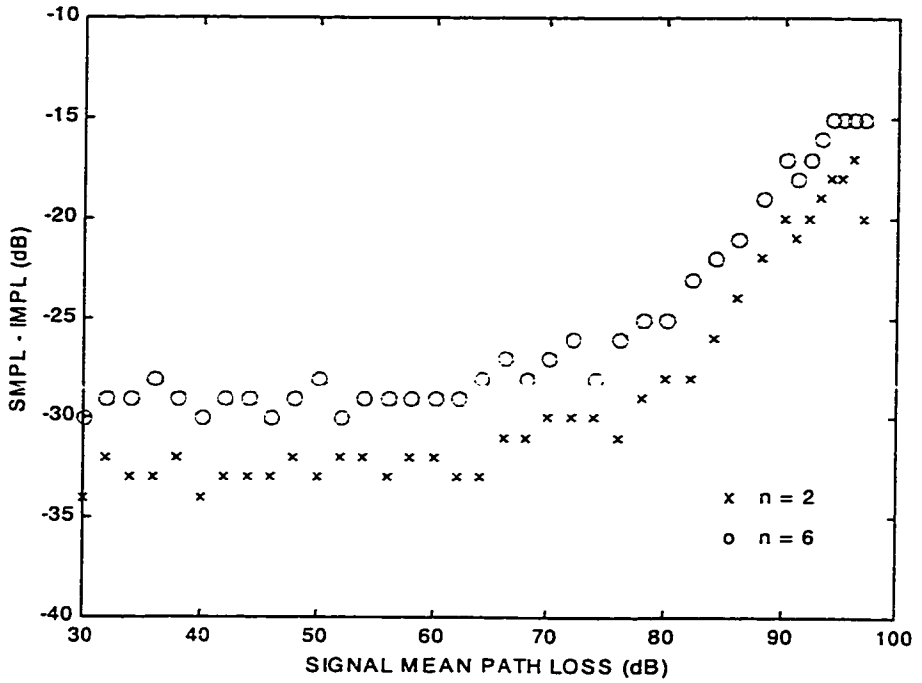

Figure 3.4 UMC with FPC, Uniform Spatial Distribution, IIP_3 = -5 dBm, Path Loss Exponents 2 and 6

3.3 NETWORK PERFORMANCE WITH ORTHOGONAL UNIFORMLY DISTRIBUTED MEMORYLESS FREQUENCY HOPPING CDMA CODES

This section contains the simulation results for Orthogonal Uniformly Distributed Memoryless Frequency Hopping Codes (O-UMC). Section 3.3.1 contains the results for the continuous maximum transmit power strategy, section 3.3.2 contains the results for the slow power control strategy and finally section 3.3.3 contains the results for the fast power control strategy.

O-UMC was evaluated with only the uniform spatial model and IIP_3 = - 5 dBm for SPC and FPC. Since O-UMC performance was also significantly below the desired performance level for the simulations completed, the other cases were not undertaken due to the significant computing time required and the minimal importance of the results.

3.3.1 CONTINOUS MAXIMUM TRANSMIT POWER

Figure 3.5 contains the simulation results for IIP_3 = -5 dBm and IIP_3 = +5 dBm. For IIP_3 = -5 dBm, the performance is dominated by intermodulation products until SMPL exceeds 50 dB. After SMPL is greater than 50 dB, the performance in dominated by the adjacent channel rejection of the system and the probability of an adjacent channel hit. For IIP_3 = +5 dBm, the performance is optimal until SMPL exceeds 40 dB. After SMPL is greater than 40 dB, the performance is dominated by the adjacent channel rejection of the system and the probability of an adjacent channel hit.

This combination of hop code and power control strategy approaches the optimal performance for the lower SMPL values. A system with a IIP_3 = +5 dBm does meet the optimal performance until SMPL exceeds 40 dB.

The path loss exponent also has no effect on the performance result therefore the results are independent of the path loss model.

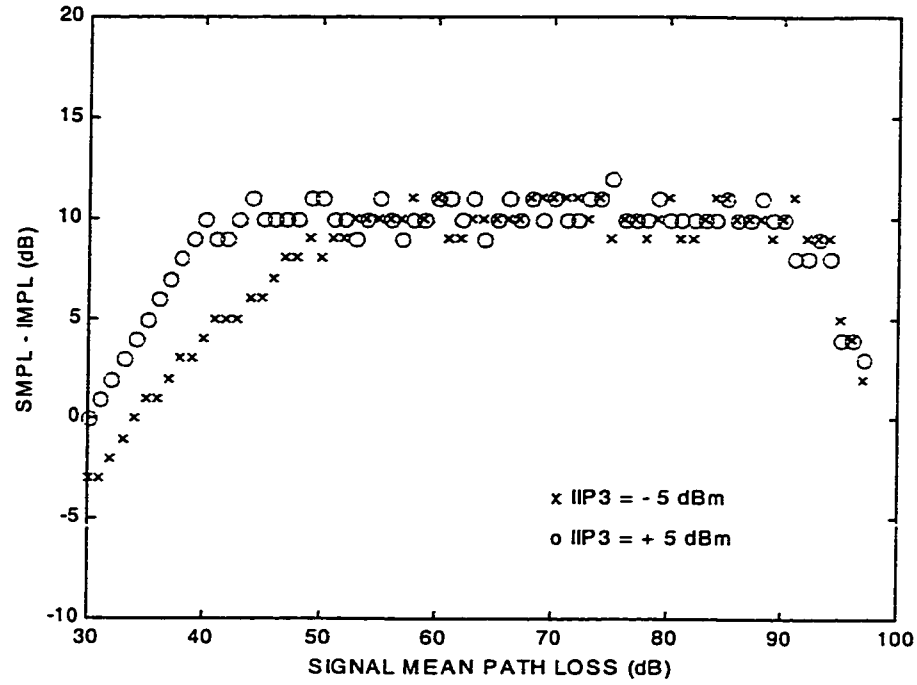

Figure 3.5 O-UMC with CMTP, IIP_3 = -5 and +5 dBm

3.3.2 SLOW POWER CONTROL

Figure 3.6 contains the results for the slow power control strategy. As can be seen from the results, the slow power control strategy performs significantly worse than the continuous maximum transmit power strategy for SMPL below 94 dB. This is attributed to the simplicity of the algorithm for the same reasons that impaired SPC with UMC. As well, performance begins to increase after 64 dB. For SMPL above 94 dB, slow power control outperforms the continuous maximum power control strategy slightly for n = 2 and by 5 to 10 dB for n = 6.

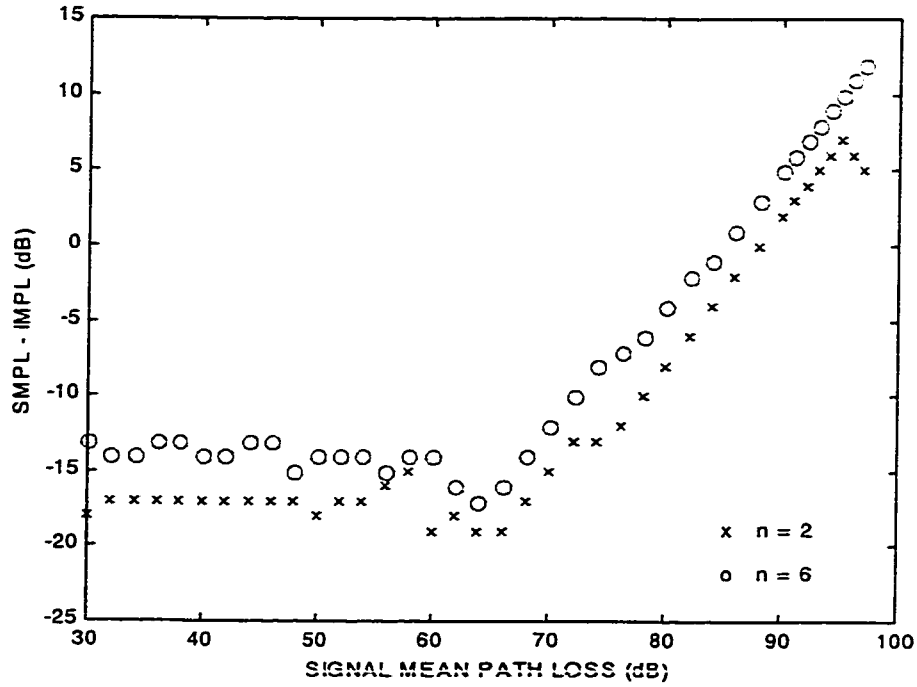

Figure 3.6 O-UMC with SPC, Uniform Spatial Distribution, IIP_3 = -5 dBm, Path Loss Exponents 2 and 6

3.3.3 FAST POWER CONTROL

Figure 3.7 contains the results for the fast power control strategy. As can be seen from the results, the fast power control (FPC) strategy performs significantly worse than the continuous maximum transmit power (CMTP) strategy but does outperform the slow power control strategy. As with SPC, the poor performance for SMPL below 90 dB is attributed to the lack of interference estimation in the power control algorithm. For SMPL above 90 dB, FPC outperforms CMTP for n = 2 and 6. As with UMC with FPC performance begins to increase as SMPL exceeds 64 dB and the power control algorithm compensates for SMPL.

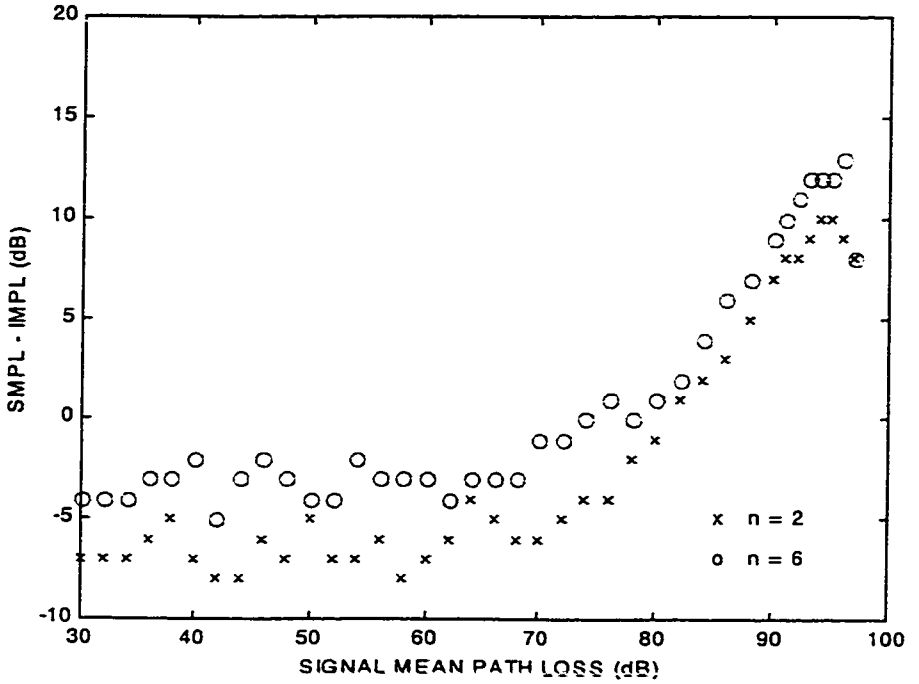

Figure 3.7 O-UMC with FPC, Uniform Spatial Distribution, IIP_3 = -5 dBm, Path Loss Exponents 2 and 6

3.4 NETWORK PERFORMANCE WITH ORTHOGONAL UNIFORMLY DISTRIBUTED MEMORYLESS FREQUENCY HOPPING CDMA CODES WITHOUT ADJACENT CHANNEL INTERFERENCE

This section contains the simulation results for Orthogonal Uniformly Distributed Memoryless Frequency Hopping Codes without Adjacent Channel Interference (O-UMC without ACI). Section 3.4.1 contains the results for the continuous maximum transmit power strategy, section 3.4.2 contains the results for the slow power control strategy and finally section 3.4.3 contains the results for the fast power control strategy.

3.4.1 CONTINOUS MAXIMUM TRANSMIT POWER

Figure 3.8 contains the simulation results for IIP_3 = -5 dBm and IIP_3 = +5 dBm. For IIP_3 = -5 dBm, the performance is dominated by intermodulation products for the full range. For IIP_3 = +5 dBm, the performance is optimal until SMPL exceeds 43 dB. After SMPL is above 43 dB, the performance is dominated by the intermodulation rejection of the system and the probability of a co-channel intermodulation product hit.

This combination of hop code and power control strategy is the nearest in performance to the optimal performance of any of the strategies evaluated to this point. A system with a IIP_3 = +5 dBm does meet the optimal performance until SMPL exceeds 43 dB.

A system with IIP_3 = + 5 dBm outperforms a system with IIP_3 = -5 dBm by approximately 6.5 dB. The significance of this result is that I_{min} is halved for a path loss exponent n = 2 thus increasing the region over which interfering units can operate without affecting performance.

For O-UMC without ACI, as with UMC and O-UMC, and continuous maximum transmit power (CMTP), the path loss exponent also has no effect on the performance.

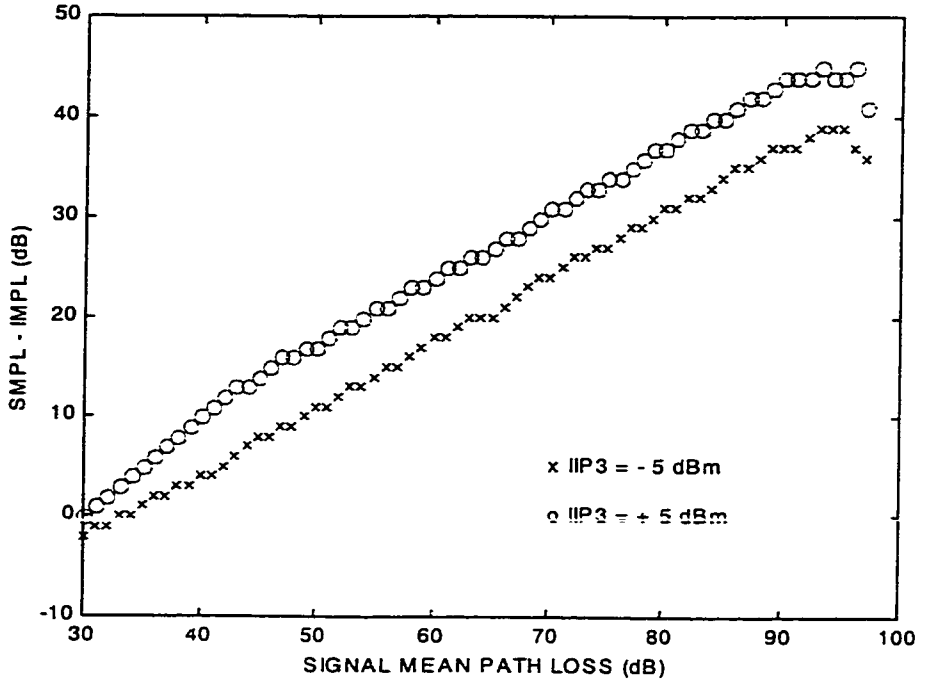

Figure 3.8 O-UMC without ACI, CMTP, IIP_3 = -5 and +5 dBm

3.4.2 SLOW POWER CONTROL

Figure 3.9 to Figure 3.13 contain the results for the slow power control strategy versus uniform, short and long spatial distributions. As can be seen from the results, the slow power control strategy performs worse than the continuous maximum transmit power strategy for SMPL below 94 dB for each spatial distribution. This is attributed to the simplicity of the algorithm for the same reasons that impaired SPC with UMC or O-UMC. For SMPL above 94 dB, slow power control outperforms the continuous maximum power

control strategy slightly for both n = 2 and n = 6. As would be expected, SPC performance improves as the spatial distribution mean value is reduced.

As the path loss exponent increases from 2 to 6 the effect of the spatial distribution becomes more pronounced.

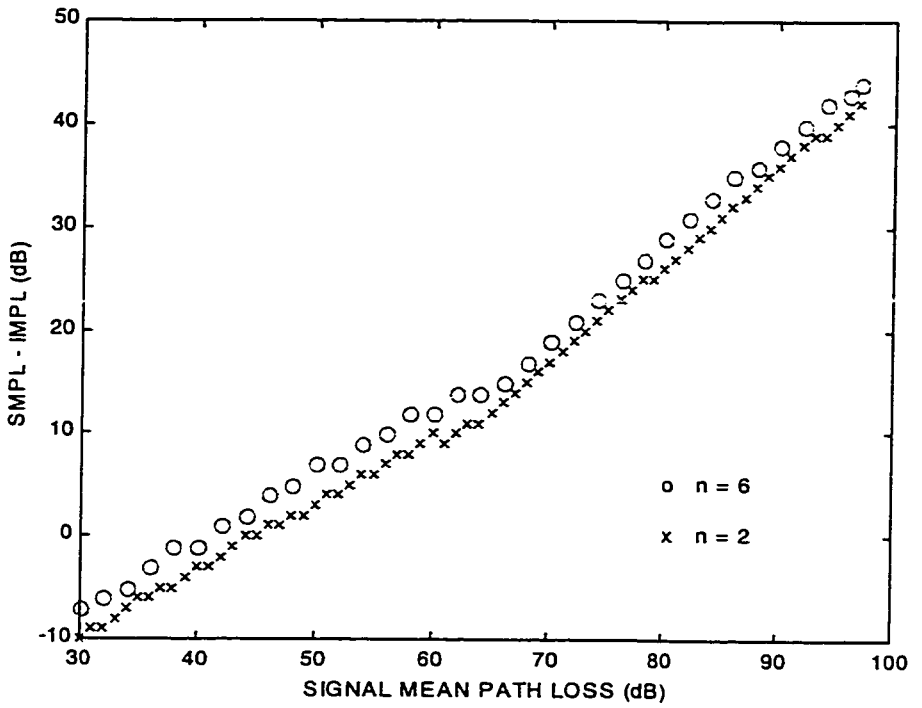

Figure 3.9 O-UMC without ACI, SPC, Uniform Spatial Distribution, IIP_3 = -5 dBm, Path Loss Exponents 2 and 6

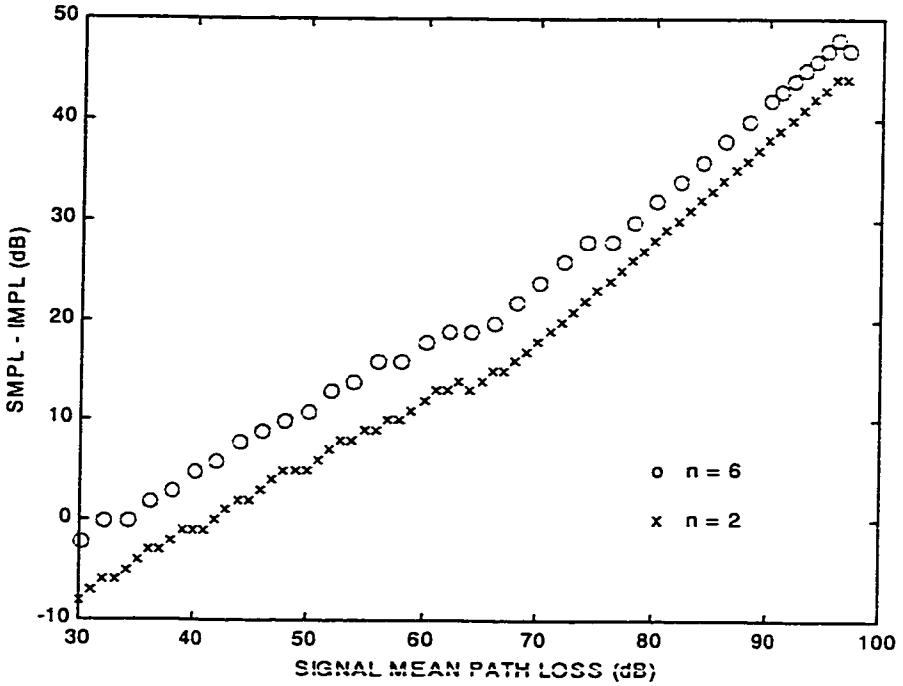

Figure 3.10 O-UMC without ACI, SPC, Short Spatial Distribution, IIP_3 = -5 dBm, Path Loss Exponents 2 and 6

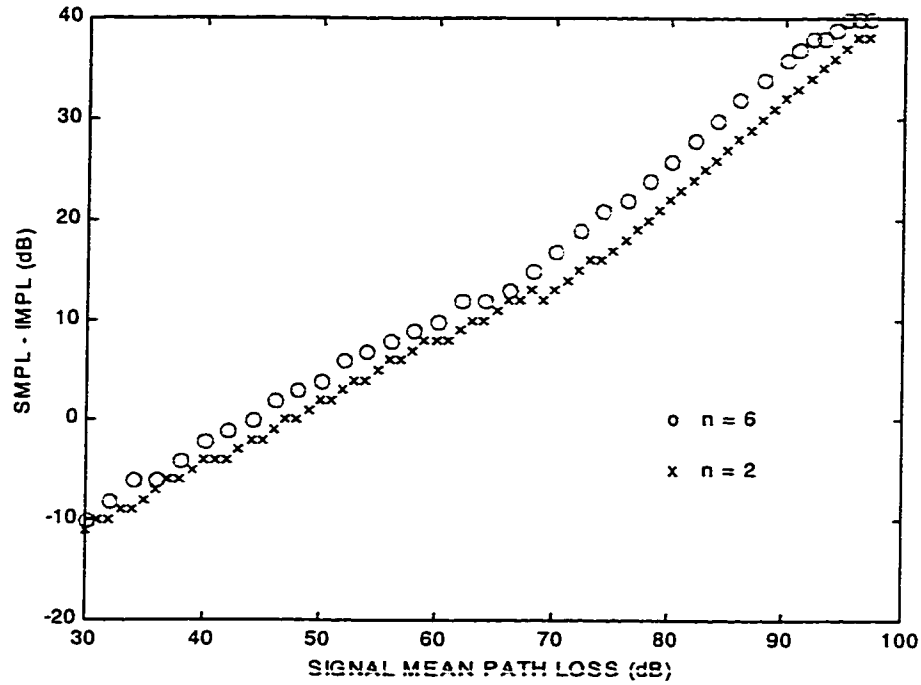

Figure 3.11 O-UMC without ACI, SPC, Long Spatial Distribution, IIP_3 = -5 dBm, Path Loss Exponents 2 and 6

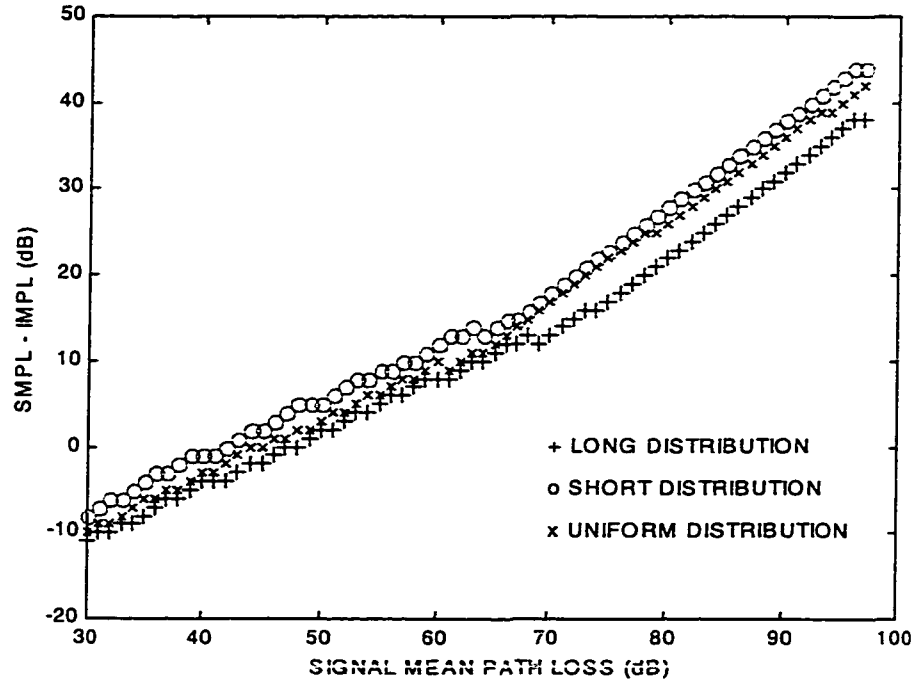

Figure 3.12 O-UMC without ACI, SPC, IIP_3 = -5 dBm and Path Loss Exponent 2 versus various Spatial Distributions

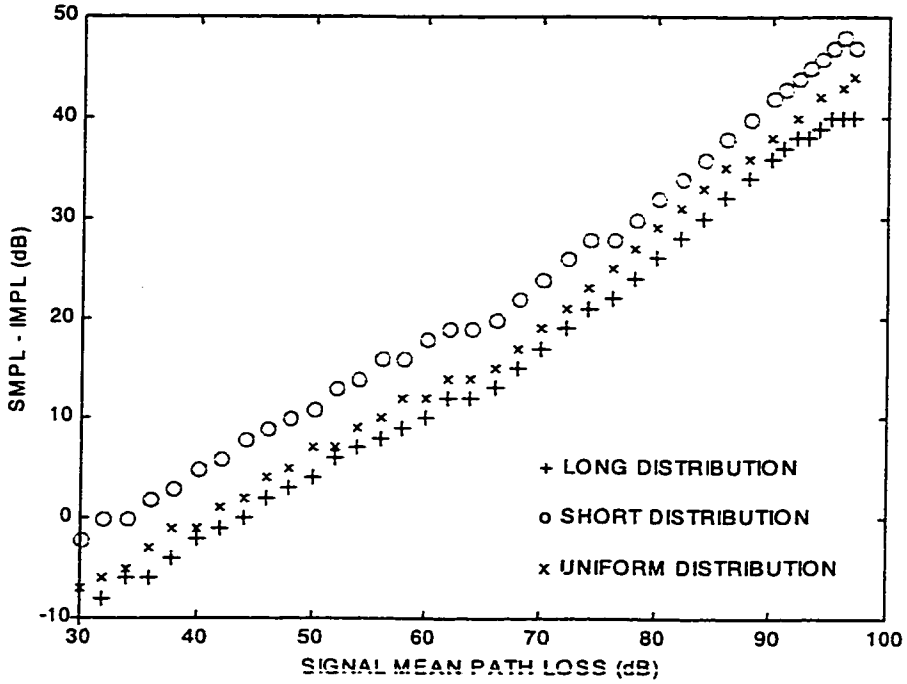

Figure 3.13 O-UMC without ACI, SPC, IIP_3 = -5 dBm and Path Loss Exponent 6 versus various Spatial Distributions

3.4.3 FAST POWER CONTROL

Figure 3.14 and Figure 3.18 contain the results for the fast power control strategy versus uniform, short and long spatial distributions. As can be seen from the results, fast power control strategy outperforms the continuous maximum transmit power strategy for each spatial distribution.

FPC, like SPC, performance improves as the spatial distribution mean value is reduced. Larger path loss exponents also increases the effects of spatial distribution on the performance of the fast power control strategy.

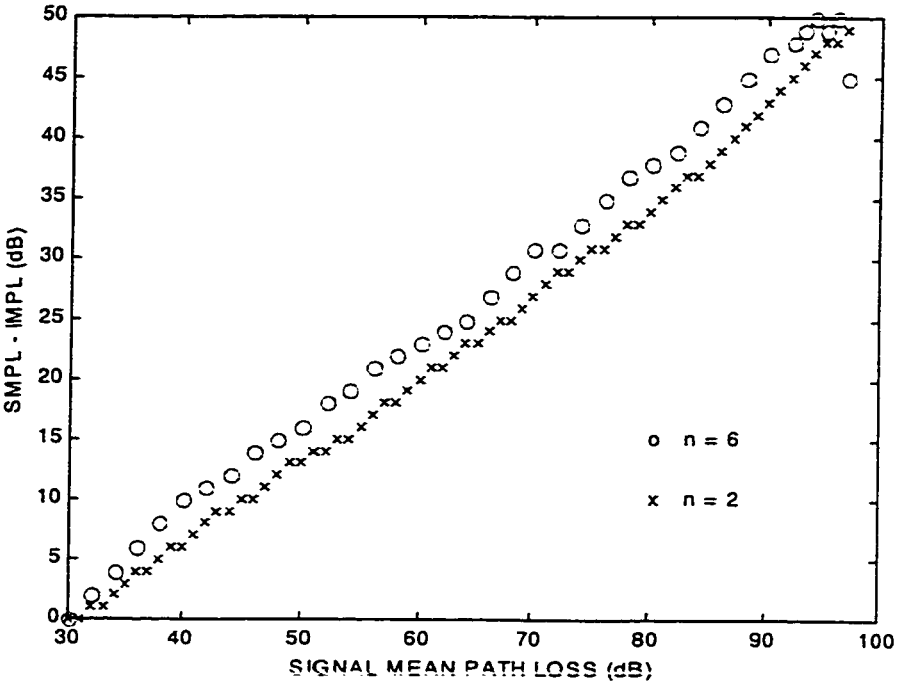

Figure 3.14 O-UMC without ACI, FPC, Uniform Spatial Distribution, IIP_3 = -5 dBm, Path Loss Exponents 2 and 6

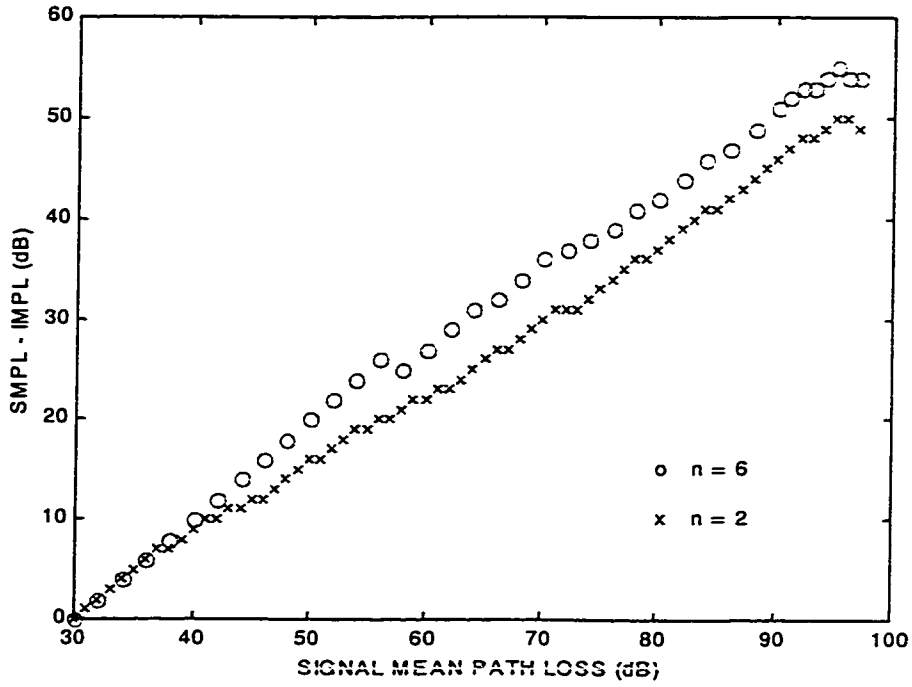

Figure 3.15 O-UMC without ACI, FPC, Short Spatial Distribution, IIP_3 = -5 dBm, Path Loss Exponents 2 and 6

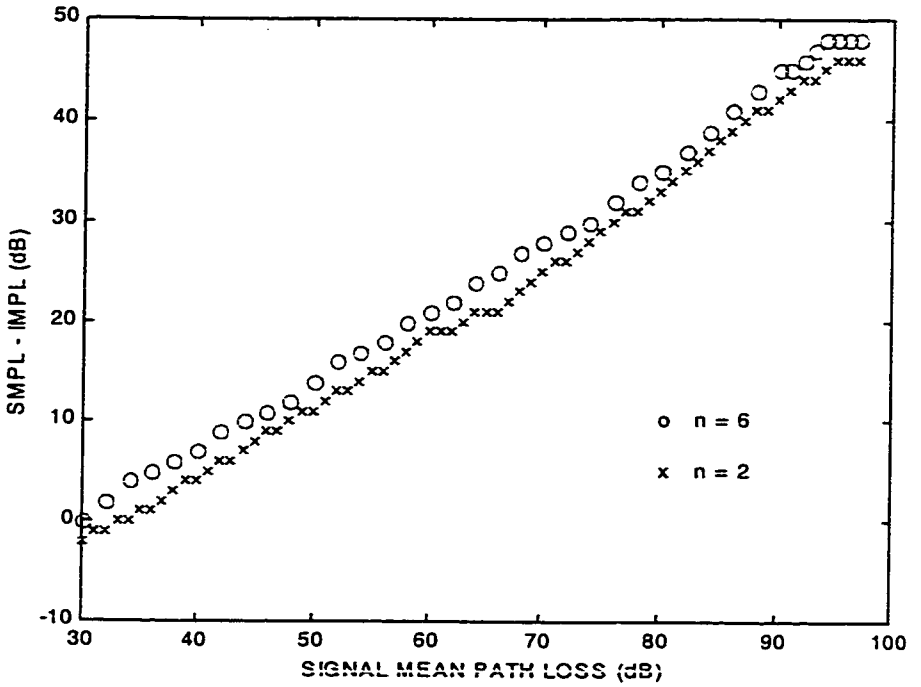

Figure 3.16 O-UMC without ACI, FPC, Long Spatial Distribution, IIP_3 = -5 dBm, Path Loss Exponents 2 and 6

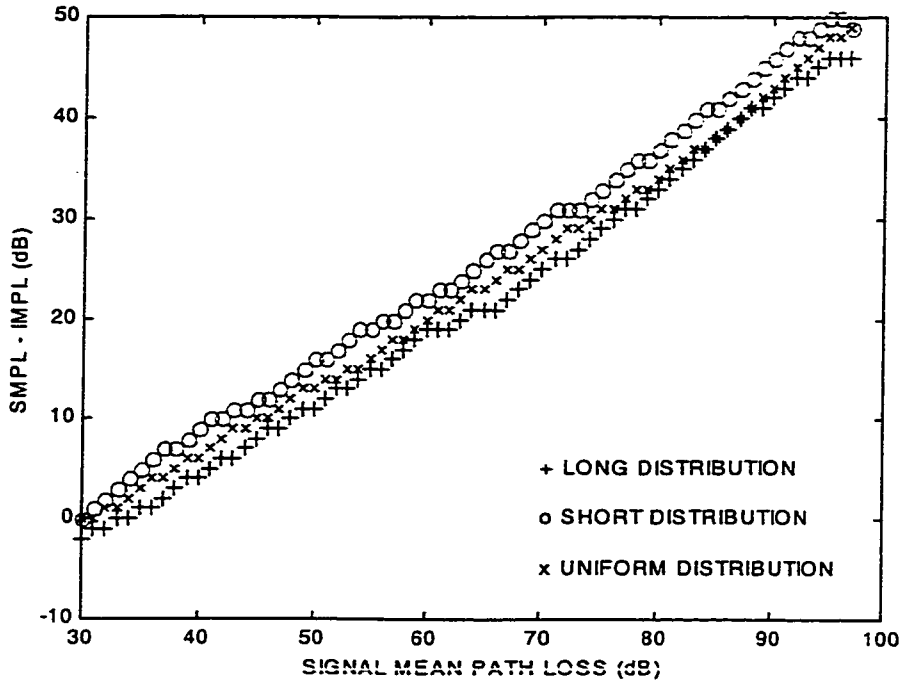

Figure 3.17 O-UMC without ACI, FPC, IIP_3 = -5 dBm and Path Loss Exponent 2 versus various Spatial Distributions

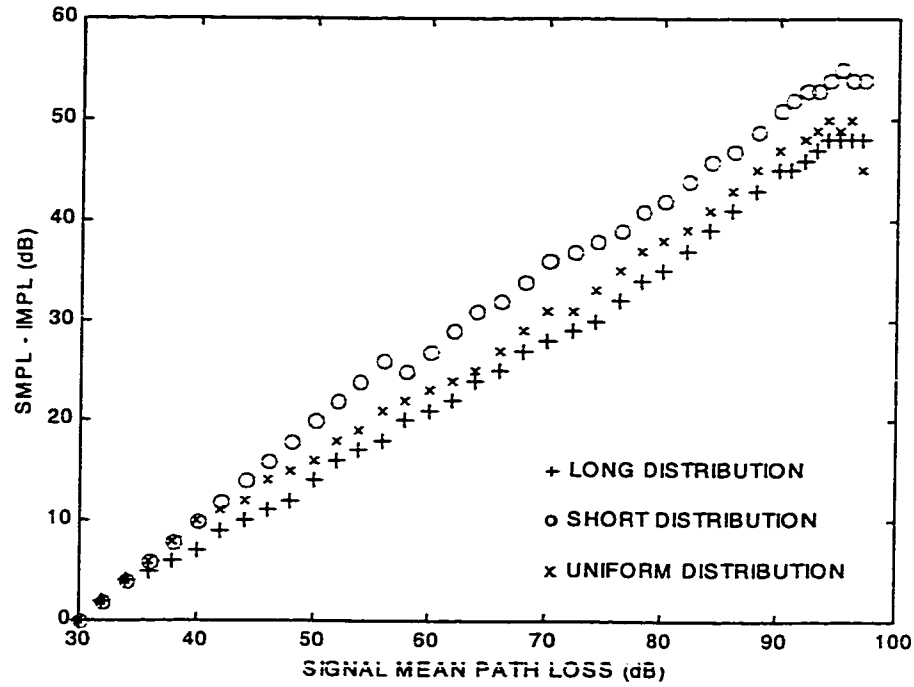

Figure 3.18 O-UMC without ACI, FPC, IIP_3 = -5 dBm and Path Loss Exponent 6 versus various Spatial Distributions

Figure 3.19 plots the performance with a IIP_3 equal to +5 dBm. In comparison to an IIP_3 equal to -5 dBm, the performance is optimal until SMPL exceeds 58 dB versus 40 dB for a path loss exponent equal to 6. At SMPL equal to 58 dB, this translates into a performance improvement of approximately 7 dB for the n equals 2 case and 6 dB for the n equals 6 case. In range terms, this translates to approximately a 55% and 21% reduction in I_{min} respectively. From the perspective of a user this would be a noticeable improvement.

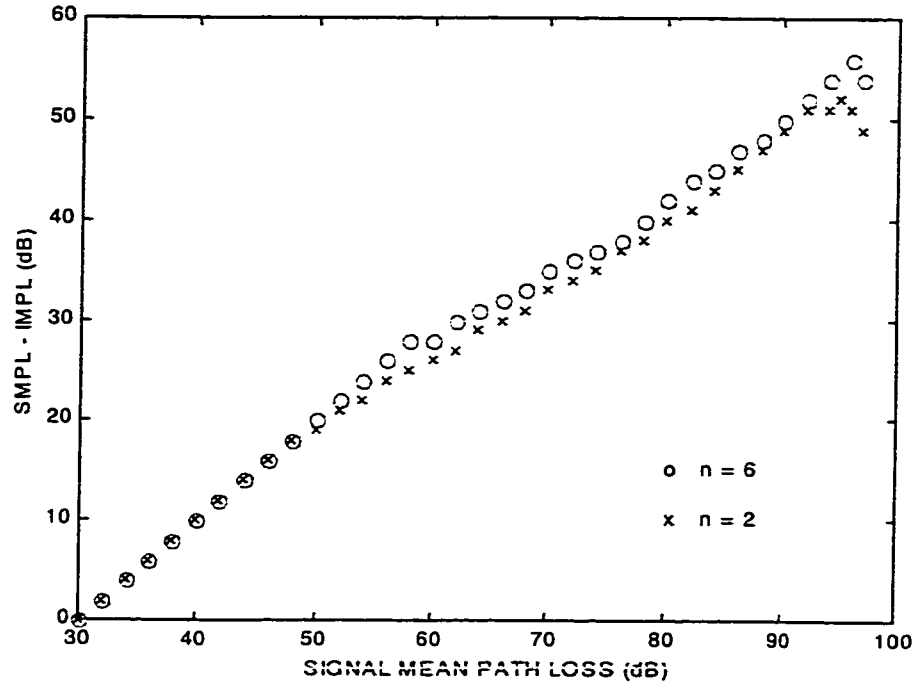

Figure 3.19 O-UMC without ACI, FPC, Uniform Spatial Distribution, IIP_3 = +5 dBm, Path Loss Exponents 2 and 6

Chapter 4

CONCLUSION

4.1 CONCLUSIONS REGARDING UNIFORMLY DISTRIBUTED MEMORY-LESS FREQUENCY HOPPING CDMA CODES

When compared to the optimal performance, the combination of UMC with any of the power control strategies has extremely poor performance. For UMC, performance is dominated by the number of direct hits and the signal strength of the interfering units relative to the desired signal. Hence, as expected, linearity and selectivity has a negligible effect on the performance of any link in the network.

Table 4.1 summarizes I_{min} relative to various coverage levels for the CTMP power control strategy which performed the best of the three strategies simulated

n	$r_{coverage}/r_{max}$	$I_{min}/r_{coverage}$
2 / 6	25%	630% / 180%
2 / 6	50%	630% / 180%
2 / 6	75%	790% / 180%
2 / 6	100%	1400% / 240%

Table 4.1 Required I_{min} to Achieve Given Coverage using UMC with CMTP, IIP_3 = -5 dBm

A smaller I_{min} corresponds to a higher performing FHSS CDMA hop code - power control strategy combination. Optimally, I_{min} should be around 1 meter independent of

SMPL. For UMC, I_{min} is so large as to loose significance. To provide a reference, the ratio of I_{min} and $r_{coverage}$ is tabulated.

For a coverage of 75% of the maximum achievable, the separation between any possible interfering units and the receiving unit is approximately 8 times the distance between the two communicating units for n equal to 2 and almost 2 times for n equal to 6. Obviously in terms of spatial density (and capacity) this is extremely poor.

The power control strategies in order of performance for UMC were CMTP, FPC and then SPC. Figure 4.1 and Figure 4.2 illustrate the relative performance of each of the power control strategies for path loss exponents 2 and 6 respectively. In both figures SPC and FPC perform much worse than CMTP until SMPL is larger than about 94 dB at which time the performance becomes comparable.

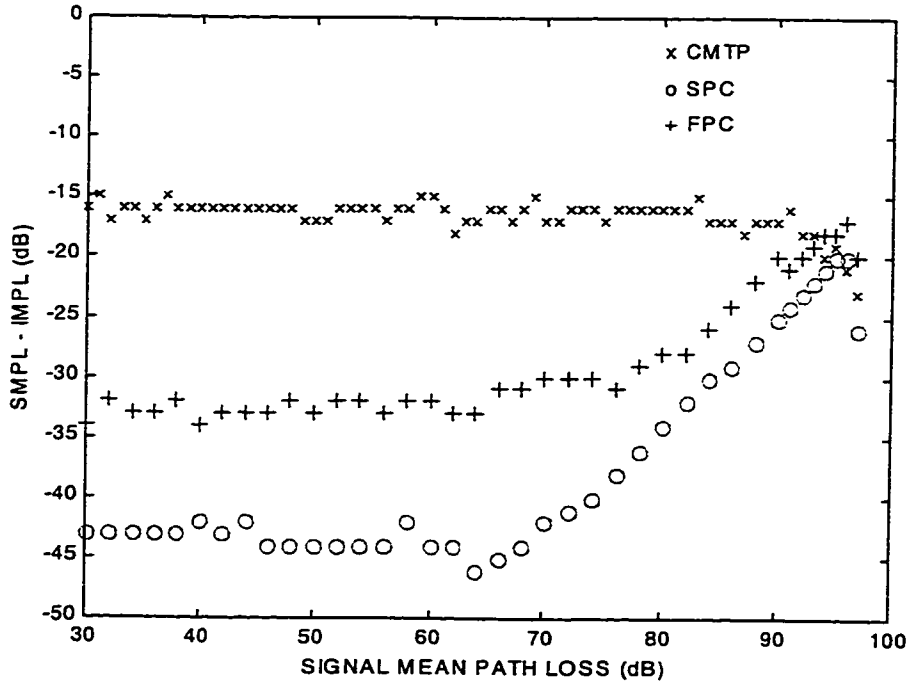

Figure 4.1 Comparison of Power Control Strategies for UMC, Uniform Spatial Distribution, IIP_3 = -5 dBm and Path Loss Exponent 2

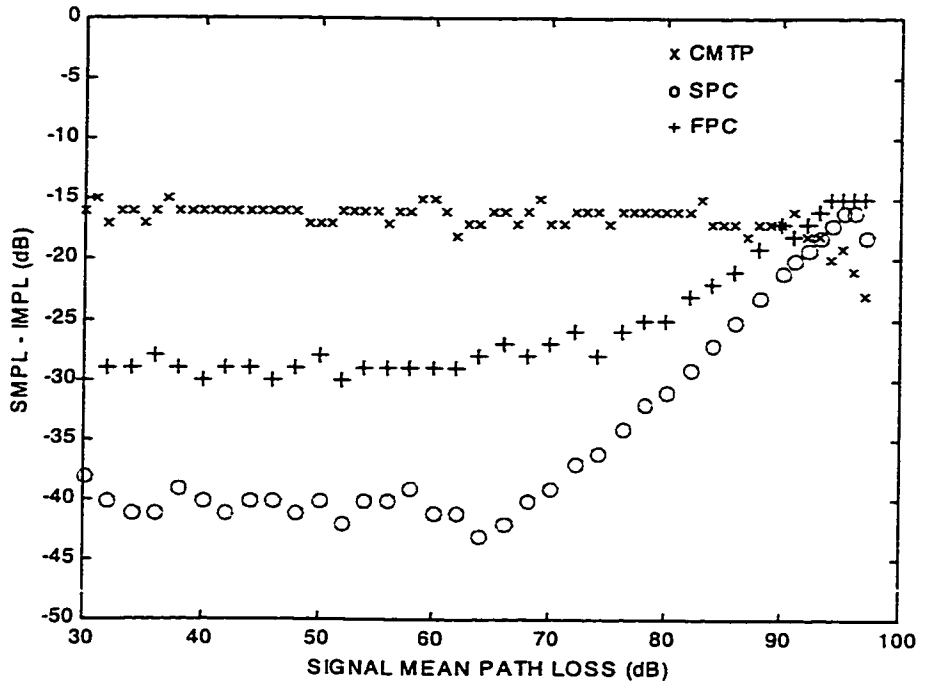

Figure 4.2 Comparison of Power Control Strategies for UMC, Uniform Spatial Distribution, IIP_3 = -5 dBm and Path Loss Exponent 6

For CMTP, the results are comprised of a single region where the probability of a co-channel hit and the mean carrier to interference (plus noise) ratio determine the performance.

For the SPC and FPC algorithms simulated, two performance regions exist in the results shown. For the lower SMPL range, the co-channel rejection is the limiting factor in the performance. This is exacerbated by the simplistic power control algorithm reducing the transmit power independent of interference levels thus decreasing the mean carrier to interference ratio (CIR). As SMPL increases, the particular power control algorithm begins to affect the performance by increasing the transmit power level and thus reducing

CIR. In the case of SPC, the second performance region begins at SMPL above about 54 dB. This is due to the nature of the SPC algorithm which attempts to maintain a constant SNR and begins to suppress the interfering signals after a SMPL of 54 dB. As can be noted from the results for SPC a local minima exists at 54 dB. This is a result of the received signal being relatively close to the sensitivity point of the receiver thus reducing the interference immunity of the receiver. The notch can be removed in one of two ways, either increasing the minimum transmit power level or increasing the desired SNR level for the power control algorithm. The transition point for FPC is not as defined as that of SPC but exists in the same general vicinity and is caused by the same factors but due to the nature of the power control objective does not exhibit the local minima affect.

For SPC and FPC with the uniform spatial model, the performance of path loss exponent 6 outperformed exponent 2. This is attributable to the effect that the path loss exponent has on translating the range into a path loss between an operating pair. As the path loss exponent increases, the mean received signal strength at the interfering pair's reverse link receiver increases. Subsequently, power control can reduce the transmit power level of the forward link unit which reduces the interference signal strength at the desired receiver.

The only option for improving performance to meet the performance target is to reduce the co-channel interference by either reducing the number of operational pairs, thus reducing the probability of a hit, or a more effective power control strategy based on the amount of inband interference. Reducing the number of users and therefore the capacity of the network is clearly against the initial purpose of this research which was to analyze simple methods to increase performance/capacity in a relatively unintelligent FHSS CDMA network. A more effective power control strategy using interference levels will

improve performance, however based on the results in this thesis it is unlikely that a more advanced power control strategy would be sufficient to improve performance to the desired level.

4.2 CONCLUSIONS REGARDING ORTHOGONAL UNIFORMLY DISTRIBUTED MEMORYLESS FREQUENCY HOPPING CDMA CODES

The power control strategies evaluated ranked in the following order for O-UMC: Continuous Maximum Transmit Power, Fast Power Control and finally Slow Power Control. This is obviously similar to the order of performance for UMC with the caveat that each of the strategies for O-UMC outperformed the same strategy with UMC. For O-UMC a power control strategy that does not incorporate relative interference levels and effects is insufficient to enhance performance over a CMTP strategy.

Table 4.2 lists the value of I_{min} relative to various coverage levels for CMTP. I_{min} , while significantly smaller than for UMC, was still fairly large so only the ratio of I_{min} to $r_{coverage}$ is tabulated.

n	$r_{coverage}/r_{max}$	$I_{min}/r_{coverage}$
2 / 6	25%	30% / 67%
2 / 6	50%	30% / 67%
2 / 6	75%	45% / 67%
2 / 6	100%	79% / 92%

Table 4.2 Required I_{min} to Achieve Given Coverage using O-UMC with CMTP, IIP_3 = -5 dBm

For a coverage radius of 75% of the maximum, I_{min} is approximately 1/2 to 2/3 of the specified coverage radius (depending on path loss exponent). While this is a significant improvement over UMC, an I_{min} of 1/2 to 2/3 the desired coverage radius is still very substantial. The achievable spatial density would still be low with O-UMC.

Figure 4.3 and Figure 4.4 compare the performance of the power control strategies for path loss exponents 2 and 6 respectively. As can be clearly discerned from the plots CMTP outperforms SPC and FPC for SMPL less than about 94 dB. Above 94 dB, SPC and FPC perform the same or slightly better.

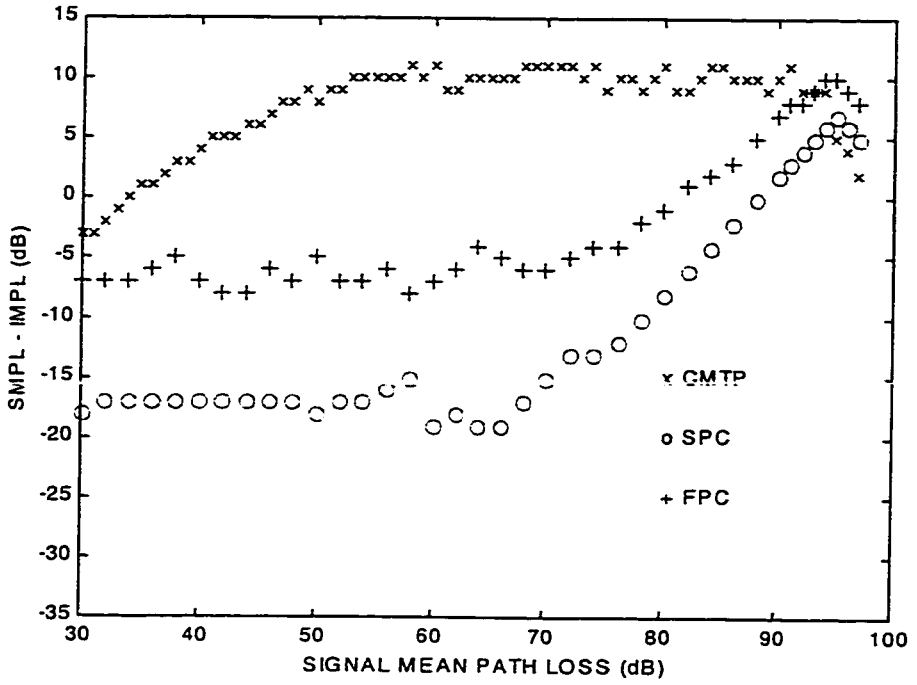

Figure 4.3 Comparison of Power Control Strategies for O-UMC, Uniform Spatial Distribution, IIP_3 = -5 dBm and Path Loss Exponent 2

O-UMC with CTMP performance can be broken into multiple regions, typically two in the results shown, a lower SMPL region where intermodulation products may or may not dominate and higher SMPL region where adjacent channel rejection dominates. The transition point between these two regions varies with the power control strategy. For CTMP with an IIP_3 = -5 dBm, the breakpoint is at SMPL equal to 50 dB, which marks the transition between the region dominated by intermodulation products and the adjacent

channel rejection region. For CTMP with an IIP_3 = +5 dBm, the breakpoint is at SMPL equal to 40 dB, a transition occurs from an optimal performance region to a region dominated by adjacent channel rejection.

If the adjacent channel rejection of the system was improved for an IIP_3 = +5 dBm system, three regions could potentially exist. An optimal region followed by a region dominated by intermodulation products then by a region dominated adjacent channel rejection.

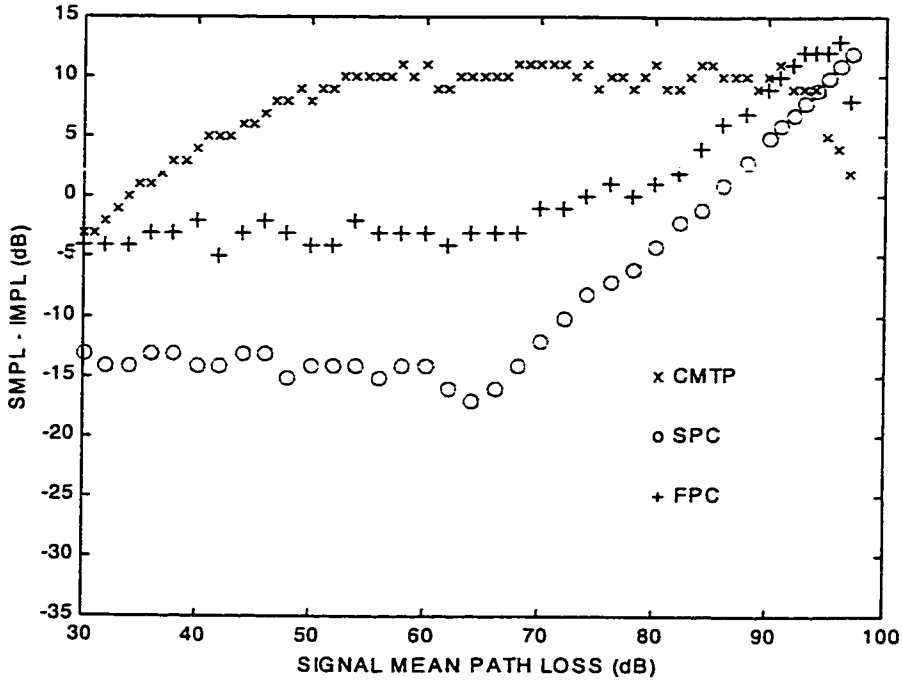

Figure 4.4 Comparison of Power Control Strategies for O-UMC, Uniform Spatial Distribution, IIP_3 = -5 dBm and Path Loss Exponent 6

For the SPC and FPC algorithms used, multiple performance regions also exist but for slightly different reasons. For the lower SMPL range, the adjacent channel rejection is the limiting factor in the performance since the simplistic power control algorithm has

reduced the transmit power independent of interference levels. As SMPL increases, the particular power control algorithm begins to affect the performance. In the case of SPC, the second performance region begins at SMPL above about 54 dB. This is due to the nature of the SPC algorithm which attempts to maintain a constant SNR and begins to suppress the interfering signals after a SMPL of 54 dB. As can be noted from the results for SPC a local minima exists at 54 dB. This is a result of the received signal being relatively close to the sensitivity point of the receiver thus reducing the interference immunity of the receiver. The notch can be removed in one of two ways, either increasing the minimum transmit power level or increasing the desired SNR level for the power control algorithm. This would however impact the performance improvement that SPC has over CMTP for SMPL above 94 dB. The transition point for FPC is not as defined as that of SPC but exists in the same general vicinity and is caused by the same factors but due to the nature of the power control objective does not exhibit the local minima affect.

For SPC and FPC with the uniform spatial model, the performance of path loss exponent 6 outperformed exponent 2. This is attributable to the effect that the path loss exponent has on translating the range into a path loss between an operating pair. As the path loss exponent increases, the mean received signal strength at the interfering pair's reverse link receiver increases. Subsequently, power control can reduce the transmit power level of the forward link unit which reduces the interference signal strength at the desired receiver.

In contrast to UMC with a CMTP strategy, the performance of O-UMC can be improved without reducing the capacity of the network. This can be achieved by increasing the adjacent channel rejection and/or IIP_3. By these means, performance could theoretically be improved until the optimal performance was reached. This would be

impractical at best or impossible to improve adjacent channel rejection and IIP_3 sufficiently at worst. However, O-UMC combined with a more intelligent power control strategy could provide a realistic compromise between selectivity, linearity and complexity to achieve optimal or near optimal performance.

4.3 CONCLUSIONS REGARDING ORTHOGONAL UNIFORMLY DISTRIBUTED MEMORYLESS FREQUENCY HOPPING CDMA CODES WITHOUT ADJACENT CHANNEL INTERFERENCE

Clearly O-UMC without ACI and FPC achieved the closest performance to the optimal level of all the options evaluated for 11 users. For O-UMC without ACI performance of the network with the chosen transmitter and receiver specifications is dominated by intermodulation products.

Table 4.3 lists I_{min} relative to various coverage radii for the FPC strategy. As compared to UMC and O-UMC, performance is significantly better.

n	$r_{coverage}/r_{max}$	$I_{min}/r_{coverage}$	I_{min} (m)
2 / 6	25%	1.3% / 41%	5.8 / 1.3
2 / 6	50%	0.6% / 24%	5.8 / 1.5
2 / 6	75%	0.4% / 17%	5.8 / 1.5
2 / 6	100%	0.4% / 15%	6.6 / 1.8

Table 4.3 Required I_{min} to Achieve Given Coverage using O-UMC without ACI, FPC, Uniform Spatial Distribution, IIP_3 = -5 dBm

For a desired coverage radius of 75% of the maximum I_{min} is between 1.5 to 5.8 m, 17% to 0.4% of the desired coverage area for n equal to 6 or 2 respectively. This is a significant improvement relative to the other code types analyzed. A FPC strategy produces an I_{min} of approximately 30% of that produced by CMTP. This validates the use of FPC and the added complexity over the use of CMTP. A worst case of 5.8 m still has a signifi-

cant reduction in the possible spatial density achievable with the network. If the system has an IIP_3 of +5 dBm I_{min}, for n equal to 2, is reduced to 3.6 m.

Figure 4.5 and Figure 4.6 plot the relative performance of each of the power control strategies for path loss exponent equal to 2 and 6 respectively for easy comparison.

Of the power control strategies evaluated for an IIP_3 equal to -5 dBm, FPC outperforms CMTP for the spatial models evaluated by a minimum of 10 dB. This would translate to a minimum reduction in I_{min} of 68% for a path loss exponent of 2 and by 37% for a path loss exponent of 6 at the extreme SMPL of 97 dB.

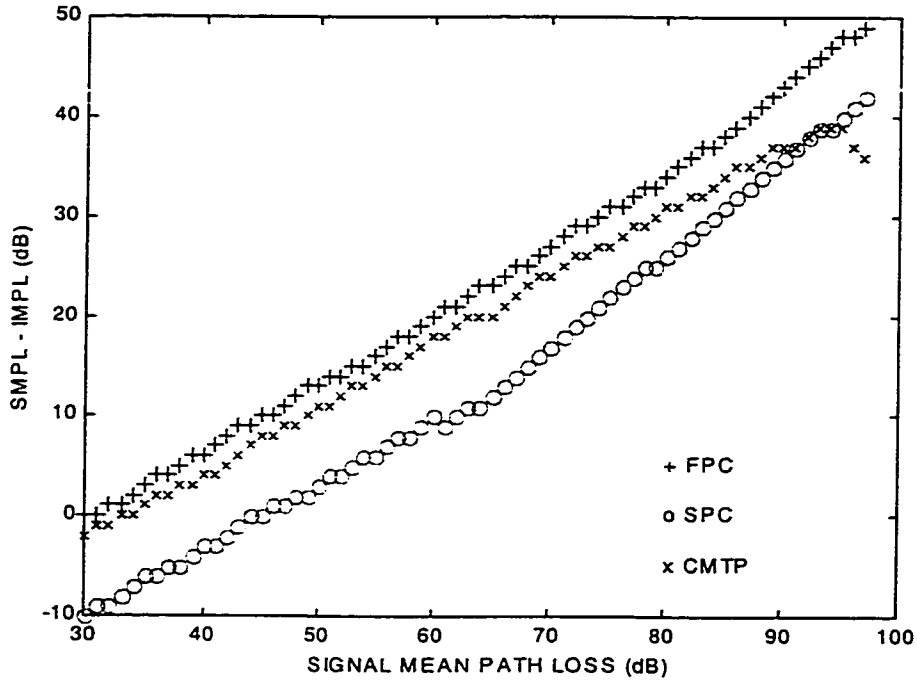

Figure 4.5 Comparison of Power Control Strategies for O-UMC without ACI, Uniform Spatial Distribution, IIP_3 = -5 dBm and Path Loss Exponent 2

For the three spatial models evaluated, the performance when the path loss exponent was 6 outperformed 2. This is attributable to effect that the path loss exponent has on

translating the range into a path loss between an operating pair. As the path loss exponent increases the effective mean received signal strength increases. Thus a system with power control based only on path loss would have a reduced transmit power level and therefor provide less interference. However, as the path loss exponent increases the deviation in performance of each spatial model increases. In an indoor environment where the path loss exponent is rarely 2, this result implies that an accurate spatial model is required to provide the most realistic results.

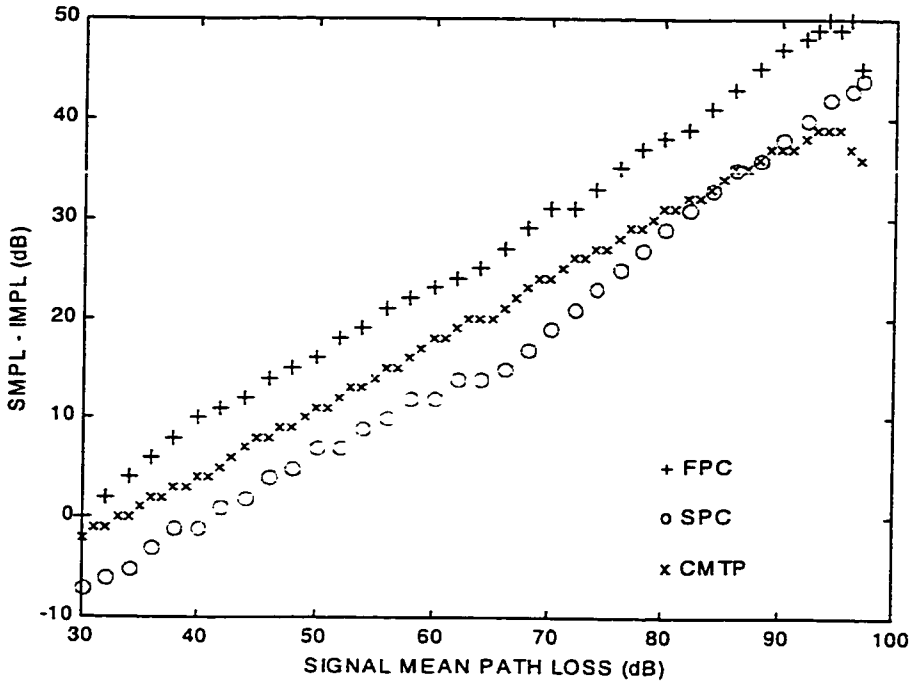

Figure 4.6 Comparison of Power Control Strategies for O-UMC without ACI, Uniform Spatial Distribution, IIP_3 = -5 dBm and Path Loss Exponent 6

Performance could be improved by reducing the mean value of the intermodulation products. This can be achieved by power control, improved receiver linearity and controlling the spatial distribution. For obvious reasons, power control and receiver linearity are

the clear choice when trying to develop an installation independent product. The effects of reducing intermodulation interference by power control has shown that even a relatively simple power control strategy based on optimizing the transmit power on each hop to account for only the path loss can outperform a CTMP strategy for a network of 11 units. A more complex strategy would be expected to improve performance levels further, perhaps achieving optimal performance without changing the transceiver specifications.

4.4 CONCLUSIONS REGARDING PERFORMANCE OF A SIMPLE FHSS CDMA NETWORK

As mentioned in the introduction of this thesis, a FHSS CDMA network is a self interference limited system and the reduction of self interference is the key task when trying to improve performance/spatial density/capacity. As intuitively expected, the simulation results have shown that co-channel interference followed by adjacent channel interference and finally intermodulation interference are the dominate sources of self interference in the network. The performance of an FHSS CDMA hopping code has been shown to be determined primarily by how these sources of interference are compensated for. UMC which makes no attempt to compensate has performance determined by co-channel interference. O-UMC which removes the possibility of co-channel interference has performance determined primarily by adjacent channel interference. O-UMC without ACI which removes co-channel and adjacent channel interference has performance determined by co-channel intermodulation products.

The value of this work is not in the comparison of the different hop code types, which is interesting in itself and included for completeness but intuitively obvious. The primary value is based on two areas, the inclusion of non-ideal transceiver effects which are seldom if ever included in the analysis of FHSS and the final performance results regarding O-UMC without ACI relative to the different power control strategies. The non-ideal effects analyzed represent realistic impairments that a FHSS network will encounter in an indoor environment and thus provide a significant level of confidence when using these results to design a FHSS network. The usefulness of the analysis of the various code options and the various power control strategies should not be understated. The cost of each increase in performance needs to be justified in many designs. The results presented

here highlight the performance improvement achieved by each increase in complexity and cost thus providing clear, concise information to perform the required design trade-off.

Figure 4.7 and Figure 4.8 illustrate the performance for the various FHSS CDMA hopping codes for CMTP power control strategy with an IIP_3 of -5 and +5 dBm respectively. As can be seen from comparing the two figures the input intercept point has a minor effect on O-UMC with CMTP while it has a major effect on O-UMC without ACI.

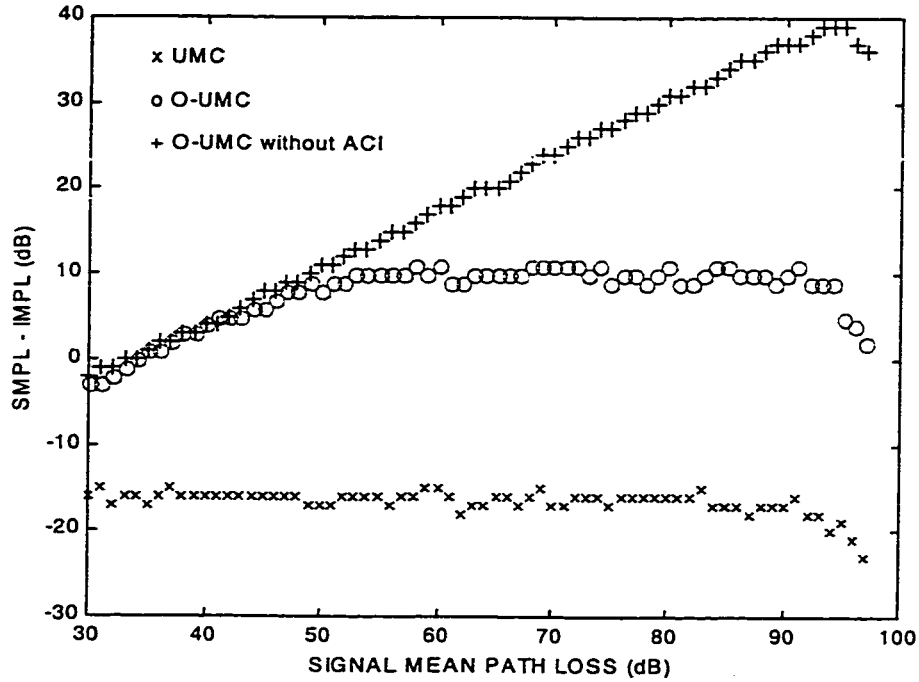

Figure 4.7 Comparison of FHSS CDMA Hopping Codes with CMTP and IIP_3 = -5 dBm

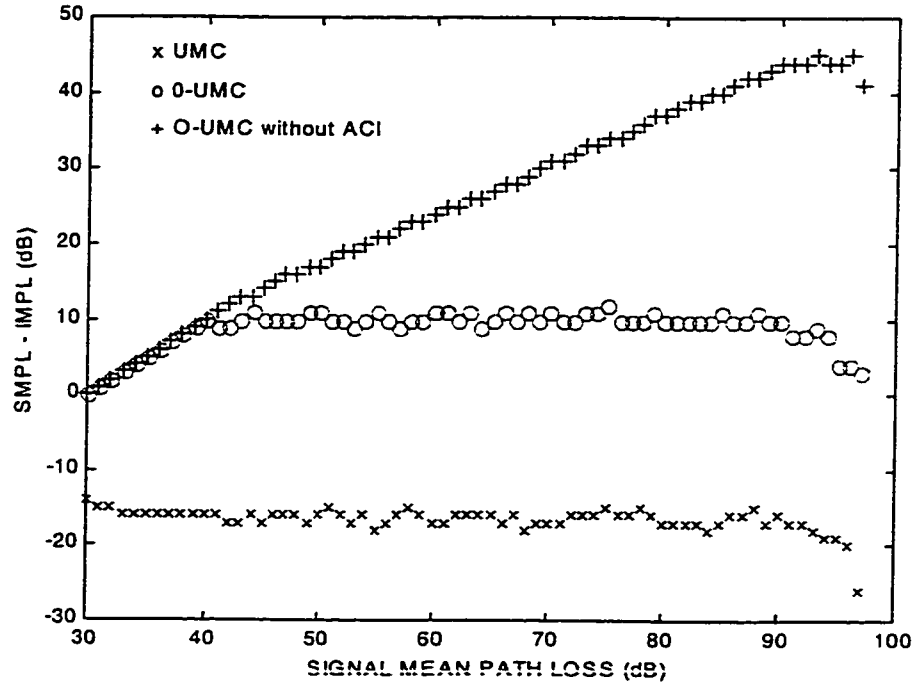

Figure 4.8 Comparison of FHSS CDMA Hopping Codes with CMTP and IIP_3 = +5 dBm

The power control strategies analyzed were shown to be insufficient in improving performance for UMC and O-UMC. O-UMC without ACI did show a significant improvement using FPC strategy over CMTP strategy. The prime reason that the power control strategies did not improve UMC and O-UMC performance was due to the lack of a carrier to interference analysis in the algorithm. If CIR was included, performance would have improved for the three code types analyzed such that the order of performance for each would have been FPC, SPC and finally CMTP. Admittedly, performance improvements due to power control would have been least for O-UMC and UMC.

Figure 4.9 and Figure 4.10 illustrate the best performing power control strategies for each of the FHSS CDMA hopping code types for IIP_3 of -5 and +5 dBm respectively.

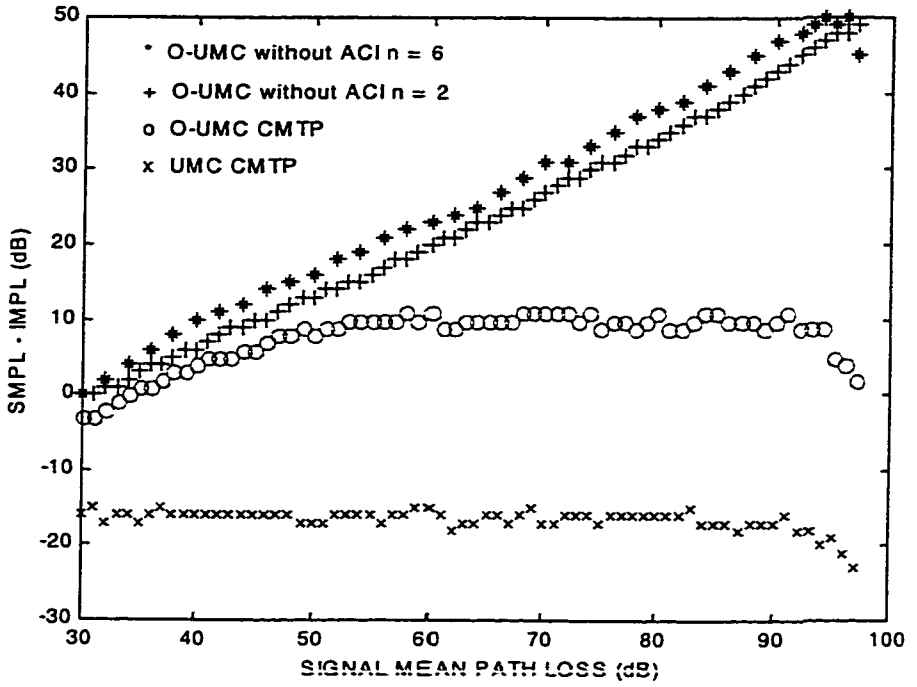

Figure 4.9 Best Performing Power Control Strategies for each of the FHSS CDMA Hopping Codes with an IIP_3 = -5 dBm

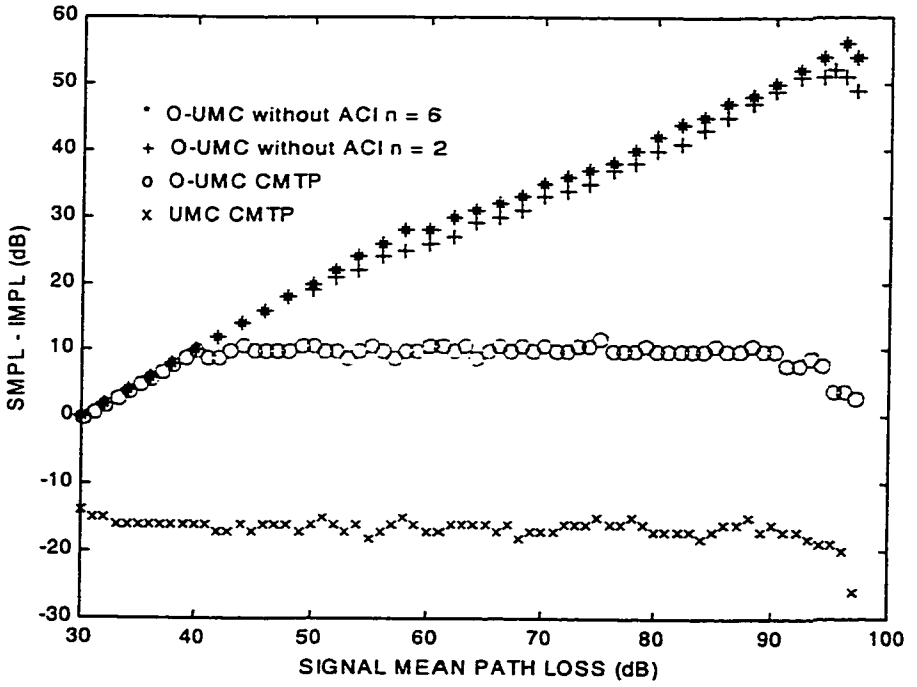

Figure 4.10 Best Performing Power Control Strategies for each of the FHSS CDMA Hopping Codes with an IIP_3 = +5 dBm

Three spatial models were used to analyze the performance of the various power control strategies with O-UMC without ACI FHSS CDMA code. Two effects of the spatial model occurred as the path loss exponent increased. The first effect was that the network performance improved with a larger path loss. This was due to the path loss exponent effecting the path loss distribution which in turn effects the interference levels. The second effect is the network performance becomes more dependent on the spatial model. The spatial model distributions effect on the path loss distribution is not as significant for lower path loss exponents as it is for larger path loss exponents. As was also expected when using power control, a network using a spatial model with a lower mean distance outperformed a network using a spatial model with a higher mean distance.

4.5 RECOMMENDATIONS FOR FUTURE WORK

This thesis analyzed the FHSS CDMA codes and transceiver performance characteristics of importance. However, the power control strategies analyzed and spatial models used were fairly simple.

Further work could be undertaken to simulate more complex power control options beyond those contained in this thesis. Realistic real-time or near real-time methods to determine CIR and/or BER accurately for use in FHSS power control algorithms could also be investigated.

The spatial models could be improved in two areas. First, when moving forward from the results presented in this thesis, I_{min} has been brought into the region where the simplistic worst case equidistant radius for all interferers begins to become a physically unrealistic situation in most applications. Work on developing a more realistic worst case close in model would allow higher accuracy for the results in this region. Secondly, research to provide empirical information on the spatial distribution models of cordless phones, wireless LANs and MODEMs would be invaluable since results have shown that the spatial models can have a significant effect on the network performance.

REFERENCES

[Balanis] C. A. Balanis, *Antenna Theory Analysis and Design*, John Wiley & Sons, 1982.

[Correia94] A. M. C. Correia, A. A. Albuquerque, "Frequency hopped spread spectrum over cellular dispersive fading channels", IEE Proceedings-Communications, vol. 141, no. 2, pp. 79 - 88, April 1994.

[Devasirvatham87] D. M. J. Devasirvatham, "Multipath Time Delay Spread in the Digital Portable Radio Environment", IEEE Communications Magazine, vol. 25, no. 6, pp. 13 - 21, June 1987.

[Gardner97] F. M. Gardner, J.D. Baker, *Simulation Techniques: Models of Communication Signals and Processes*, John Wiley & Sons, 1997.

[Geraniotis82] E. A. Geraniotis, M. B. Pursley, "Error Probabilities for Slow-Frequency-Hopped Spread-Spectrum Multiple-Access Communications over Fading Channels", IEEE Transactions on Communications, vol. COM-30, pp. 996-1009, May 1982.

[Hegde90] M. V. Hegde, W. E. Stark, "Capacity of Frequency-Hop Spread Spectrum Multiple Access Communication Systems", IEEE Transactions on Communications, vol. 38, no. 7, pp. 1050 - 1059, July 1990.

[Ishifuji94] T. Ishifuji, E. Amada, "Performance of Slow Frequency Hopping Spread Spectrum Transmission in Rayleigh Fading Indoor Channels", IEICE Transactions on Communications, vol. E77-B, no. 7, pp 876 - 882, July 1994.

[Jeruchim92] M. C. Jeruchim, P. Balaban, K.S. Shanmugan, *Simulation of Communication Systems*, Plenum Press, 1992.

[Kasahara96] H. Kasahara, S. Hara, N. Morinaga, "Modeling and Simulation Analysis of Indoor Packet Radio Communication Systems", Electronics and Communications in Japan, Part 3, vol. 79, no. 5, 1996.

[Kim94] S. W. Kim, Y. H. Lee, S. Kim, "Bandwidth tradeoffs among coding, processing gain and modulation in frequency-hopped multiple access communications, IEE Proceedings-Communications, vol. 141, no. 2, pp. 63 - 69, April 1994.

[Kim94_2] S. W. Kim, " Bandwidth Efficient Frequency-Hopped Multiple-Access Communication With Reed-Solomon Coded MFSK Signaling, IEEE Globecom 94, vol 3, pp 1304 - 1310, 1994.

[Kocaturk94] M. Kocaturk, S. C. Gupta, "Simulation of Cochannel Interference in Coexisting Cellular TDMA Networks", IEEE Transactions on Vehicular Technology, pp. 753 - 761, Part 2 August 1994.

[Maric95] S. V. Maric, "Construction of Optimal Frequency Hopping sequences for minimizing bit errors in selective fading

channels characteristic to digital cellular systems", IEE Proceedings-Communications, vol. 142, no. 4, pp. 271 - 273, August 1995.

[Matsumoto92] T. Matsumoto, A. Higashi, "Performance Analysis of RS-Coded M-ary FSK for Frequency-Hopping Spread Spectrum Mobile Radios", IEEE Transactions on Vehicular Technology, vol. 41, no. 3, pp 266 - 270, August 1992.

[Maxemchuk77] N.F. Maxemchuk, L. Schiff, "Third Order Intermodulation Interference-Bounds and Interference-Free Channel Assignment", IEEE Transactions on Communications, vol. COM-25, no. 9, pp. 1041 - 1046, September 1977.

[Molta96] D. Molta, "There's Relief Ahead For Your Wireless Woes", Network Computing, issue 720, December 15 1996.

[Pahlavan] K. Pahlavan, A. Levesque, *Wireless Information Networks*, John Wiley & Sons, 1995.

[Parsons] J. D. Parsons, *The Mobile Radio Propagation Channel*, John Wiley & Sons, 1992.

[Pawula81] R. F. Pawula, "On the Theory of Error Rates for Narrow-Band Digital FM", IEEE Transactions on Communications, vol COM-29, no. 11, pp. 1634 - 1643, November 1981.

[Proakis] J. G. Proakis, *Digital Communications, 2nd Edition*, McGraw-Hill, 1989.

[Sagers82] R. C. Sagers, "Intercept Point and Undesired Responses", IEEE Transactions on Vehicular Technology, vol. VT-32, no. 1, pp. 121 - 123, February 1983.

[Stark85_1] W. E. Stark, "Coding for Frequency-Hopped Spread-Spectrum Communication with Partial-Band Interference - Part I: Capacity and Cutoff Rate", IEEE Transactions on Communications, vol. COM-33, no. 10, pp. 1036 - 1044, October 1985.

[Stark85_2] W. E. Stark, "Coding for Frequency-Hopped Spread-Spectrum Communication with Partial-Band Interference - Part II: Coded Performance", IEEE Transactions on Communications, vol. COM-33, no. 10, pp. 1045 - 1057, October 1985.

[Tjhung70] T. T. Tjhung, P. H. Wittke, " Carrier Transmission of Binary Data in a Restricted Band", IEEE Transactions on Communication Technology, vol. COM-18, no. 4, pp. 295 - 304, August 1970.

[Wang95] C. C. Wang, G. J. Pottie, "Interference Avoidance and Power Control Strategies for Coded Frequency Hopped Cellular Systems", Proceedings IEEE International Conference on Communications ICC 95, vol. 3, pp. 1737-1741, June 1995.

[Weber95] S. Weber, "RF ICs critical to growth in mobile arena", EE Times, issue 868, October 2 1995.

[Woerner94] B. D. Woerner, A. I Wardhana, "Throughput of a FHMA System for Variable Rate Coding and Interference Estimates", Proceedings of Tactical Communications Conference, pp. 167 - 177, 1994.